DOT/FAA/AR-07/49

Air Traffic Organization
Operations Planning
Office of Aviation Research
and Development
Washington, DC 20591

Analyses of Fatigue Crack Growth Databases for Use in a Damage Tolerance Approach for Aircraft Propellers and Rotorcraft

November 2007

Final Report

U.S. Department of Transportation
Federal Aviation Administration

NOTICE

This report is available at the Federal Aviation Administration William J. Hughes Technical Center’s Full-Text Technical Reports page: actlibrary.tc.faa.gov in Adobe Acrobat portable document format (PDF).

Technical Report Documentation Page

1. Report No.	2. Government Accession No.	3. Recipient's Catalog No.
DOT/FAA/AR-07/49		

4. Title and Subtitle	5. Report Date
ANALYSES OF FATIGUE CRACK GROWTH DATABASES FOR USE IN A DAMAGE TOLERANCE APPROACH FOR AIRCRAFT PROPELLERS AND ROTORCRAFT	November 2007
	6. Performing Organization Code

7. Author(s)	8. Performing Organization Report No.
James C. Newman, Jr.	

9. Performing Organization Name and Address	10. Work Unit No. (TRAIS)
Mississippi State University P.O. Box 6156 Mississippi State, MS 39762	
	11. Contract or Grant No. 01-C-AW-MSU Amd 002, 004, 008

12. Sponsoring Agency Name and Address	13. Type of Report and Period Covered
U.S. Department of Transportation Federal Aviation Administration Air Traffic Organization Operations Planning Office of Aviation Research and Development Washington, DC 20591	Final Report
	14. Sponsoring Agency Code ASW-112

15. Supplementary Notes

The FAA William J. Hughes Technical Center Airport and Aircraft Safety R&D Division Technical Monitors were Dy Le and Cu D. Nguyen.

16. Abstract

A large portion of the fatigue crack growth threshold data in this report is inappropriate due to the load reduction test procedure that was used to generate these data. The author, in collaboration with National Aeronautics and Space Administration (NASA) Langley Research Center (LaRC) personnel, is developing new test procedures to generate threshold data under steady-state constant-amplitude loading conditions without any load history effects. The new test method involves using compression precracking to generate a crack at a V-notch and then to test the specimen under constant-amplitude loading. A large test program on the development of these fatigue crack growth databases, for use in damage-tolerant analyses for aircraft propellers and rotorcraft components, was conducted at NASA LaRC under a Memorandum of Agreement with the Federal Aviation Administration (FAA). Some materials tested and analyzed herein were 7050-T7451 and 7075-T7351 aluminum alloys and D6AC and 4340 steels. Only the steels were tested as part of the FAA program. The 7075 alloy was tested at the NASA Johnson Space Center, and the 7050 and 7075 alloys were tested at NASA LaRC. This test program was conducted to generate more accurate representations of fatigue crack growth rate behavior in the near-threshold regime and approaching fracture under a wide range of constant stress ratio ($R = P_{min}/P_{max}$) conditions. The objective of the proposed research grant was to analyze the test data on selected propeller and rotorcraft materials to develop the effective stress-intensity factor range against crack growth rate relationship for use in damage tolerance analyses. The resulting relationships can then be used in the strip-yield model in NASGRO (Stripy), AFGROW, or used to generate the stress-intensity factor range (ΔK) against crack growth rate curves for use in NASGRO, AFGROW, or any other life-prediction code requiring linear elastic fracture mechanics procedures.

17. Key Words	18. Distribution Statement
Fatigue, Fatigue crack growth, Fracture, Damage tolerance, Threshold behavior, Stress analysis, Stress-intensity factor, Fracture toughness	This document is available to the U.S. public through the National Technical Information Service (NTIS), Springfield, Virginia 22161.

19. Security Classif. (of this report)	20. Security Classif. (of this page)	21. No. of Pages	22. Price
Unclassified	Unclassified	93	

TABLE OF CONTENTS

LIST OF FIGURES

LIST OF TABLES

LIST OF SYMBOLS AND ACRONYMS

B	Specimen thickness, mm
C_i	Crack growth coefficient for segment i
c	Crack length, mm
c_n	Notch length, mm
c_i	Initial crack length, mm
dc/dN	Fatigue crack growth rate, m/cycle
$dk/dc/K$	Normalized K gradient
F_i	Boundary correction on stress-intensity factor for various loading
f	Crack mouth-opening-displacement gage force, kN
G_i	Boundary correction on crack surface displacements for various loading
E	Modulus of elasticity, MPa
K_{Ie}	Elastic stress-intensity factor at failure, MPa√m
K	Applied stress-intensity factor, MPa√m
k_g	Crack mouth-opening-displacement gage stiffness, N/mm
N	Newton
n_i	Crack growth power for segment i
P	Applied load, kN
R	Stress ratio (K_{min}/K_{max}, P_{min}/P_{max} or S_{min}/S_{max})
S	Applied stress, MPa
S_o	Crack-opening stress, MPa
V_i	Crack mouth-opening displacement for various loading, mm
V_g	Crack mouth-opening displacement gage displacement, mm
W	Width of C(T) and total width of M(T) specimen, mm
x	Cartesian coordinate measured along crack plane, mm
α	Constraint factor
Δc	Crack growth increment, mm
ΔK	Stress-intensity factor range, MPa√m
ΔK_{th}	Stress-intensity factor range threshold, MPa√m
ΔK_{eff}	Effective stress-intensity factor range, MPa√m
ΔK_{eff}-rate	Effective stress-intensity factor range against rate
$(\Delta K_{eff})_T$	Effective stress-intensity factor range at flat-to-slant crack growth, MPa√m
ΔK-rate	Stress-intensity factor range against rate
σ_o	Flow stress (average of σ_{ys} and σ_u), MPa
σ_{ys}	Yield stress (0.2 % offset), MPa
σ_u	Ultimate tensile strength, MPa
AGARD	Advisory Group for Aerospace Research and Development
ASTM	American Society of Testing and Materials
COD	Crack-opening displacement
C(T)	Compact tension specimen
CPCA	Compression-compression precracking constant-amplitude
CPCK	Compression-compression precracking constant ΔK
FAA	Federal Aviation Administration
L	Longitudinal

LaRC	Langley Research Center
LEFM	Linear elastic fracture mechanics
LT	Longitudinal transverse
JSC	Johnson Space Center
MSU	Mississippi State University
M(T)	Middle crack tension specimen
NASA	National Aeronautics and Space Administration
ONR	Office of Naval Research
S	Short
T	Transverse
TL	Transverse longitudinal

EXECUTIVE SUMMARY

A large portion of the fatigue crack growth threshold data in this report is inappropriate due to the load reduction test procedure that was used to generate these data. The author, in collaboration with National Aeronautics and Space Administration (NASA) Langley Research Center (LaRC) personnel, is developing new test procedures to generate threshold data under steady-state constant-amplitude loading conditions without any load history effects. The new test method involves using compression precracking to generate a crack at a V-notch and then to test the specimen under constant-amplitude loading. A large test program on the development of these fatigue crack growth databases, for use in damage-tolerant analyses for aircraft propellers and rotorcraft components, was conducted at NASA LaRC under a Memorandum of Agreement with the Federal Aviation Administration (FAA). Some materials tested and analyzed herein were 7050-T7451 and 7075-T7351 aluminum alloys, and D6AC and 4340 steels. Only the steels were tested as part of the FAA program. The 7075 alloy was tested at the NASA Johnson Space Center, and the 7050 and 7075 alloys were tested at NASA LaRC. This test program was conducted to generate more accurate representations of the fatigue crack growth rate behavior in the near-threshold regime and approaching fracture under a wide range of constant stress ratio ($R = P_{min}/P_{max}$) conditions. The objective of the proposed research grant was to analyze the test data on selected propeller and rotorcraft materials to develop the effective stress-intensity factor range against crack growth rate relationship for use in damage tolerance analyses. The resulting relationships can then be used in the strip-yield model in NASGRO (Stripy), AFGROW, or used to generate the stress-intensity factor range (ΔK) against crack growth rate curves for use in NASGRO, AFGROW, or any other life prediction code requiring linear elastic fracture mechanics procedures.

1. INTRODUCTION.

1.1 PURPOSE.

The objective of this project was to analyze the test data from the Federal Aviation Administration (FAA) sponsored test program at National Aeronautics and Space Administration (NASA) Langley Research Center (LaRC), test data generated at NASA LaRC, and at NASA Johnson Space Center (JSC) to support the validation of the newly developed test methods. This test program was conducted to generate more accurate representations of the fatigue crack growth rate behavior in the near-threshold regime and approaching fracture under a wide range of stress ratio (R) conditions. The FAA test program studied a variety of propeller and rotorcraft materials. Some of the materials tested and analyzed herein were 7050-T7451 and 7075-T7351 aluminum alloys and D6AC and 4340 steels. Only the steels were tested as part of the FAA program. The 7075 transverse longitudinal (TL) alloy was tested at NASA JSC, and the 7050 and 7075 longitudinal transverse (LT) alloys were tested at NASA LaRC. Tests were conducted on two specimen types (compact and middle crack tension specimens). Four test procedures were used: (1) constant-amplitude loading, (2) American Society of Testing and Materials (ASTM) E647 load reduction method [1], (3) K_{max} equal constant test procedure [2], and (4) a compression-compression precracking constant-amplitude (CPCA) procedure [3]. An additional test procedure, compression-compression precracking constant ΔK (CPCK) loading, was used on some of the compact tension (C(T)) specimens to study the extent of the tensile residual stresses caused by compression yielding at the crack starter notch.

Test data on selected propeller and rotorcraft materials were analyzed to develop the effective stress-intensity factor range (ΔK_{eff}) against crack growth rate relationship for use in damage tolerance analyses. The resulting relationships can then be used in the strip-yield model in NASGRO (Stripy) [4], AFGROW [5], or used to generate the stress-intensity factor range (ΔK) against crack growth rate curves for use in NASGRO, AFGROW, or any other life prediction code requiring linear elastic fracture mechanics (LEFM) procedures.

1.2 BACKGROUND.

Fatigue crack growth in a metallic material is typically quantified by the size of the crack (c) and the rate at which the crack propagates (dc/dN). The crack growth rate in a given material is defined in terms of the LEFM parameter and ΔK at a given stress ratio (R = minimum to maximum load ratio). The relationship between ΔK and dc/dN was originally shown to be nearly linear on a log(ΔK)-log(dc/dN) scale by Paris and Erdogan [6] for a large number of materials. However, the relation between ΔK and dc/dN is nonlinear when the cracked body is approaching fracture [7] and when the crack growth rate is very slow [8]. Therefore, the three regions of crack growth are defined as the threshold region (slow growth), the linear mid-region (Paris regime), and the fracture region (rapid growth).

The fatigue crack growth threshold is defined as the value of ΔK at which dc/dN is extremely slow (10^{-10} m/cycle) [9]. Traditionally, the threshold is used as a limit for damage-tolerant design [10]; e.g., if the stress-intensity factor for a given crack is below the threshold value, the crack is assumed to be nonpropagating. However, it has been shown by Pearson [11] that small

cracks propagate at stress-intensity factor levels below the large crack threshold defined by the ASTM standard test procedure [1]. Newman [12 and 13] has demonstrated that the discrepancy between small crack data under constant-amplitude loading and large crack data generated with the load reduction procedure was due to "remote" closure effects on the large crack data. Thus, the anomaly is the large crack threshold at low stress ratios (R). Therefore, if the fatigue crack growth threshold is to be established as a lifing criterion, then the most accurate representation of the threshold for a material needs to be defined.

2. DISCUSSION.

Accurate representation of fatigue crack thresholds, the region defining crack growth as either very slow or nonexistent, is extremely important for many structural applications. If the measured threshold is unconservatively high, then a structural component designed with these data may fail long before the fatigue analysis predicts. Currently, in North America, the threshold crack growth regime is experimentally defined using ASTM Standard E 647 [1], which has been shown to exhibit anomalies due to the load reduction test procedure. The load reduction test procedure has been shown to induce high crack closure loads [14] and remote crack surface closure [12], which prematurely slows down crack growth and produces an abnormally high threshold. Several other investigators [15 and 16] have used other methods to generate threshold values that appear to not be affected by the test procedure.

Alternative test methods have also been proposed, such as the constant K_{max} test procedure [2], to define the low crack growth rate and threshold regimes. But the current K_{max} test procedure produces data at variable R and fatigue crack growth thresholds at extremely high stress ratios (> 0.9). The K_{max} test procedure also produces what has been referred to as the "K_{max} effect" because lower thresholds are obtained using higher K_{max} values [17 and 18]. But extensive literature data reviewed by Vasudevan, et al. [19] on a wide variety of materials do not show the so-called K_{max} effect. These mixed results suggest that something is different in either the test procedure or test specimens that exhibit different behavior in the near-threshold regime.

The current test method defined by ASTM is designed to fully reproduce the range of fatigue crack thresholds (e.g., low and high stress ratios) needed to characterize loading conditions for many structural applications. The ASTM load reduction test procedure [1] was based on stress-intensity factors changing at an exponential rate. A typical load reduction example is shown in figure 1. The ratio of the current maximum applied load, P_{max}, to the initial maximum applied load, $(P_{max})_i$, is plotted against crack length. In this example, the initial crack length (c_i) of the load reduction procedure was 20 mm in a large middle crack tension specimen. The solid curves are based on a constant rate of change in normalized plastic zone size with crack extension. The normalized K-gradient, $(dK/dc)/K$, was -0.08 mm^{-1} for the upper solid curve, as recommended in the standard. This is equivalent to a 5% change in stress every 0.5 mm of crack extension, as shown by the stair-step lines. The standard also allows a 10% change every 0.5 mm of crack extension, if computerized, and smooth load reduction capability is not available. This is equivalent to a normalized K-gradient of -0.2 mm^{-1}, as shown by the lower solid curve. These procedures have been used over the past 25 years to generate fatigue crack growth thresholds for a wide variety of materials. It would be expected that a load history effect may occur if the residual plastic deformation left along the advancing crack surface causes premature closure [12 and 20]. During the past decade, some of these thresholds have been shown to be satisfactory,

such as those for high-strength materials (steels) using middle crack tension specimens, but for lower-strength materials (aluminum and titanium alloys), the thresholds are estimated to be as much as a factor of 2 to 3 too high (in terms of ΔK).

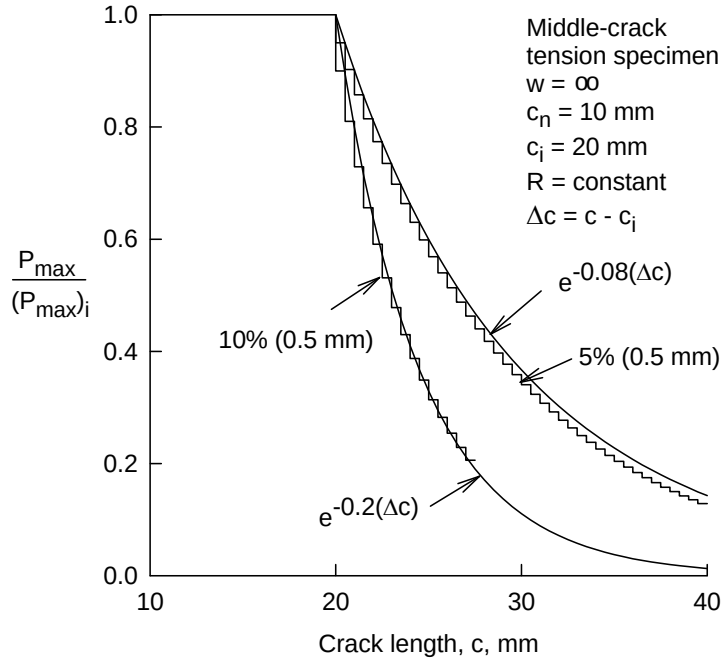

Figure 1. ASTM E 647 Load Reduction Procedure for Threshold Testing

The problem associated with using the load reduction procedure to generate fatigue crack growth rate data is illustrated in figure 2. Forman, who works for NASA JSC generated fatigue crack growth data on a 7075 aluminum alloy forging at three different stress ratios using the load reduction procedure. Using the FASTRAN crack-opening stress equations [21] under steady-state, constant-amplitude loading conditions, the data for the various *R* ratios were correlated quite well in the middle and upper regions, but the model was unable to correlate the data in the near-threshold regime for the low *R* ratios. The near-threshold data "fans out" as a function of the stress ratio. The rise in the crack-opening stresses (due to remote closure) was not accounted for in the steady-state, crack-opening stress equations. The crack closure theory predicts that data generated under constant-amplitude loading should not fan out in the near-threshold regime, and that the low *R* ratio data should correlate with the high *R* ratio data. The basic problem is that the aerospace community is now using the low *R* ratio data stress-intensity factor range against rate (ΔK-rate) as if it is the intrinsic fatigue crack growth rate behavior. These high threshold values can result in very unconservative life predictions, especially for high-cyclic fatigue components.

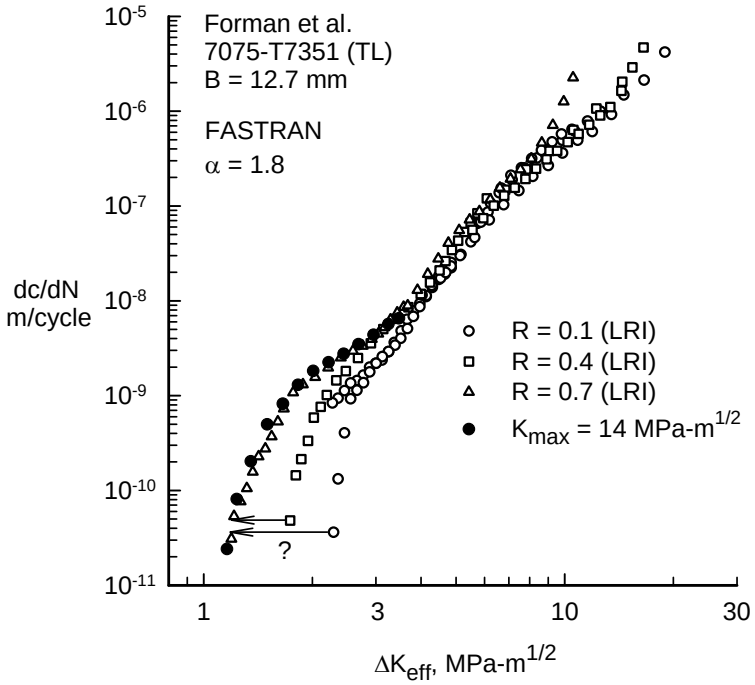

Figure 2. Effective Stress-Intensity Factor Against Rate for 7075 Forging Material

To generate fatigue crack growth rate data in the near-threshold regime for any stress ratio without load reduction effects, a compression-compression precracking method, developed over the years by Hubbard [22], Topper and Au [23], Au, et al. [24], Suresh [25], and Pippan, et al. [3], was used in the current study. Using this procedure, prenotched specimens were cycled under compression-compression precracking to produce an initial crack, which naturally stops growing. Then, the specimen was subjected to a constant-amplitude fatigue loading to generate fatigue crack growth rate data in the near-threshold regime at the desired stress ratio. The CPCA loading, as shown in figure 3, was designed to generate fatigue crack growth rates in the threshold regime under constant-amplitude loading conditions with minimal load history effects [26 and 27]. This type of loading is expected to produce fatigue cracks at machined notches with minimal load history effects, after the crack has grown several compressive plastic zone sizes. James, et al. [28], using finite element analyses, has shown that the crack should have grown about 3 compressive plastic zone sizes to ensure steady-state crack growth rate conditions.

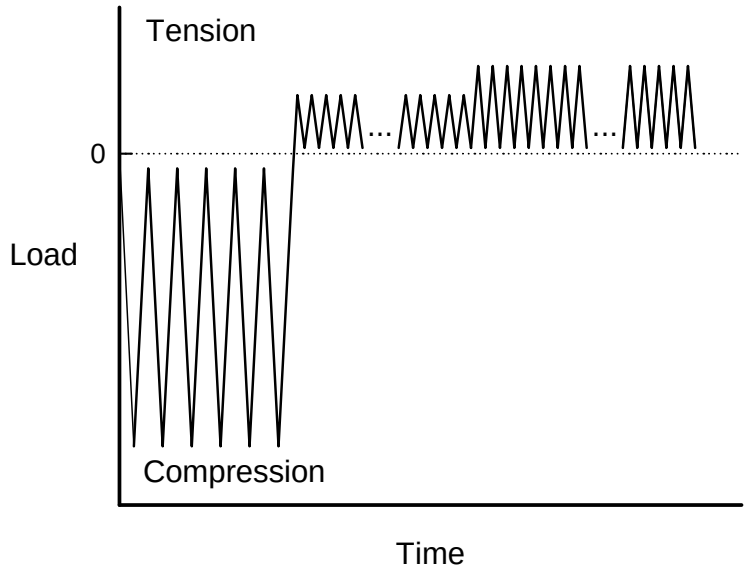

Figure 3. Loading Sequence to Initiate Crack at Notch With Minimal Load History Effects

Once a fatigue crack has been initiated at the crack starter notch, a tensile loading is then applied to grow the crack under constant-amplitude loading from threshold to near fracture conditions. Currently, trial and error procedures are required to select the initial tensile loading to start the test at the unknown ΔK threshold value. If a tensile load is selected that would produce a stress-intensity factor range below the threshold, then the crack will not grow; however, if the load is high enough, then the crack will grow. The task is to locate this particular tensile loading, which will result in a stress-intensity factor that is only slightly higher than the true ΔK threshold. However, one objective of the existing grant was to develop the equations to estimate the threshold at a given stress ratio. This will minimize the number of tests required to establish the threshold values and data in the near-threshold regime.

A schematic of the expected behavior for the load reduction procedure and the proposed CPCA loading procedure is shown in figure 4. The objective is to determine the steady-state, constant-amplitude curve (solid curve in the figure) at a constant R ratio, without any load history effects. The traditional load reduction scheme has been shown to induce higher ΔK_{th} thresholds than steady-state conditions [12 and 14]. Also, the thresholds have been shown to be influenced by the initial ΔK level at which the load reduction procedure was applied [29], as shown in figure 4. On the other hand, cracks grown under the CPCA loading are fully open at the start of constant-amplitude loading, rapidly slow down and approach the steady-state curve from above. The cracks are growing because of tensile residual stresses induced by the compressive yielding at the crack starter notch. At low initial values of ΔK_i, an over shoot (rates below the steady-state condition) may occur in the results based on FASTRAN [21] simulations. It is estimated that the crack must grow several compressive plastic-zone sizes before steady-state conditions are met [28]. The ΔK_{eff} curve (dash-dot curve) is the ΔK-rate curve for high R ratios and is the characteristic behavior of a fully open crack. The ΔK_{eff} curve may or may not be parallel to the steady-state curve due to three-dimensional constraint and environmental effects.

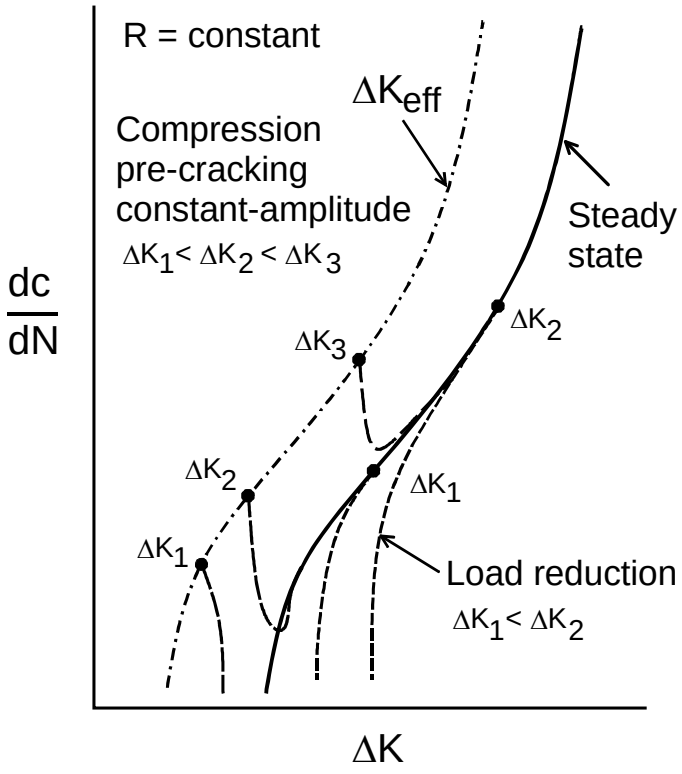

Figure 4. Schematic of Fatigue Crack Growth Rates From Load Reduction and Compression Precracking Methods in Relation to Steady-State Behavior Under a Constant Stress Ratio

The introduction of the CPCA threshold test procedure now gives two methods to determine the near-threshold and threshold behavior for metallic materials. The CPCA procedure would effectively give a lower bound on the threshold behavior, and the load reduction procedure would give an upper bound. Ideally, if there are no load history effects, then both methods should reproduce the same behavior.

3. EVALUATION APPROACH.

3.1 TEST SPECIMENS.

The primary test specimen used at both the NASA LaRC and NASA JSC was the C(T) specimen (see figure 5). The specimens were nominally W = 76 mm and B = 11 to 13 mm. Some smaller C(T) specimens (W = 51 mm and B = 6.35 mm) were also tested at NASA LaRC. Fatigue crack growth rate data generated from an Advisory Group for Aerospace Research and Development (AGARD) study [30] on the 4340 steel used middle crack tension (M(T)) specimens (W = 76 mm and B = 5.1 mm), as shown in figure 5.

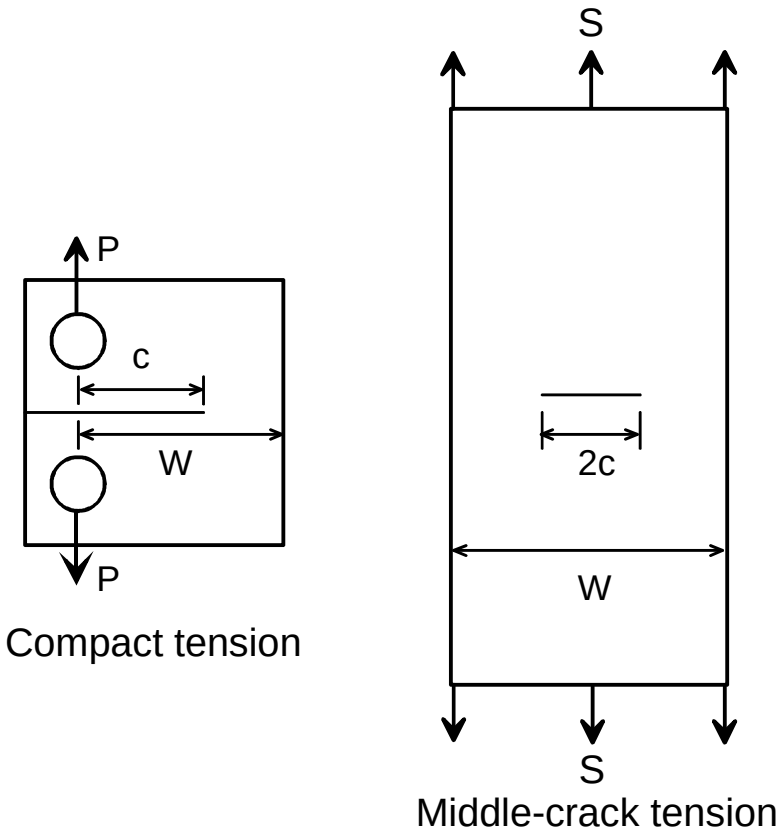

Figure 5. Test Specimens Used to Generate Fatigue Crack Growth Rate Data

3.2 MATERIALS.

The four materials (7050-T7451 and 7075-T7351 aluminum alloys, and D6AC and 4340 steels) were obtained from a propeller or rotorcraft manufacturer and tested at NASA LaRC. The aluminum alloy test results were obtained from Forth, et al. [26 and 27]; and the test data on the two steels were obtained from Forth, et al. [31]. In general, specimens were machined and tested in three material orientations, but only tests conducted in the longitudinal (L or LT) orientation were analyzed herein. NASA JSC (Forman) also tested 7075-T7351 in the TL orientation and these results were also analyzed.

3.2.1 Aluminum Alloy 7050-T7451.

NASA LaRC machined all 7050 specimens from a 152-mm-thick plate that had been obtained in an overaged T7451 heat-treat condition per specification AMS 4050G [32]. The chemical composition of this alloy is listed in table 1.

Table 1. Chemical Composition of 7050 Aluminum Alloy [33]

Element	Symbol	7050 Aluminum Alloy
Aluminum	Al	Balance
Chromium	Cr	0.04%
Copper	Cu	2.0%-2.6%
Iron	Fe	0.15%
Magnesium	Mg	1.9%-2.6%
Manganese	Mn	0.1%
Silicon	Si	0.12%
Titanium	Ti	0.06%
Zinc	Zn	5.7%-6.7%
Zirconium	Zr	0.08%-0.15%
Others	—	0.2%

Tensile tests were conducted according to ASTM Standard E8 using 6.4-mm round-bar tension specimens. The specimens were tested in the both the L and short (S) transverse orientations at room temperature. The yield stress, ultimate tensile strength, and modulus of elasticity were calculated from two tests for each orientation. For the L orientation at room temperature, the yield stress was 470 MPa, the ultimate tensile strength was 525 MPa, and the modulus of elasticity was 76 GPa.

3.2.2 Aluminum Alloy 7075-T7351.

Test results on the 7075-T7351 aluminum alloys were obtained from two sources. NASA LaRC machined specimens in the LT orientation from plates that had been obtained in a T7351 heat-treat condition from a rotorcraft manufacturer. NASA JSC (Forman) machined specimens from 52-mm-thick plates that were also provided by the same manufacturer, but these specimens were tested in the TL orientation. Unfortunately, tensile tests were not preformed. Thus, handbook values of the tensile properties were used herein. For the LT orientation at room temperature, the yield stress was 430 MPa, the ultimate tensile strength was 508 MPa, and the modulus of elasticity was 72 GPa; whereas, in the TL orientation, the yield stress was 415 MPa, the ultimate tensile strength was 490 MPa, and the modulus of elasticity was 72 GPa. Again, chemical compositions were not performed on these particular alloys, but the nominal chemical composition is listed in table 2.

Table 2. Chemical Composition of 7075 Aluminum Alloy [33]

Element	Symbol	7050 Aluminum Alloy
Aluminum	Al	Balance
Chromium	Cr	0.18%-0.28%
Copper	Cu	1.2%-2.0%
Iron	Fe	0.5%
Magnesium	Mg	2.1%-2.9%
Manganese	Mn	0.3%
Silicon	Si	0.4%
Titanium	Ti	0.2%
Zinc	Zn	5.1%-6.1%
Others	—	0.2%

3.2.3 D6AC Steel.

NASA LaRC [31] machined test specimens from a hammer-forged D6AC steel block that was provided by a propeller manufacturer. The details of the heat treatment and material source are proprietary to the manufacturer. Material directions were defined with respect to the local block configuration. The L coincided with the length of the block. The T and S directions coincided with the longest and shortest cross-sectional dimensions, respectively. The block was cut into fatigue crack growth rate specimens (C(T) and M(T)) and tensile specimens to measure mechanical properties. Herein, only the longitudinal direction (L) specimens were analyzed. The chemical composition of this alloy is listed in table 3.

Table 3. Chemical Composition of D6AC Steel [34]

Element	Symbol	D6AC Steel
Carbon	C	0.45%-0.50%
Chromium	Cr	0.90%-1.20%
Copper	Cu	< 0.35%
Iron	Fe	Balance
Manganese	Mn	0.60%-0.90%
Molybdenum	Mo	0.90%-1.10%
Nickel	Ni	0.40%-0.70%
Phosphorous	P	< 0.015%
Silicon	Si	0.15%-0.30%
Sulphur	S	< 0.015%
Vanadium	V	0.08%-0.15%

Tensile tests were conducted according to ASTM Standard E8 using 13-mm-wide rectangular tension specimens. The specimens were tested in the L, T, and S direction at three temperatures. The yield stress, ultimate tensile strength, and modulus of elasticity were calculated from the results of three tests for each orientation. For the L orientation at room temperature, the yield

stress was 1120 MPa, the ultimate tensile strength was 1235 MPa, and the modulus of elasticity was 210 GPa.

3.2.4 4340 Steel.

Again, NASA LaRC [31] machined test specimens from a 4340 steel block that was provided by a propeller manufacturer. Details on the heat treatment and material source are proprietary. Material directions were defined with respect to the local block configuration. The L direction coincided with the length of the block. The T and S directions coincided with the longest and shortest cross-sectional dimensions, respectively. The block was cut into fatigue crack growth rate specimens (C(T) and M(T)) and tensile specimens to measure mechanical properties. Herein, only the L specimens were analyzed. The chemical composition of this alloy is listed in table 4.

Table 4. Chemical Composition of 4340 Steel [34]

Element	Symbol	4340 Steel
Carbon	C	0.38%-0.43%
Chromium	Cr	0.70%-0.90%
Iron	Fe	Balance
Manganese	Mn	0.60%-0.80%
Molybdenum	Mo	0.20%-0.30%
Nickel	Ni	1.65%-2.00%
Phosphorous	P	< 0.035%
Silicon	Si	0.15%-0.30%
Sulphur	S	< 0.040%

Tensile tests were conducted according to ASTM Standard E8 using 13-mm-wide rectangular tension specimens. The specimens were tested in the L, T, and S direction at three temperatures. The yield stress, ultimate tensile strength, and modulus of elasticity were calculated from the results of three tests. For the L orientation at room temperature, the yield stress was 500 MPa, the ultimate tensile strength was 730 MPa, and the modulus of elasticity was 210 GPa.

3.3 TEST METHODS.

In generating fatigue crack growth rate data (crack length against cycles) on metallic materials, various test methods have been used over the past 30 years (see ASTM E 647 [1]). The primary goal has been to determine the constant-amplitude fatigue crack growth rate behavior at various mean and alternating load conditions. However, to generate fatigue crack growth rate data in the near-threshold regime, constant-amplitude loading conditions have not been able to initiate a crack at a crack starter notch at the extremely low stress-intensity factors required. Thus, Schmidt and Paris [35] and Hudak, et al. [9] developed a load reduction scheme to initiate cracks at higher ΔK and slowly reduce the ΔK until the near-threshold and threshold behavior has been obtained. The load reduction procedure assumed that the crack growth rate was totally controlled by the ΔK value. This procedure was standardized in ASTM E 647 and has been used for over 25 years to generate fatigue crack growth rate data from threshold to fracture conditions.

Herman, et al. [2] developed a load reduction procedure to reduce ΔK (by reducing the load amplitude), but held the K_{max} value constant. This procedure generated low crack growth rates at very small ΔK values, but the stress ratio near and at threshold was extremely high, generally greater than 0.9. Procedures to maintain a constant ΔK value have also been used to study environmental effects. This procedure, which is also a load reduction procedure to maintain a constant ΔK value as the crack grows, has been widely used. All of these methods assume that the crack tip behavior is totally controlled by the ΔK.

However, fatigue crack closure under cyclic loading (Elber [36]) brings the influence of load history on crack growth behavior, such as the plastic wake and residual stresses. Thus, the ΔK does not control fatigue crack growth. Contact of the crack surfaces and residual stresses in the plastic zone influences the crack growth rate behavior. Since Elber's discovery, several other closure mechanisms, such as fretting oxide debris and roughness induced closure, have been discussed and modeled [37-39]. The test environment, even laboratory air, has a tremendous influence on the crack growth mechanisms that are activated, which can influence crack closure behavior and must be considered in developing any damage tolerance life-prediction method.

Recently, there has been a renewed interest in using compression precracking test procedures, as proposed by Hubbard [22], Topper and Au [23], Au, et al. [18], Suresh [25], Pippan, et al. [3], and Forth, et al. [26 and 27], to generate a crack under compressive loading and then to apply either a small ΔK or small constant-amplitude loading slightly above the steady-state ΔK threshold at a given stress ratio. This test procedure should generate fatigue crack growth rate data in the near-threshold regime that minimizes any load history effects, after the crack has grown several compressive plastic zone sizes [28].

In the following, several fatigue crack growth rate test methods will be presented and discussed. They are: (1) constant-amplitude loading tests, (2) load reduction threshold tests, (3) constant K_{max} tests, (4) CPCK tests, and (5) CPCA threshold tests.

3.3.1 Constant-Amplitude Loading Tests.

In fracture mechanics terminology, constant-amplitude loading is described in terms of the maximum load (P_{max}) or maximum stress (S_{max}) and the stress ratio ($R = P_{min}/P_{max} = S_{min}/S_{max}$), as shown in figure 6. In fatigue terminology, constant-amplitude loading has been defined in terms of the alternating and mean load or stress. Thus, two parameters (P_{max} and R; or alternating and mean) are required to define constant-amplitude loading. The primary objective of constant-amplitude test procedures is to generate steady-state behavior at a given stress ratio. Steady-state behavior is when the crack front plastic deformations and the residual plastic deformations in the wake are mutually associated. Transient effects, such as accelerated or retarded crack growth at the start of a test or at a change in load amplitude, are not included.

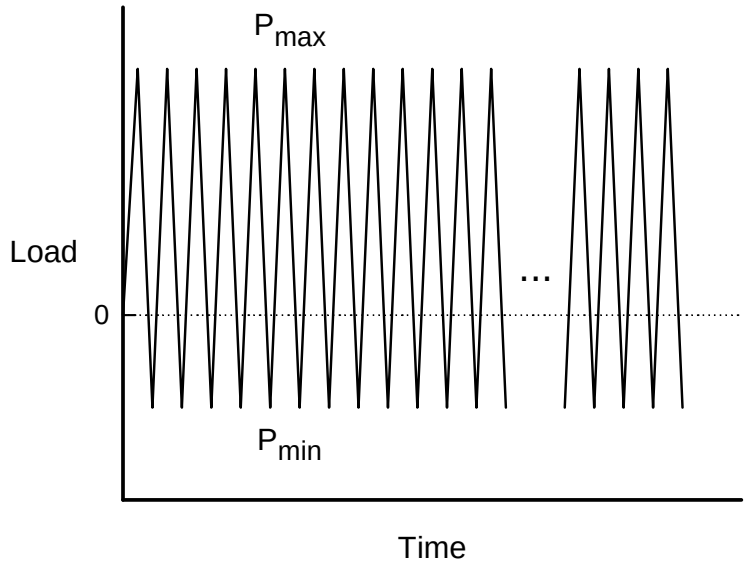

Figure 6. Definition of Constant-Amplitude Loading

Constant-amplitude fatigue crack growth rate data at various stress ratios are used in many damage-tolerant life prediction codes to predict crack growth from an initial damage state (i.e., initial crack size) using either linear-cumulative damage or retardation/acceleration routines.

3.3.2 Load Reduction Threshold Tests.

The current load reduction test method defined by ASTM E 647 is designed to fully reproduce the range of fatigue crack thresholds (e.g., low and high stress ratios) needed to characterize loading conditions for many structural applications. The ASTM load reduction test procedure [1] was based on stress-intensity factors changing at an exponential rate. A typical load reduction example is shown in figure 7. The ratio of the current applied load, P_{max}, to the initial applied load, $(P_{max})_i$, is plotted against crack length. The solid curves are based on a constant rate of change in normalized plastic zone size with crack extension. The normalized K-gradient, $(dK/dc)/K$, was -0.08 mm^{-1} for the upper solid curve, as recommended in the standard. This is equivalent to a 5% change in stress every 0.5 mm of crack extension, as shown by the stair-step lines. The standard also allows a 10% change every 0.5 mm of crack extension, if computerized, smooth load reduction capability is not available. This is equivalent to a normalized K-gradient of -0.2 mm^{-1}, as shown by the lower solid curve. These procedures have been used over the past 25 years to generate fatigue crack growth thresholds for a wide variety of materials.

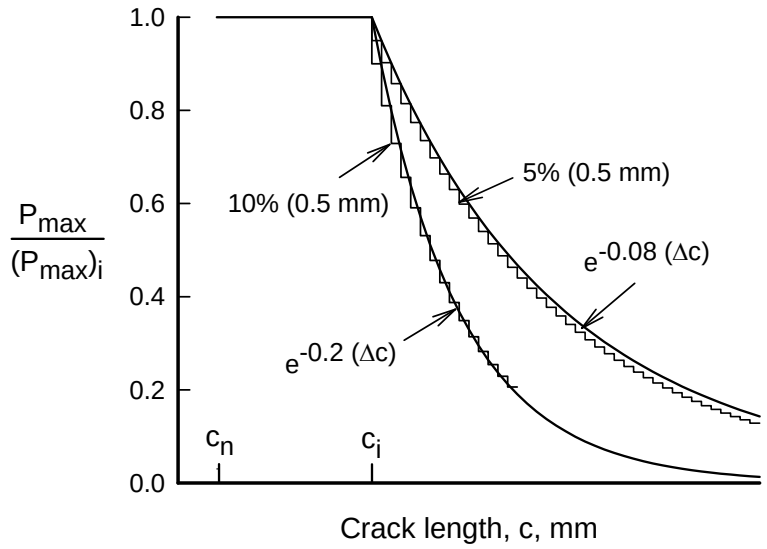

Figure 7. Definition of ASTM E 647 Load Reduction Procedure

3.3.3 Constant K_{max} Tests.

Herman, Hertzberg, and Jaccard [2] developed a simplified laboratory test method to generate fatigue crack growth rate data that would be able to predict short crack growth behavior, referred to as the "K_{max} test." Their assumption was that short crack behavior was closure free and that high-stress ratio data would agree with short crack data. Of course, this is not the case for short or small crack behavior. Only in the initial stages of short or small crack growth will the crack be closure free. However, this test has been frequently used to generate closure-free (high R) data for large cracks. These high R data are also frequently used to generate the effective stress-intensity factor curve for use in the crack closure models, such as FASTRAN.

The K_{max} test is a K-controlled test where the K_{max} value is held constant and the minimum K value is slowly increased with crack length, as shown in figure 8. In the example shown, the initial R value was 0.5, and the R value will increase as the crack length becomes larger. As the ΔK value decreases, the corresponding crack growth rate will also decrease and approach a threshold condition. Generally, the threshold value will be at an extremely high R value, such as 0.9 to 0.95.

However, K_{max} testing has also introduced another phenomenon called the K_{max} effect on threshold behavior [17 and 18]. Larger values of K_{max} have generated lower thresholds. The reason for this behavior is not clear, but appears to be related to the fracture process. For the aluminum alloys and larger K_{max} values, Newman, et al. [18] has shown more dimpling and tunneling on the fatigue surface as the threshold is approached.

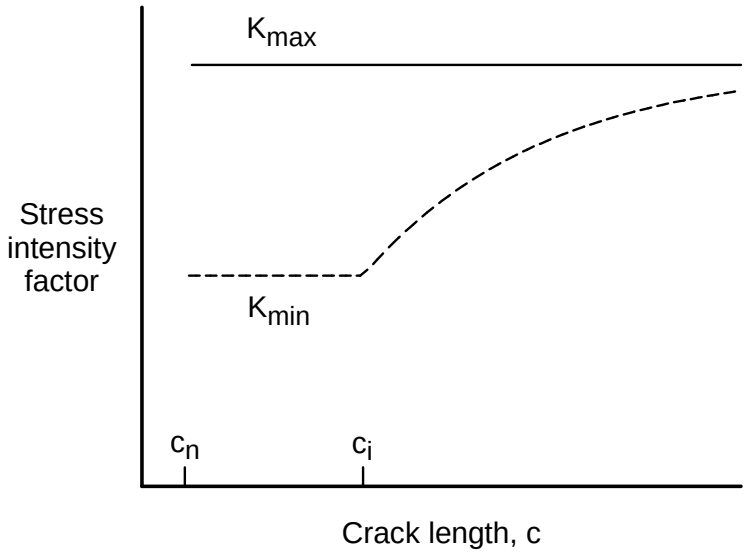

Figure 8. Definition of Constant K_{max} Test Procedure

3.3.4 The CPCK Tests.

During the current study, the researchers at NASA LaRC proposed to use a compression precracking method, which is basically a *K*-controlled test, as shown in figure 9. Using a notched specimen, a cyclic compressive loading would be applied to initiate a crack at the notch. Then, the specimen would be subjected to a constant ΔK (above the apparent ΔK_{th} threshold) for a given *R* value. The compressive loading, which yields the notch root, induces a tensile residual stress in front of the notch. The objective in using this technique was to identify the extent of the influence of these residual stresses. But, this technique is also a load reduction procedure because the applied load has to be decreased with larger crack lengths to maintain the constant ΔK value.

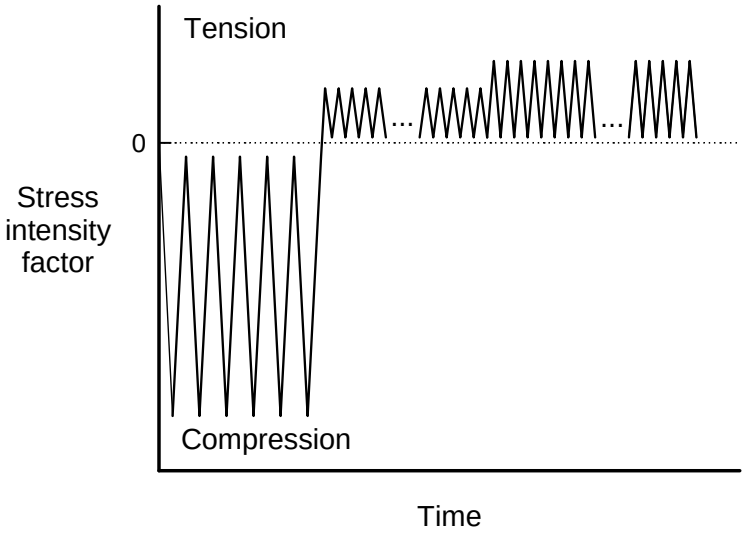

Figure 9. Definition of CPCK Loading

3.3.5 The CPCA Threshold Tests.

The compression-compression precracking procedure, as shown in figure 10, was designed to generate fatigue crack growth rates in the near-threshold regime under constant-amplitude loading conditions with minimal load history effects. This type of loading has been demonstrated to produce fatigue cracks at machined notches with minimal load history effects on both compact and middle crack tension specimens [26 and 27]. Once a fatigue crack has been initiated at the notch root, then very small tensile loading can be applied to grow the crack under steady-state constant-amplitude loading from threshold to fracture conditions. Currently, trial-and-error procedures are required to select the initial tensile loading to start the test at the unknown threshold value. If a tensile load is selected that would produce a ΔK below the threshold, then the crack will not grow; however, if the load is high enough, then the crack will grow. One objective of the current grant was to develop the equations to estimate the threshold at any given stress ratio. This will minimize the number of tests required to establish the threshold values and data in the near-threshold regime.

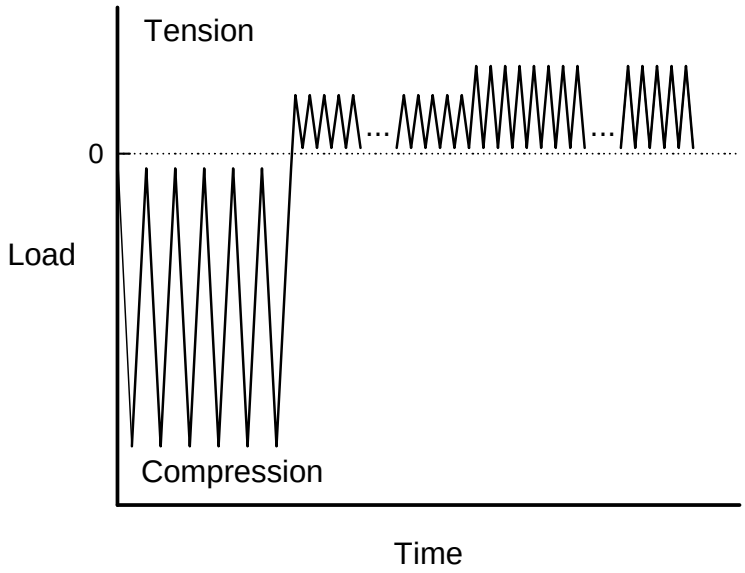

Figure 10. Definition of CPCA Loading

3.4 ANALYSES OF TEST METHODS.

FASTRAN [21], which is a life-prediction code, is an advanced strip-yield model based solely on the plasticity-induced crack closure mechanism. The code is perhaps the most accurate life-prediction code under variable amplitude loading. The key feature of the model is the ability to account for the three-dimensional stress state effects using a constraint factor on crack tip yielding and the plastic wake. Plane-stress (thin-sheet) conditions are modeled with the constraint factor $\alpha = 1$ and plane-strain (thick-plate) conditions are modeled with $\alpha = 3$. But, the code is only a two-dimensional model. As with any model, there are limitations and approximations that are made to produce a rapid life-prediction code and improvements can always be made.

In the following, the FASTRAN code will be used to simulate fatigue crack growth under the various test methods that have been developed to generate crack growth rate data. These are: (1) constant-amplitude loading tests, (2) load reduction threshold tests, (3) constant K_{max} tests, and (4) CPCA threshold tests.

3.4.1 Constant-Amplitude Loading Tests.

In generating fatigue crack growth rate data under constant-amplitude loading, two specimens, the C(T) and M(T) specimens, are most commonly used. In FASTRAN, the two-dimensional (strip-yield) crack closure model is that for a central crack in a finite width plate under remote tension, which is ideal for M(T) specimens. However, to calculate the crack-opening stresses (or loads) for C(T) specimens, the concept of *K*-analogy [21] is used. McClung [40] has used the two-dimensional, elastic-plastic, finite element method; and Daniewicz and Bloom [41] have used weight functions and a two-dimensional strip-yield model to analyze several difference crack configurations under plane stress conditions. Their results confirm that under small-scale yielding conditions, the same maximum stress-intensity factor and *R* ratio will produce the same stabilized crack-opening stresses (or loads). Thus, *K*-analogy can be used to predict the crack-opening stresses for other crack configurations under small-scale yielding conditions.

The stress-intensity factor for the C(T) specimen is

$$K_{ct} = P/(B\sqrt{W})\, F = P/(BW)\, \sqrt{(\pi c)}\, F_{ct} = S_{ct}\, \sqrt{(\pi c)}\, F_{ct} \quad (1)$$

where P is the applied load, F is the usual boundary correction factor in ASTM E 647, S_{ct} is a characteristic stress, $P/(BW)$, and F_{ct} is the corresponding boundary correction factor. The stress-intensity factor for the M(T) specimen is

$$K_{mt} = S_{mt}\, \sqrt{(\pi c)}\, F_{mt} \quad (2)$$

where S_{mt} is the applied stress and F_{mt} is the usual boundary correction factor. Equating equations 1 and 2 gives

$$S_{mt} = [P/(BW)]\, F_{ct}/F_{mt} \quad (3)$$

Thus, S_{mt} is the stress applied to the M(T) specimen strip-yield model that will be used to calculate crack-opening stress levels for the same crack length in a C(T) specimen. Figure 11 shows calculations from FASTRAN for C(T) specimens subjected to very low loads like those used in threshold testing. The specimens were subjected to a characteristic stress range, ΔS, of 3 MPa at three different stress ratios (R = 0, 0.4, and 0.7). The simulations were conducted on a high-strength aluminum alloy under a high constraint, $\alpha = 2$, condition. Under these conditions, the normalized crack-opening stresses stabilize very rapidly and approach a nearly constant value until near the end of the test (at longer crack lengths and at fracture). The dotted lines show the minimum stress at each stress ratio condition. The vertical arrow shows the effective stress range, ΔS_{eff}, normalized by the maximum applied stress, which controls crack growth.

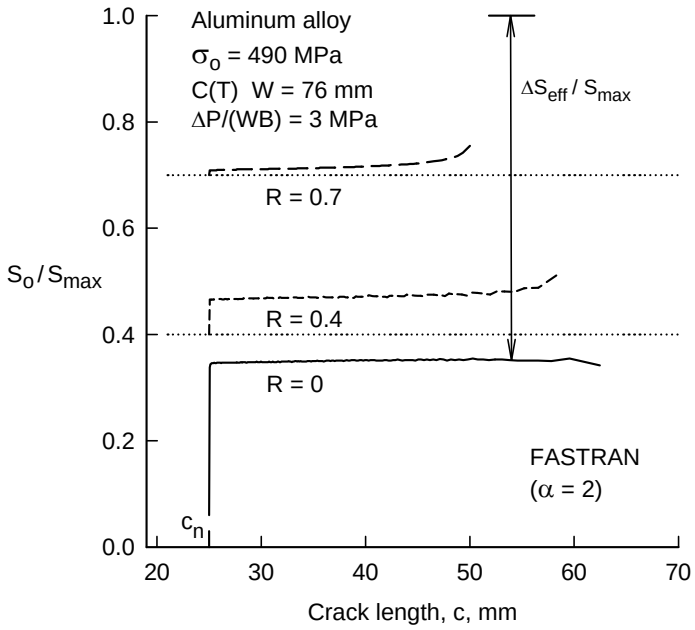

Figure 11. Calculated Crack-Opening Stresses at Very Low Loads on C(T) Specimens Under High Constraint During Constant-Amplitude Loading

FASTRAN simulations made on M(T) specimens subjected to an applied stress level like those used in aircraft fuselage structures are shown in figure 12. The M(T) specimens were subjected to a maximum applied stress of 70 MPa at R = 0 and -1 conditions. The simulations were conducted on thin-sheet aluminum alloy. The material model simulated the flat-to-slant crack growth (constraint-loss) regime characteristic of thin-sheet materials (α = 2 for low rates and α = 1 for high rates). Under these conditions, the normalized crack-opening stresses show a steady rise due to the loss of constraint and faster crack growth rates. (The oscillations in the crack-opening stresses are due to "lumping" in the model to combine some adjacent elements to keep the degrees of freedom in the model to a reasonable level.) Near the end of the test simulation, the plastic zone size is a large percentage of the remaining net section and a drop in the opening stress occurs. For the R = -1 condition, the crack has to grow somewhat before the crack-opening levels are positive, but the crack-opening levels are lower than those at R = 0, which indicates that the crack will be growing faster under R = -1 than under R = 0 conditions.

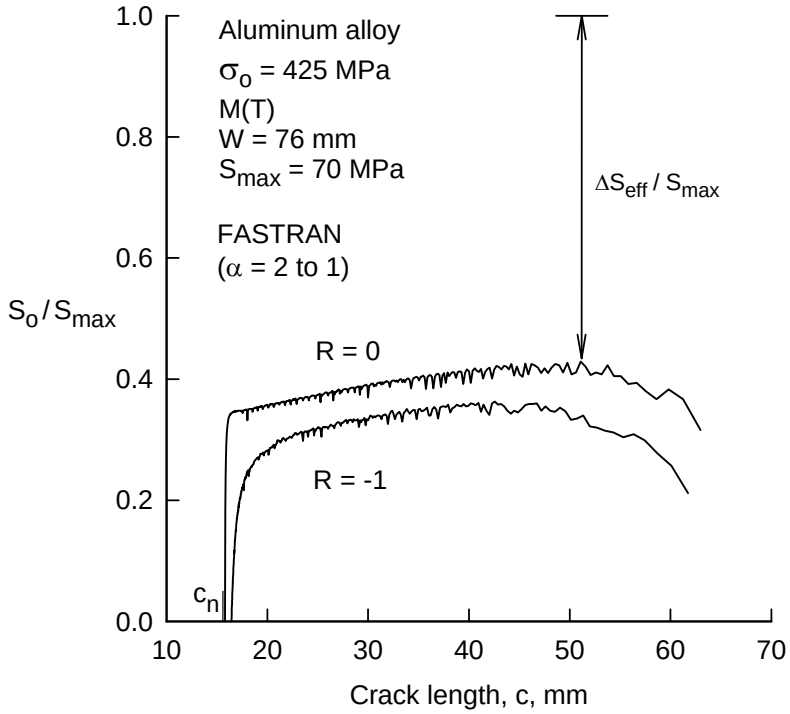

Figure 12. Calculated Crack-Opening Stresses on M(T) Specimens Under Variable Constraint Conditions During Constant-Amplitude Loading at Two Stress Ratios

In reference 42, crack-opening stress (S_o) equations for constant-amplitude loading were developed from the strip-yield crack closure model. These equations were fit to the results from the crack closure model (see figures 13 and 14) and gave S_o as a function of stress ratio (R), maximum stress normalized by the flow stress (S_{max}/σ_o) and the constraint factor (α). The equations will be presented here for completeness. The equations were given by

$$S_o/S_{max} = A_0 + A_1 R + A_2 R^2 + A_3 R^3 \qquad \text{for } R \geq 0 \tag{4}$$

and

$$S_o/S_{max} = A_0 + A_1 R \qquad \text{for } R < 0 \tag{5}$$

where $R = S_{min}/S_{max}$, $S_{max}/\sigma_o < 0.8$, $S_{min} > -\sigma_o$, $S_o = S_{min}$ if S_o/S_{max} is less than R, and $S_o/S_{max} = 0$ if S_o/S_{max} is negative. The A_1 coefficients are functions of α and S_{max}/σ_o and are given by

$$A_0 = (0.825 - 0.34\ \alpha + 0.05\ \alpha^2)\ [\cos(\pi\ S_{max}/(2\sigma_o)]^{(1/\alpha)} \tag{6}$$

$$A_1 = (0.415 - 0.071\ \alpha)\ S_{max}/\sigma_o \tag{7}$$

$$A_2 = 1 - A_0 - A_1 - A_3 \tag{8}$$

$$A_3 = 2A_0 + A_1 - 1 \tag{9}$$

These equations are used in the computer codes in appendix B to develop the effective stress-intensity factor relations for a given material and to predict the ΔK-rate curves for a specified material for various stress ratios over a wide range in rates.

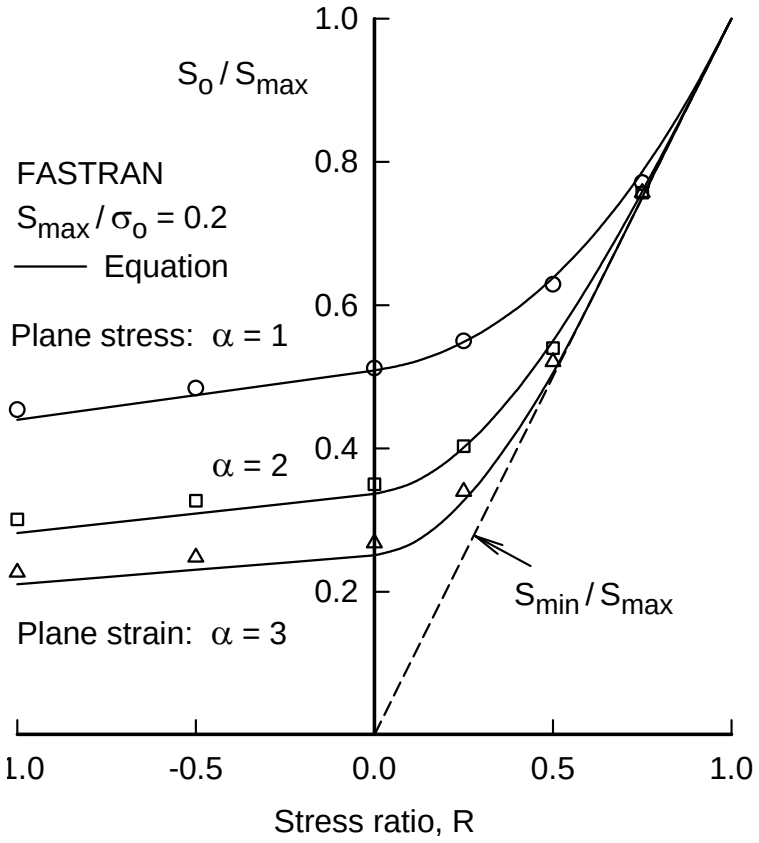

Figure 13. Stabilized Crack-Opening Stresses as a Function of Stress Ratio and Stress Level Under a High-Constraint Condition for M(T) Specimens

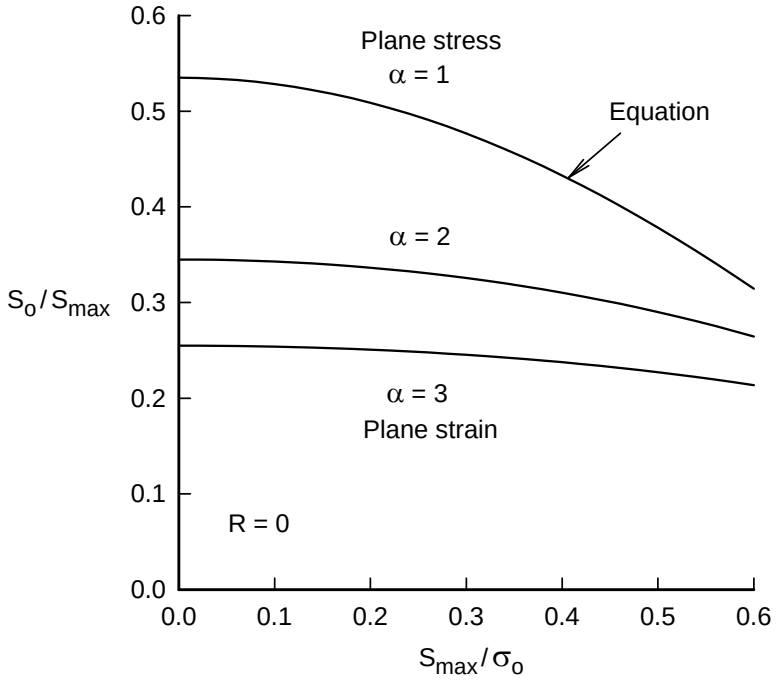

Figure 14. Stabilized Crack-Opening Stresses as a Function of Stress Level for Various Constraint Conditions for M(T) Specimens

3.4.2 Load Reduction Threshold Tests.

The FASTRAN code has been used to simulate the load reduction test [20]. In the current simulation, a very large M(T) specimen made of an aluminum alloy was selected. The material had a constant constraint factor $\alpha = 2$. The specimen had an initial saw cut and was subjected to fatigue precracking loads to grow a crack from the saw cut to a specified crack length under constant-amplitude loading, $(S_{max})_{CA} = 115$ MPa. After the crack had reached the specified length, the load reduction procedure was initiated. Figure 15 shows the local crack-opening displacements (COD) along the crack surfaces for $R = 0$ loading after the load reduction test simulation. The current crack tip is at x = 54 mm. The saw cut, fatigue precracking region, and the load reduction regions are as indicated along the x axis. The solid and dashed curves show the CODs at maximum and minimum applied stress, respectively. The solid symbols show the displacement at the centroid of the elements in the model. These results show that the crack surfaces close remotely at the minimum applied stress. Although not apparent from the figure, the crack surfaces at the crack tip (c = 54 mm) are also closed at minimum load. The remote closure causes a high value of crack-opening stress to develop and this greatly reduces the cyclic crack tip strains, which causes the crack to stop growing at an inappropriately high threshold value. The objective in developing new test procedures is to eliminate the "remote" closure effect in the near-threshold regime. Crack closure mechanisms that develop at the crack tip, such as plasticity, roughness, and oxide-debris induced closure, will develop naturally as the crack grows under constant-amplitude loading or under an increasing stress-intensity factor field.

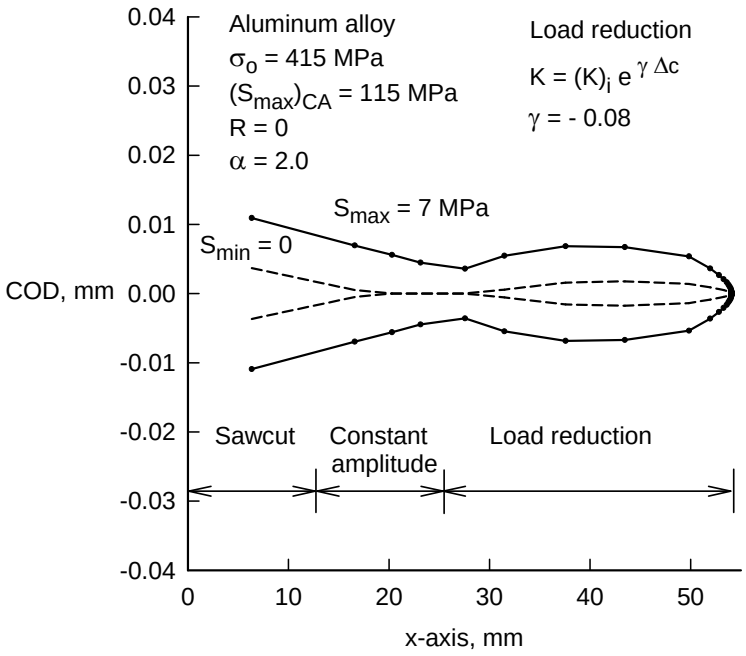

Figure 15. Calculated Crack Surface Profile After the Load Reduction Procedure

Realistic crack growth properties for an aluminum alloy were chosen to study the effects of stress ratio and the load reduction procedure on crack-opening stresses during threshold testing. For the thin-sheet alloy analyzed herein, a constraint factor of 2 was selected for low rates and 1.15 for high rates. The constraint loss regime was assumed to occur in the crack growth rate regime of 1.0E-07 to 2.0E-06 m/cycle. M(T) specimens were fatigue precracked at either $R = 0$ or 0.7 conditions and then subjected to the load reduction procedure. The normalized crack-opening stress results as a function of ΔK are shown in figure 16.

For the $R = 0$ simulation, the solid triangular symbol shows the initial ΔK value for the saw cut (no prior plastic history). After a small amount of crack growth, the S_o/S_{max} value stabilized and the load reduction test was initiated at a ΔK of 30 MPa$\sqrt{m}$. The crack-opening stresses during the load reduction phase are shown as the lower solid curve. A rise in opening stresses (and threshold development) occurred at low values of ΔK. (At $R = 0$, the load reduction threshold in the aluminum alloys generally occurs at a ΔK_{th} value of about 3 MPa$\sqrt{m}$.) It must be noted that the crack growth simulation at $R = 0$ must violate threshold-testing procedures, in that the initial ΔK value at the start of the load reduction scheme is very high. However, this may be the source of some of the high values of thresholds and specimen size effects being reported in this document. On the other hand, the results at $R = 0.7$ seems to be a more realistic test condition. To initiate cracks from saw cuts in aluminum alloys, a ΔK value of about 4 to 6 MPa$\sqrt{m}$ is generally required. The crack was precracked at $(S_{max})_{CA}$ of 135 Mpa, and the ΔK value at the start of load reduction phase was about 10 MPa$\sqrt{m}$. The crack-opening stresses are generally near the minimum applied stress, but the analysis shows a rapid rise at a ΔK value of about 2 MPa$\sqrt{m}$. This corresponds quite closely to the development of the threshold value at $R = 0.7$ for some aluminum alloys.

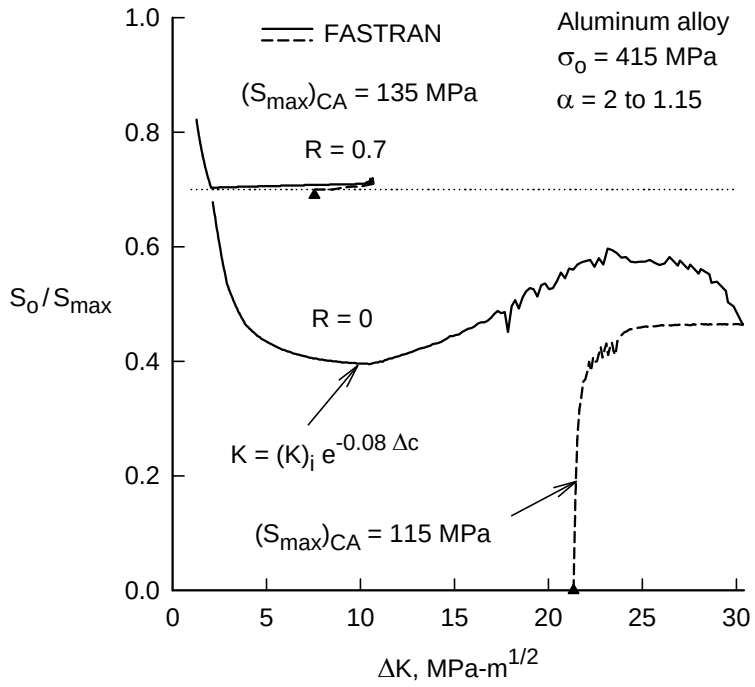

Figure 16. Calculated Crack-Opening Stresses During Simulated Load Reduction Testing at Two Stress Ratios

3.4.3 Constant K_{max} Tests.

The K_{max} test [2] has been proposed as an alternative test to obtain low crack growth rate data. A crack growth and closure analysis of the K_{max} test conducted on an M(T) specimen is shown in figure 17. The upper dashed line is the K_{max} (22 MPa$\sqrt{m}$) value and the lower dashed curve is the K_{min} values. The initial notch half-length was c_n, and the crack half-length c_i denotes the start of the increasing K_{min} test. The solid curve shows the crack-opening (K_o) calculations from the model. At a stress ratio of about 0.8, the crack surfaces became fully open at the minimum stress-intensity factor (crack length about 7.7 mm). At the end of the test simulation, the R value was about 0.95 and the ΔK value was 1.2 MPa$\sqrt{m}$. Thus, at the end of the K_{max} test the crack is fully open and the ΔK-rate curve may be used as the effective stress-intensity factor range against rate (ΔK_{eff}-rate) curve. However, the K_{max} test has introduced a "K_{max} effect" in that larger K_{max} values produce lower high R thresholds.

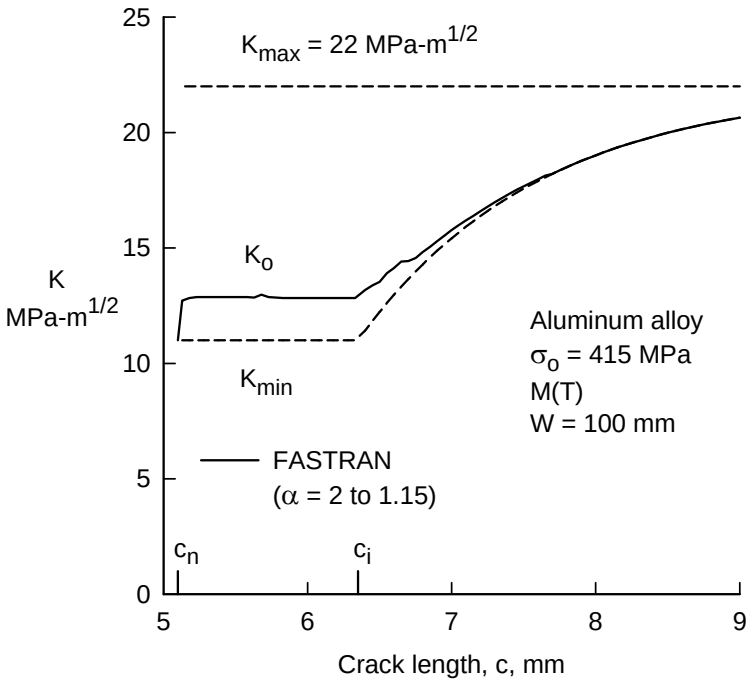

Figure 17. Calculated Crack-Opening Stresses Under Constant K_{max} Testing

The standard K_{max} test usually starts at a high positive stress ratio, such as 0.5, and produces an extremely high R value when the ΔK_{th} threshold is reached, such as 0.9 or higher. If the K_{max} value is selected as a very small value and the K_{min} value is negative, then it may be possible to reach the ΔK_{th} at a lower R value. This type of simulation is shown in figure 18. A crack is grown under tension compression loading from the notch length, c_n, to the initial crack length, c_i. Then the K_{min} value is slowly increased as the crack grows. The solid curve shows the calculated crack-opening (K_o) values. Here, the K_o values are always increasing, while the ΔK_{eff} values are deceasing. After some crack growth, the K_o values stabilize. This type of test may be designed to reach the ΔK_{th} at a low R value.

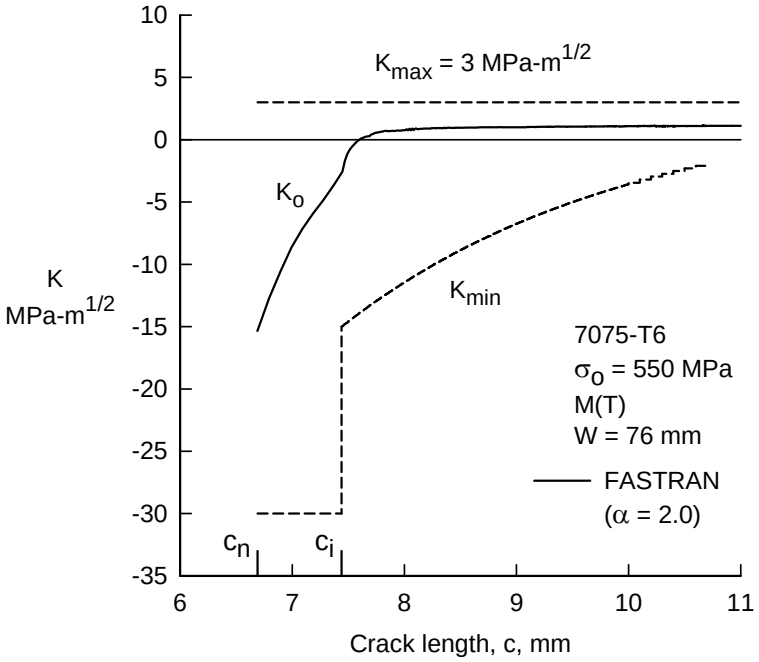

Figure 18. Calculated Crack-Opening Stresses Under Compression Precracking Constant K_{max} Testing

3.4.4 The CPCA Threshold Tests.

FASTRAN has been used to simulate CPCA threshold test conditions on a compact specimen, like those that are being tested at NASA LaRC on the 7075-T7351 alloy. The issue of compressive yielding at the crack starter V-notch and the influence of the resulting tensile residual stresses on crack growth rates and crack closure behavior must be understood if the new threshold test procedures are to be accepted by the technical community.

A compact specimen (W = 76 mm) was subjected to 0 to -12 MPa (P/WB) loading for about 2 million cycles. The crack rapidly grew from the V-notch and reached a threshold condition after about 0.75 mm of crack growth (see figure 19 for $c = c_i$). The figure shows the calculated crack-opening loads (P_o) as a function of crack length. The crack-opening load is at the minimum load (notch is fully open) and rapidly rises as the crack grows and leaves the residual plastic deformed material in the crack wake. After the threshold condition was reached, a positive loading of 1.2 MPa was applied at $R = 0$ conditions for about 20 million cycles (specimen cycled to failure). The crack-opening loads slowly increased during the $R = 0$ (positive) loading and stabilized after about 0.15 mm of crack growth.

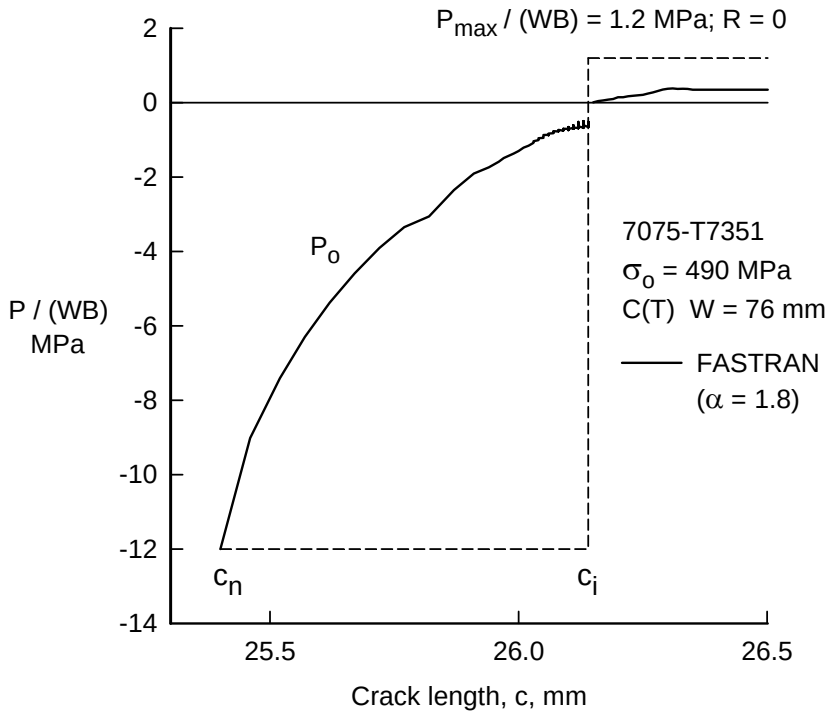

Figure 19. Calculated Crack-Opening Stresses Under CPCA Loading

Figure 20 shows a comparison between the crack-opening loads under constant-amplitude loading and those under the previous CPCA loading. This figure shows that the steady-state constant-amplitude behavior $(P_o)_{ca}$ stabilizes very quickly, but the tensile residual stresses are delaying the attainment of the steady-state conditions until the crack has grown about "1" compressive plastic-zone size. As seen in reference 28, analyses and testing indicate that the crack must be grown at least 3 compressive plastic zone sizes to reach steady-state conditions.) Thus, this is an area that needs further study using both the finite element method and strip-yield models.

To study the detailed stresses in front of the crack (plastic zone) and along the crack surfaces (due to crack closure), a very refined FASTRAN model was developed. The element size was reduced from 0.2 to 0.05 times the cyclic plastic zone. (This will allow more accurate crack-opening stresses under high *R* conditions, especially for rotorcraft and propeller components.) The number of elements in the plastic zone was also increased from 10 to 60. The intact (plastic zone) and contact (crack surfaces) stresses from the nonlinear contact problem are determined from an iteration procedure. The iteration error check was also reduced from 0.02 to 0.001 times the flow stress of the material. In general, the number of iterations to convergence doubled. (Comparisons made between FASTRAN Version 3.8 and the highly refined model indicated that crack-opening stresses were not greatly affected by the plastic zone refinement.)

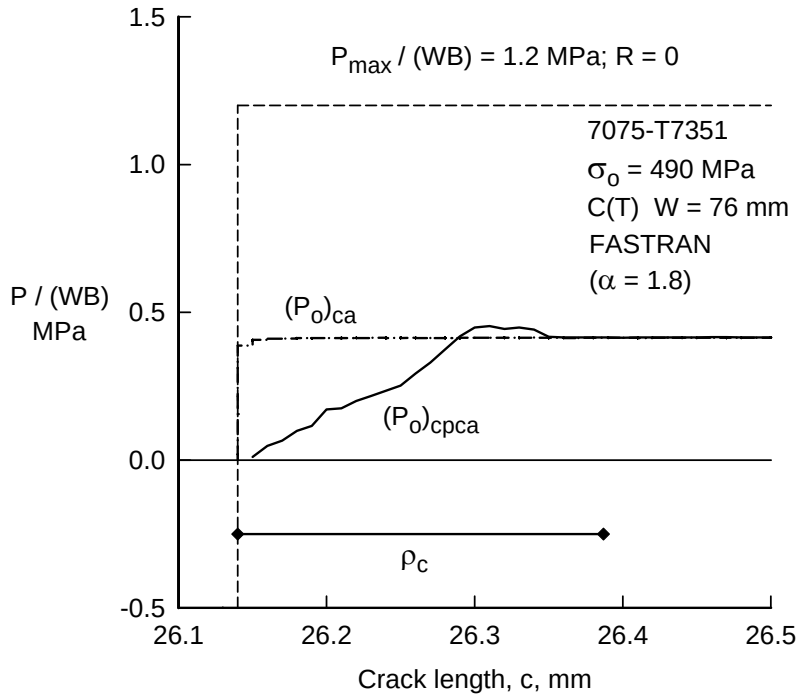

Figure 20. Comparison of Crack-Opening Stresses Under Constant-Amplitude and CPCA Loading

In the FASTRAN simulation, a C(T) specimen was subjected to 0 to -12 MPa (P/WB) loading for about 2 million cycles. After the crack had reached a threshold under zero-to-compression loading, the constant-amplitude loading (1.2 MPa at $R = 0$) was applied. After a small amount of crack growth, the residual stresses at minimum and maximum loads were determined (see figures 5-11). The element stress is plotted against the distance along the crack plane, as shown in figure 21. The x axis is measured along the crack plane and extends from the crack tip to the compressive plastic zone. The crack tip material is either at the tensile yield stress or at the compressive yield stress, depending upon the applied loading, due to the very high strain concentration in the model. The dashed curve shows the tensile residual stresses in the compressive plastic zone region. The tensile residual stresses are balanced by small compressive stresses acting over much of the compressive plastic zone. The solid curve is the tensile stresses in front of the crack tip under the applied tensile loading (1.2 MPa). (A comparison made with elastic-plastic, finite element results from NASA LaRC (Mark James, et al. [28]) showed good agreement on the extent of the compressive plastic zone size.) The highly refined model was needed to simulate the crack tip yielding during the application of the very small stress-intensity factor levels to the model. As the crack grows, the plastic deformations, responsible for the tensile residual stresses, will decay. (To simulate this behavior with the finite element method would require extremely small elements.)

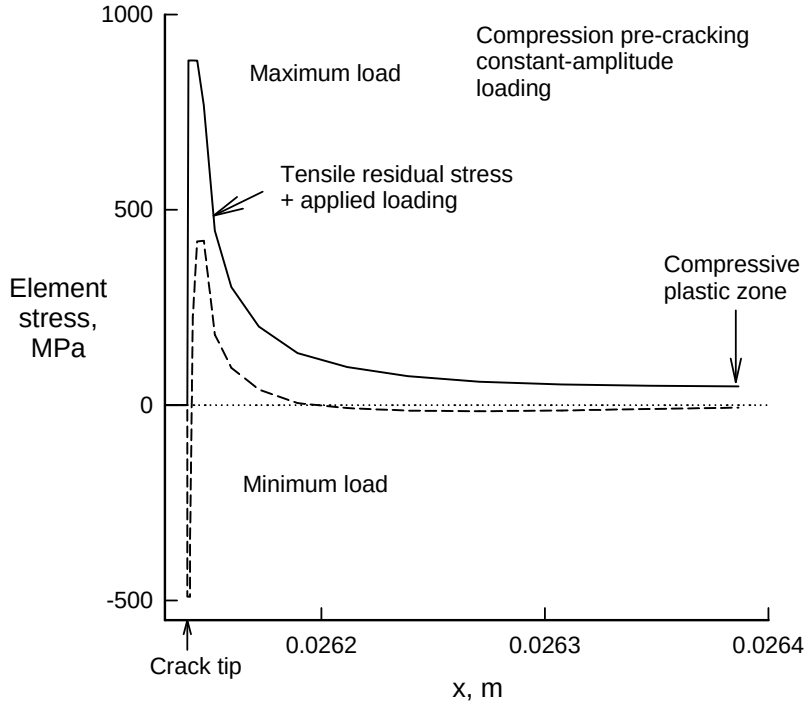

Figure 21. Element Stresses From the FASTRAN Code After CPCA Loading

The issue of residual stresses in front of the crack and crack closure behavior behind the crack tip has been actively debated for more than 30 years. Is it the residual stresses, the crack closure behavior, or a combination of both affecting the crack growth rate behavior? The issue has resulted into, at least, two or more technical approaches. To convince the technical community that the compression precracking threshold test procedure is not inducing severe residual stress effects, this issue will have to be resolved. This can only be done with critical tests and highly refined analyses. The results shown in figure 22 are focusing on the crack tip region during both compression precracking followed by constant-amplitude loading or during constant-amplitude loading only. The figure shows the applied load against the cyclic crack tip displacement, δ. These two cases were selected to have the same crack-opening load, P_o. These results show that the effective stress-intensity factor (ΔK_{eff}), the change in cyclic crack tip displacements ($\Delta\delta$), and the cyclic crack tip hysteresis energies (H) are nearly the same. These results indicated that crack closure theory would account for residual stress effects on crack tip deformations. This is an extremely important observation, which needs to be confirmed with highly refined finite element analyses. Another observation is that the hysteresis energy below the crack-opening level is very small. Crack growth rates should be directly proportional to the cyclic hysteresis energy.

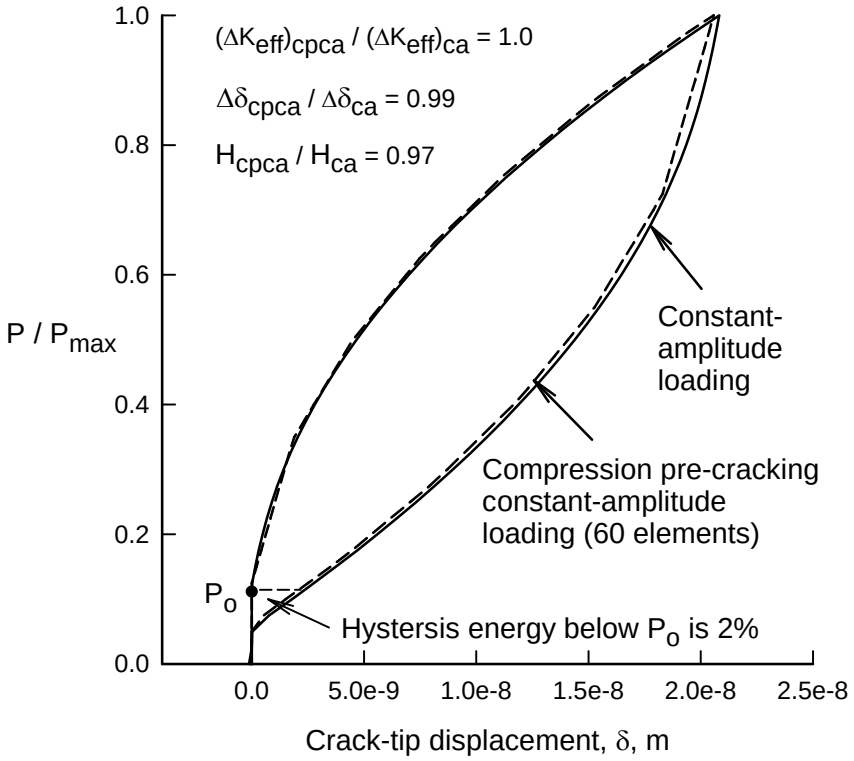

Figure 22. Cyclic Crack Tip Displacements From a Refined FASTRAN Model Under Both Constant-Amplitude and CPCA Loading

A comparison of measured fatigue crack growth rates under load reduction and CPCA loading on C(T) specimens made of the 7075-T7351 (TL) alloy is shown in figure 23. The open symbols show ΔK-rate for a load reduction test at $R = 0.1$, which shows a threshold slightly greater than 3 MPa-m$^{1/2}$. The solid symbols show the results of a CPCA tests on the same alloy tested at Mississsippi State University (MSU) under an Office of Naval Research (ONR) grant. The open diamond symbol shows the three compressive plastic zone size criteria (plane stress conditions), which appear to occur at the minimum rate on the CPCA test results. For higher rates, the CPCA results are assumed to be steady-state constant-amplitude results with no load history effects. These results show that, not only is the threshold region affected by the load reduction procedure, but rates above the threshold region are also affected. Above rates of 1E-8 m/cycle, the CPCA and load reduction data, which is most likely K increasing data, agreed very well.

In figure 23, the dashed curve is the ΔK_{eff}-rate curve generated for this alloy using a constraint factor of 1.8. The solid curve is the predicted behavior for CPCA loading from FASTRAN. As noted, the crack closure model predicts that the influence of tensile residual stresses, due to compressive yielding, is only 1 compressive plastic zone size, whereas the test data indicates that about 3 compressive plastic zone sizes would be a better criterion (diamond symbol near minimum CPCA rate). The reason for this discrepancy is not known and further study is needed. For ΔK values above 3 MPa-m$^{1/2}$, the predicted results agreed very well with the CPCA test data.

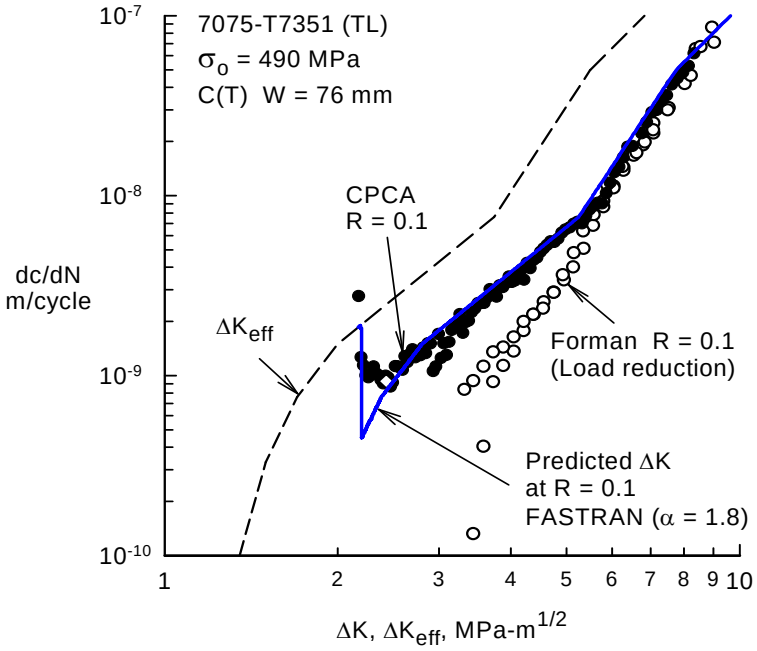

Figure 23. Comparison of Measured and Predicted Crack Growth During CPCA Loading

3.5 ALUMINUM ALLOYS.

3.5.1 Aluminum Alloy 7050-T7451.

The fatigue crack growth test results and material properties for the 7050-T7451 alloy were obtained from references 26, 27, and 43. C(T) specimens were used for all tests (W = 76 mm, B = 12.7 mm, initial notch length of 19 mm). Three testing procedures were used to generate the threshold and near-threshold data: (1) load reduction, (2) constant K_{max}, and (3) CPCA loading.

The constant R load reduction method generated fatigue crack growth rates into the threshold region by reducing the applied load on the specimen in a controlled manner such that the load ratio, R, remains constant, e.g., the maximum and minimum load are continuously reduced throughout the test. The constant K_{max} load reduction method also reduces both the maximum and minimum load to generate threshold data; however, the value of K_{max} is held constant, i.e., R increases. The load reduction tests were precracked at a constant ΔK level that is equivalent to the first data point in the load reduction test. Specimens were precracked until the crack length to width (c/W) ratio was approximately 0.3.

The CPCA test procedure was implemented to produce fatigue crack growth data with minimal load history effects. This was accomplished by first producing a crack from a notch using a high compressive loading. The precracking loads, with a maximum load of -0.44 kN and a minimum load of -13.6 kN, were applied for 10,000 cycles. Then, the crack was propagated using a small tensile load, with a maximum load of 0.20 kN and a minimum load of 0.02 kN, to grow the crack out of the residual tensile stress field caused by the compressive loading. Finally, constant-amplitude loading was applied at a specific R value starting at an assumed ΔK_{th} and generating the entire fatigue crack growth rate curve in one test.

The results from these three test methods are shown in figure 24 at two stress ratios. The solid symbols show the load reduction results, the triangular symbols show the K_{max} test results, and the other open symbols show the CPCA test results. For each R ratio, the results from load reduction and CPCA loading gave essentially the same results. The CPCA results were only slightly lower than the load reduction test results.

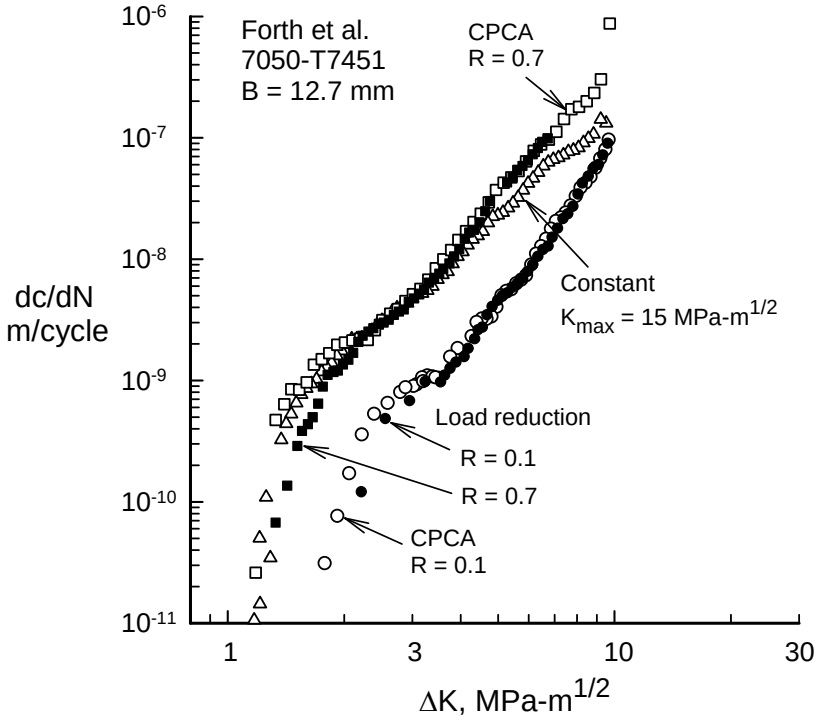

Figure 24. Fatigue Crack Growth Rates From Various Tests on 7050-T7451 Alloy

The CPCA and K_{max} test results were analyzed with the crack closure model (see appendix A) to find a constraint factor, which would correlate all of the data along a single curve. The ΔK_{eff} at the transition from flat-to-slant crack growth $(\Delta K_{eff})_T$ was calculated to see whether a constraint loss region was needed [44]. The relation for the transition from flat-to-slant crack growth is given by

$$(\Delta K_{eff})_T = 0.5\ \sigma_o\ \sqrt{B} \tag{10}$$

where σ_o is the flow stress of the material and B is the thickness. For the 7050 alloy and thick C(T) specimens, the $(\Delta K_{eff})_T$ was 28 MPa-$m^{1/2}$. Because the largest ΔK value from the test was 10 MPa-$m^{1/2}$, a constant constraint factor would be sufficient. Figure 25 and table 5 gives the ΔK_{eff}-rate against rate correlation of data and the baseline ΔK_{eff}-rate curve, respectively. The data correlated fairly well, but not as good as other aluminum alloys. The ΔK_{eff} baseline curve was fitted to the average of all tests, but followed the K_{max} test results much closer than either the low or high R ratio tests. The curve was extrapolated beyond 10 MPa-$m^{1/2}$. The baseline curve

is a multilinear curve fit of the data. Each pair of data points defines a linear segment. The crack growth relation used in FASTRAN is

$$dc/dN = C_i\,(\Delta K_{eff})^{n_i} / [1 - (K_{max}/C_5)^q] \qquad (11)$$

where C_i and n_i are the coefficient and power for each linear segment, K_{max} is the maximum stress-intensity factor, C_5 is the cyclic fracture toughness and q is the power on the fracture term. The table lookup form is used because many materials, especially aluminum alloys, show sharp changes in the crack growth rate curves at unique values of rate. These sharp changes have been associated with monotonic and cyclic plastic zone sizes, grain sizes, and environments [45 and 46]. The fracture term is very similar to the term used by Forman in the crack growth rate equation in the NASGRO code [4]. In general, C_5, which is equal to K_{Ie}, the elastic stress-intensity factor at failure (under cyclic loading), is a function of crack length, specimen width, and specimen type. A method to correlate fracture and to predict K_{Ie} (or C_5) for a given material and crack configuration has been developed by Newman [47]. Herein, C_5 and q are held constant; and they are treated as fitting parameters. A trial and error procedure is used to select C_5 and q to fit fatigue crack growth rate data during the cyclic fracture stage.

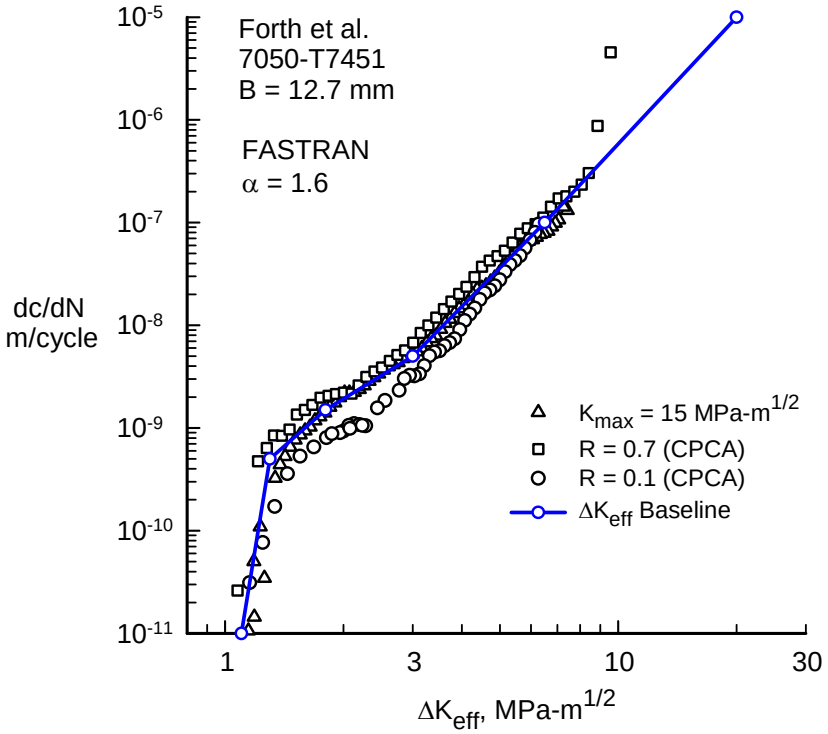

Figure 25. Effective Stress-Intensity Factor for Various Tests on 7050-T7451 Alloy

Table 5. Effective Stress-Intensity Factor Relation and Properties for 7050-T7451

ΔK_{eff} MPa-m$^{1/2}$	dc/dN m/cycle
1.1	1.0E-11
1.3	5.0E-10
1.8	1.5E-09
3.0	5.0E-09
6.5	1.0E-07
20	1.0E-05
35	1.0E-04
$\alpha = 1.6$	All
$C_5 = 38$	$q = 2$

To see how well equation 11 fits the data, figure 26 shows the ΔK-rate curves for the low and high R CPCA test results, which are steady-state constant-amplitude results. The curves are predicted behavior using equation 11 and the computer code described in appendix B. The equation correctly correlated the influence of stress ratio on the threshold behavior, as well as fitting the high R ratio test as the cracks grew to failure. As previously mentioned, these data did not correlate as well as other aluminum alloys, especially for the low R ratio tests, but the resulting relationship is conservative for low R. The high R ratio curve is fairly close to the test data over the complete range in rates.

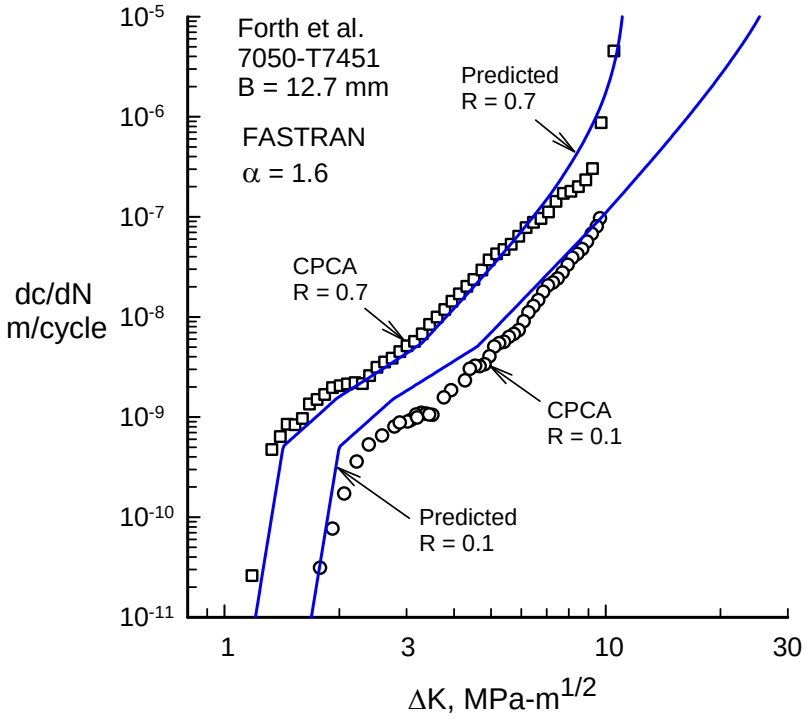

Figure 26. Predicted ΔK-Rate Behavior for 7050-T7451 Alloy at Two R Ratios

3.5.2 Aluminum Alloy 7075-T7351.

The fatigue crack growth test results and material properties for the 7075-T7351 alloy were obtained from NASA LaRC [26 and 27] and JSC (unpublished). C(T) specimens made from TL and LT orientations were used for all tests (W = 76 mm, B = 12.7 mm). Again, three test procedures were used to generate the threshold and near-threshold data: (1) load reduction, (2) constant K_{max}, and (3) CPCA loading.

3.5.2.1 TL-Orientation.

Figure 27 shows fatigue crack growth rate data generated at NASA JSC using the load reduction and load increasing test procedures. A very wide range in stress ratios were considered, and these tests produced rates over many orders of magnitude from threshold to fracture. After the load reduction test was conducted, the specimen was loaded under load-increasing conditions to generate the upper portion of the curves.

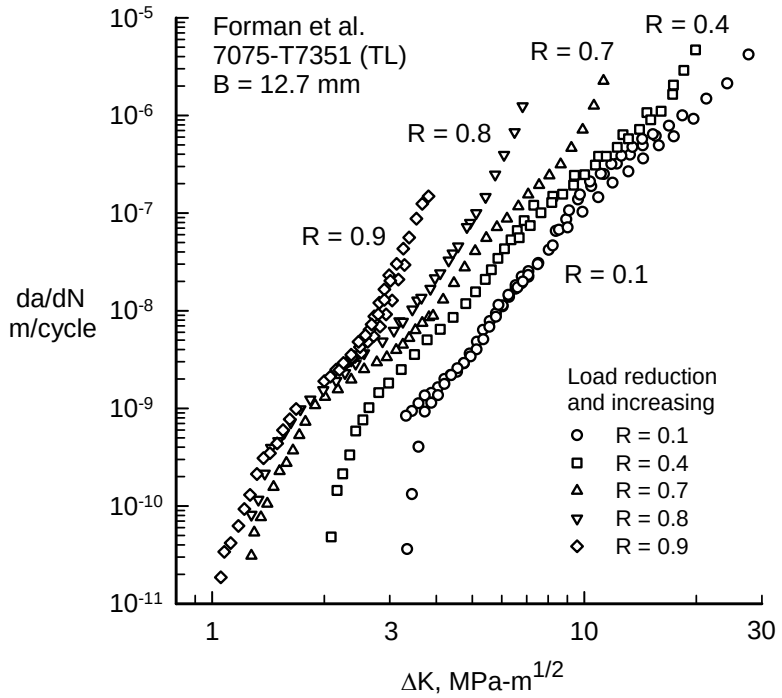

Figure 27. Fatigue Crack Growth Rates From Various Tests on 7075-T7351 (TL) Alloy

These data were analyzed with the crack closure model and the ΔK_{eff}-rate results and are shown in figure 28. These results also include a constant K_{max} test. Because of the high strength and thickness, a single constraint factor was used in an attempt to correlate the data onto a single curve. The constraint factor was 1.8. As can be seen from the figure, the data did not correlate onto a single curve. It is suspected that the data in the near-threshold and threshold regimes are being affected by the load reduction procedure, especially at the low R conditions. The load reduction procedure induces a load history effect on the data due to elevated closure levels [12, 13, and 14]. The data in the high-rate regime for high R values are approaching fracture.

Effective stress-intensity factor analyses, which are based on linear elastic fracture mechanics, cannot correlate these data onto a single curve. The crack growth rate from equation 11 would be needed to fit these data. The solid curve is the ΔK_{eff} baseline curve for the 7075-T7351 (TL) data (see table 6). Again, the curve has been extrapolated beyond the last data points.

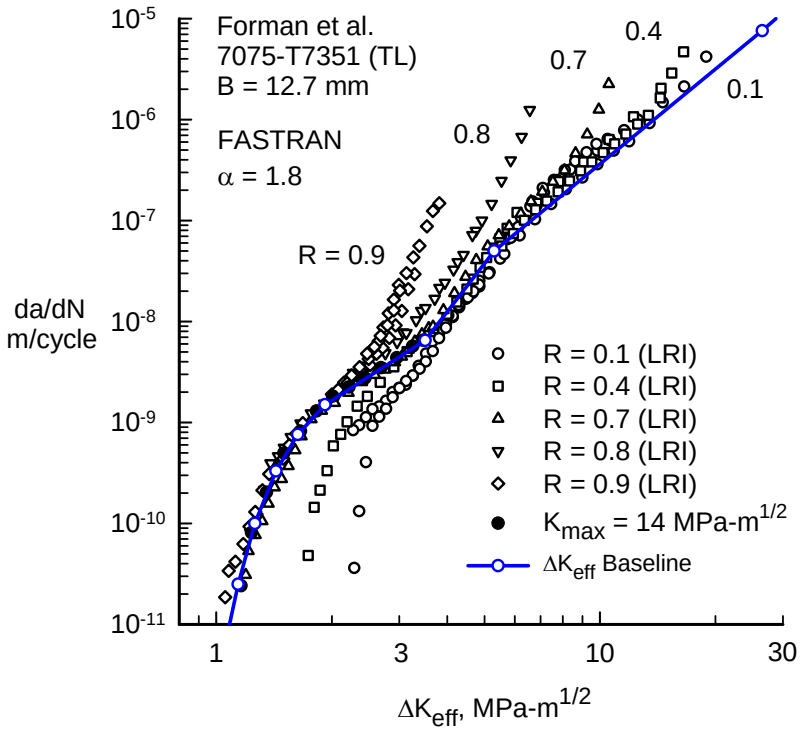

Figure 28. Effective Stress-Intensity Factor for Various Tests on 7075-T7351 (TL) Alloy

Table 6. Effective Stress-Intensity Factor Relation and Properties for 7075-T7351 (TL)

ΔK_{eff} MPa-m$^{1/2}$	*dc/dN* m/cycle
1.05	2.5E-12
1.15	2.5E-11
1.25	1.0E-10
1.42	3.3E-10
1.62	7.6E-10
1.92	1.5E-09
3.50	6.5E-09
5.30	5.0E-08
26.5	7.6E-06
$\alpha = 1.8$	All
$C_5 = 38$	$q = 2$

Again, to see how well equation 11 fits these data, figure 29 shows the predicted ΔK-rate curves for the various constant R tests using the computer code described in appendix B. The equation calculated the behavior at the high R ratios in the near-threshold regime fairly well, as well as fitting the various R ratio tests as the cracks grew to failure. The main issue is the low R ratio load reduction test results, which show much higher thresholds than those predicted from plasticity-induced crack closure theory. Further study is needed on this material to resolve the apparent problem with the load reduction threshold data. (Note that this material is currently being tested under an ONR grant using the CPCA-loading procedures.)

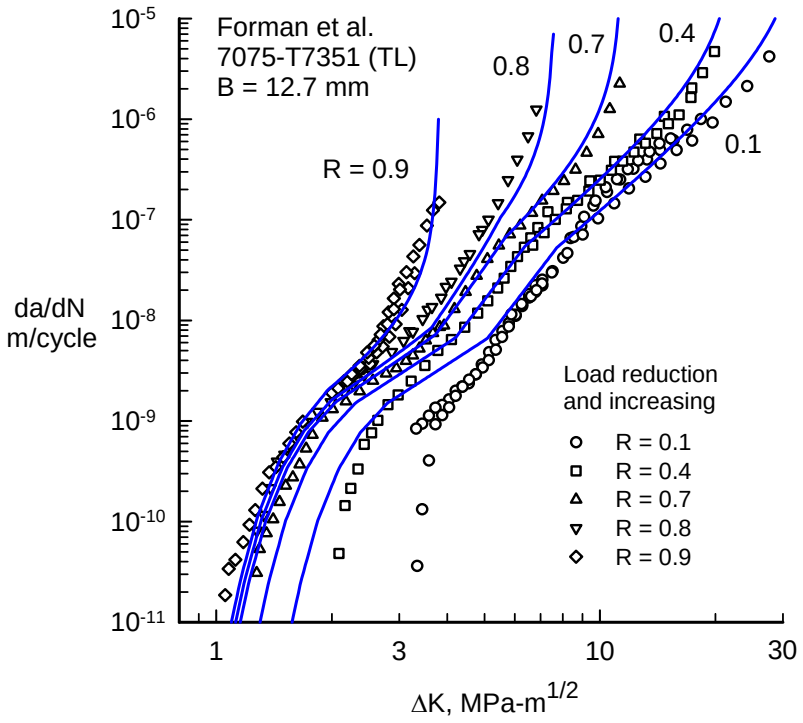

Figure 29. Predicted ΔK-Rate Behavior for 7075-T7351 (TL) Alloy at Various R Ratios

3.5.2.2 LT Orientation.

The fatigue crack growth test results and material properties for the 7075-T7351 alloy tested in the LT orientation were obtained from references 26 and 27. C(T) specimens were, again, used for all tests (W = 76 mm, B = 12.7 mm, initial notch length of 19 mm). The three test procedures (load reduction, constant K_{max}, and CPCA loading) were used to generate the threshold and near-threshold data.

Results from these three test methods are shown in figure 30 at two stress ratios. The solid symbols show load reduction test results, the triangular symbols show the K_{max} test results, and the other open symbols show the CPCA test results. For this alloy and the low R ratio tests, the CPCA results showed a substantially lower threshold than the load reduction threshold. But, the high R ratio CPCA results were only slightly lower than the load reduction results.

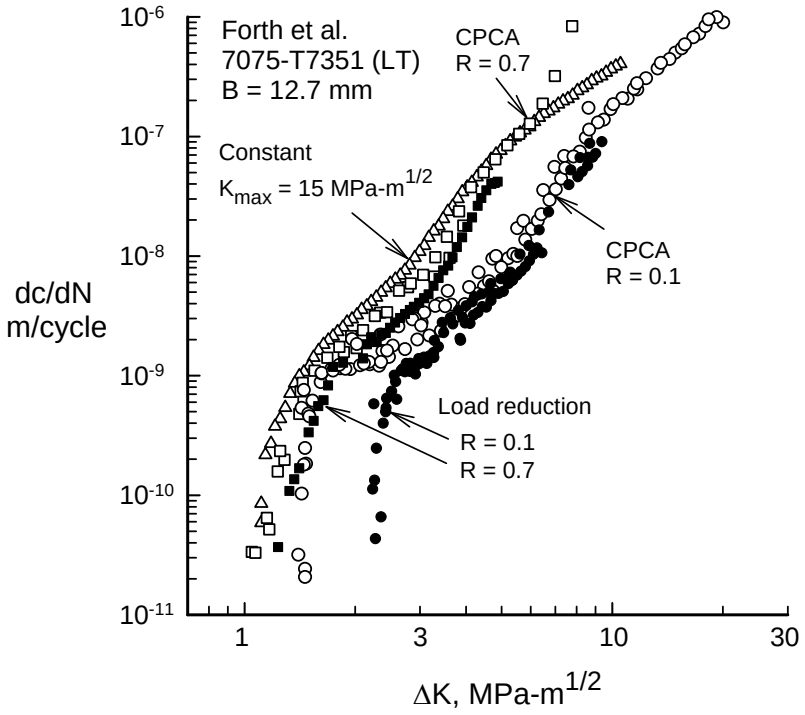

Figure 30. Fatigue Crack Growth Rates From Various Tests on 7075-T7351 (LT) Alloy

The CPCA and K_{max} test results were analyzed with the crack closure model (see appendix A) to find a constraint factor, which would correlate all data along a single curve. Figure 31 and table 7 give the ΔK_{eff}-rate correlation of data and the baseline ΔK_{eff}-rate curve, respectively. The data correlated fairly well, but again, not as good as other aluminum alloys. The ΔK_{eff} baseline curve was fitted to the average of all tests, but followed the high R and K_{max} test results more closely than the low R ratio tests. The low R ratio data showed some oscillations about the baseline curve at low rates, but showed the approach to fracture at the higher rates. The baseline curve was extrapolated beyond 30 MPa-m$^{1/2}$, but fell below the data because equation 11 will amplify the rates as K_{max} approaches C_5.

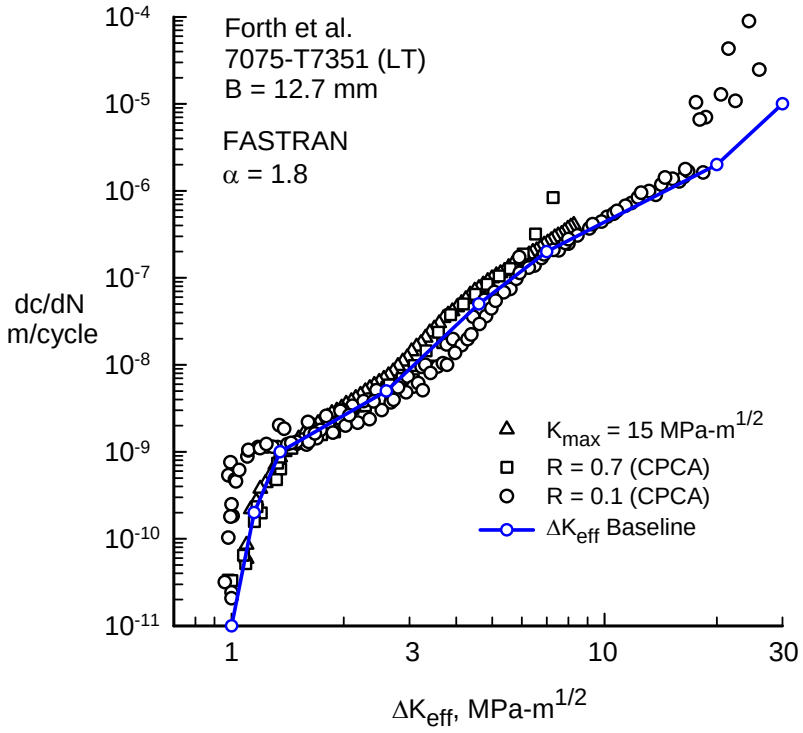

Figure 31. Effective Stress-Intensity Factor for Various Tests on 7075-T7351 (LT) Alloy

Table 7. Effective Stress-Intensity Factor Relation and Properties for 7075-T7351 (LT)

ΔK_{eff} MPa-m$^{1/2}$	*dc/dN* m/cycle
1.00	1.0E-11
1.15	2.0E-10
1.35	1.0E-09
2.60	5.0E-09
4.60	5.0E-08
7.00	2.0E-07
20.0	2.0E-06
30.0	1.0E-05
$\alpha = 1.8$	All
$C_5 = 38$	$q = 2$

Again, to see how well equation 11 fits the data, figure 32 shows the Δ*K*-rate curves for the low and high *R* CPCA test results, which are steady-state constant-amplitude results. The curves are the predicted behavior using equation 11 and the computer code described in appendix B. The equation fit the high *R* results extremely well, but the low *R* results, again, showed some oscillations about the predicted curve. Further testing at high *R* values would be required to verify the use of equation 11. The equation predicted slightly higher rates for most of the low *R* results, but fit the approach to fracture very well.

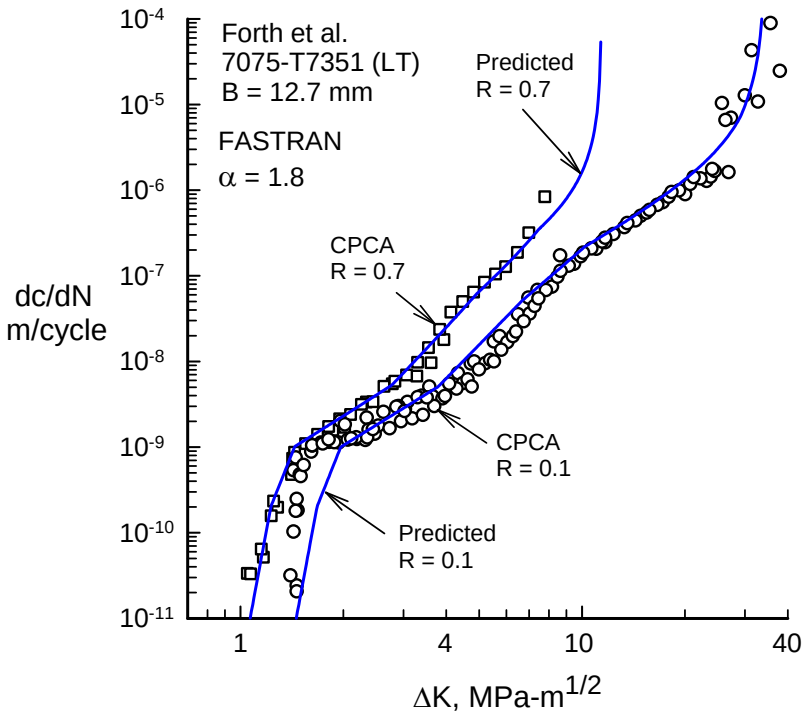

Figure 32. Predicted Δ*K*-Rate Behavior for 7075-T7351 (LT) Alloy at Two *R* Ratios

3.6 STEELS.

3.6.1 D6AC Steel.

The fatigue crack growth test results and material properties for the D6AC steel were obtained from reference 31. C(T) specimens were used for all tests (W = 76 mm and *B* = 12.7 mm, except where noted). Three testing procedures were used to generate the threshold and near-threshold data: (1) load reduction, (2) constant K_{max}, and (3) CPCK loading. (CPCA loading was not used to study the near-threshold behavior.)

CPCK loading was used to assess the influence of the tensile residual stresses caused by compressive yielding at the notch on near-threshold behavior. Testing was conducted by first applying compressive loads at the top and bottom of the specimen via the clevises and loading blocks to initiate a crack at the notch root. Then, tensile loading was applied via pin loading, and the specimen was cycled using constant Δ*K* control. These results are presented after the baseline data.

ASTM Standard E 647 defines two methods for generating fatigue crack growth rate data. The constant *R* load reduction test procedure reduces the maximum and minimum load applied to a cracked specimen such that the load ratio, *R*, remains constant. The constant K_{max} test procedure imposes a constant K_{max}, while increasing K_{min}. The specimens were precracked at a constant Δ*K* that is equivalent to the first data point in the load reduction test. These loads were applied until the crack length to width ratio (c/W) was about 0.28.

The fatigue crack growth rate data was generated using fixed stress ratios of 0.1, 0.3, 0.7, 0.8, and 0.9 and using constant K_{max} values of 16.5, 22, and 33 MPa-m$^{1/2}$. Only the specimen tested in the LT orientation will be present here. These results are shown in figure 33.

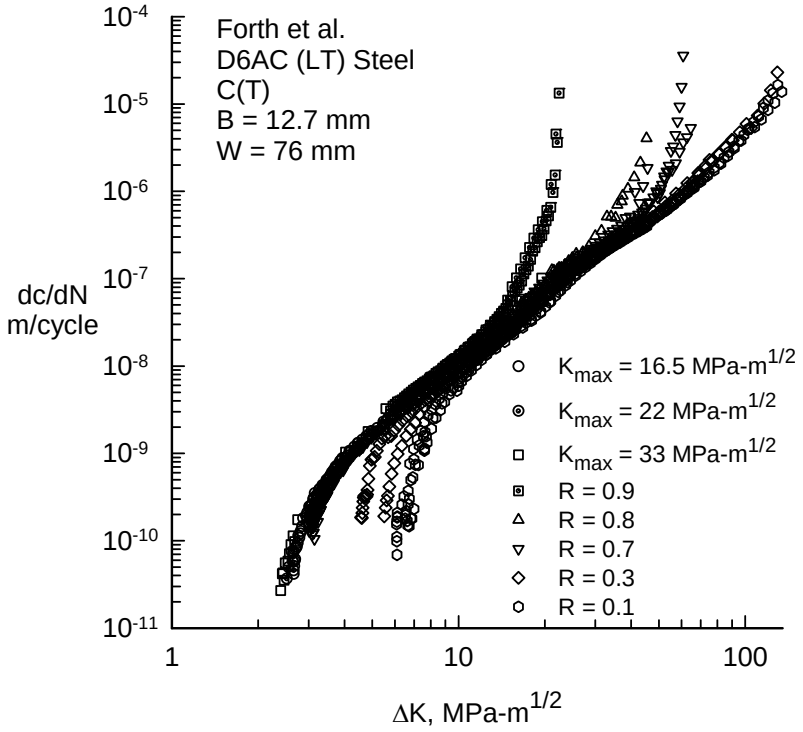

Figure 33. Fatigue Crack Growth Rates From Various Tests on D6AC Steel

These data were analyzed with the crack closure model, and the ΔK_{eff}-rate results are shown in figure 34 (see appendix A). Again, because of the high strength and thickness, a single constraint factor was used in an attempt to correlate the data onto a single curve. The constraint factor (α) was selected as 3, because an observation was made that there was very little stress ratio shift in the ΔK-rate curves, which would indicate "plane-strain" behavior. Based on the tensile properties and thickness, the $(\Delta K_{eff})_T$ was 66 MPa-m$^{1/2}$, which would indicate a flat-to-slant crack growth (or constraint loss) behavior near this value. However, for simplicity, a single constraint factor was used for the complete data set. As can be seen from the figure, the data did not correlate onto a single curve. Again, it was suspected that the data in the near-threshold and threshold regimes are being affected by the load reduction procedure, especially at the low R conditions. The data in the high-rate regime for high R values are approaching fracture. Effective stress-intensity factor analyses, which are based on linear elastic fracture mechanics, cannot correlate these data onto a single curve. The crack growth rate from equation 11 would be needed to fit these data. The solid curve is the ΔK_{eff} baseline curve for the D6AC steel data (see table 8). The baseline curve was chosen to fit the R = 0.7 data in the threshold regime and the low R ratio results in the high-rate regime. (Note that the ΔK_{eff}-rate curve beyond the last data point is a linear extrapolation using the last two data points.)

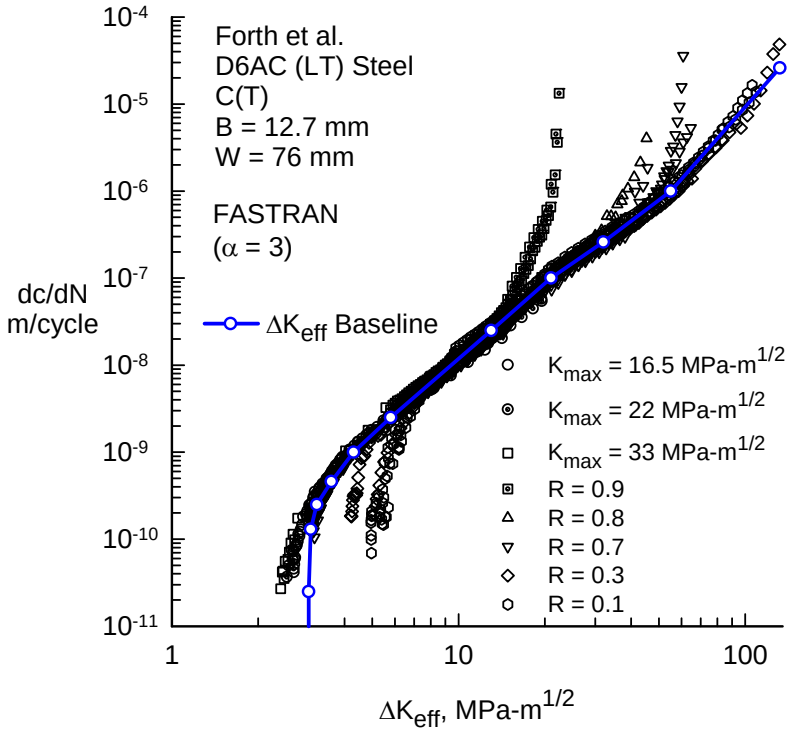

Figure 34. Effective Stress-Intensity Factor for Various Tests on D6AC Steel

Table 8. Effective Stress-Intensity Factor Relation and Properties for D6AC Steel

ΔK_{eff} MPa-m$^{1/2}$	*dc/dN* m/cycle
3.00	2.5E-11
3.05	1.3E-10
3.20	2.5E-10
3.60	4.6E-10
4.30	1.0E-09
5.80	2.5E-09
13.0	2.5E-08
21.0	1.0E-07
32.0	2.6E-07
55.0	1.0E-06
132.0	2.6E-05
$\alpha = 3.0$	All
$C_5 = 220$	$q = 3$

The C_5 and q parameters (equation 11) were chosen (by trial-and-error) to fit the ΔK-rate data, and these results are shown in figure 35. The q value was 3, and C_5 was 220 MPa-m$^{1/2}$. The fracture term in equation 11 fit the crack growth rate test data in the cyclic fracture regimes extremely well. At first glance, the value of C_5 seems extremely large, but previous testing on

D6AC steel [48] indicated that the cyclic fracture toughness (K_{Ie}) could be as high as 200 MPa-$m^{1/2}$ on higher-strength steel than that tested in reference 31. A comparison of the calculated ΔK-rate curves using equation 11 is shown in figure 35a. Further CPCA testing is needed to resolve the issue of load reduction thresholds at low R values. Another issue is the effects of K_{max}, that higher K_{max} values produce lower thresholds. The K_{max} effect is beyond the scope of the present study. Because of the tight correlation of data in the mid-rate range, figures 35b to 35e show comparisons for each R ratio, respectively.

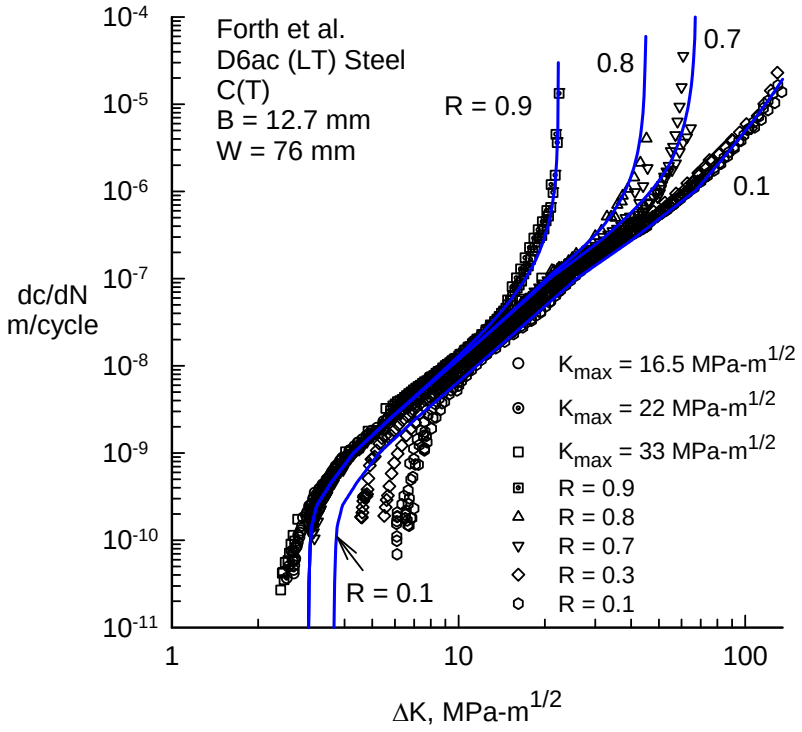

Figure 35a. Predicted ΔK-Rate Behavior for D6AC Steel at Various R Ratios

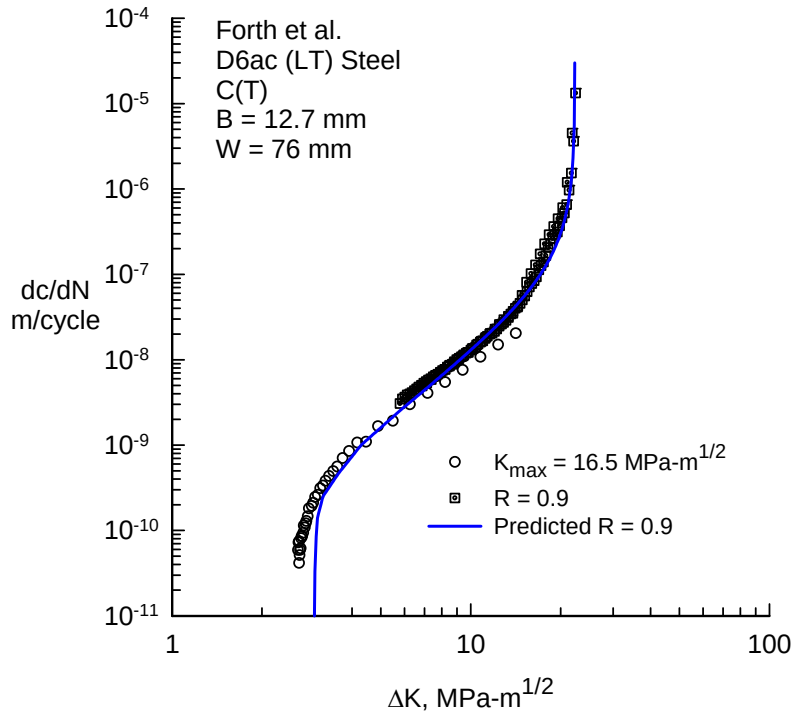

Figure 35b. Predicted Δ*K*-Rate Behavior for D6AC Steel at *R* = 0.9

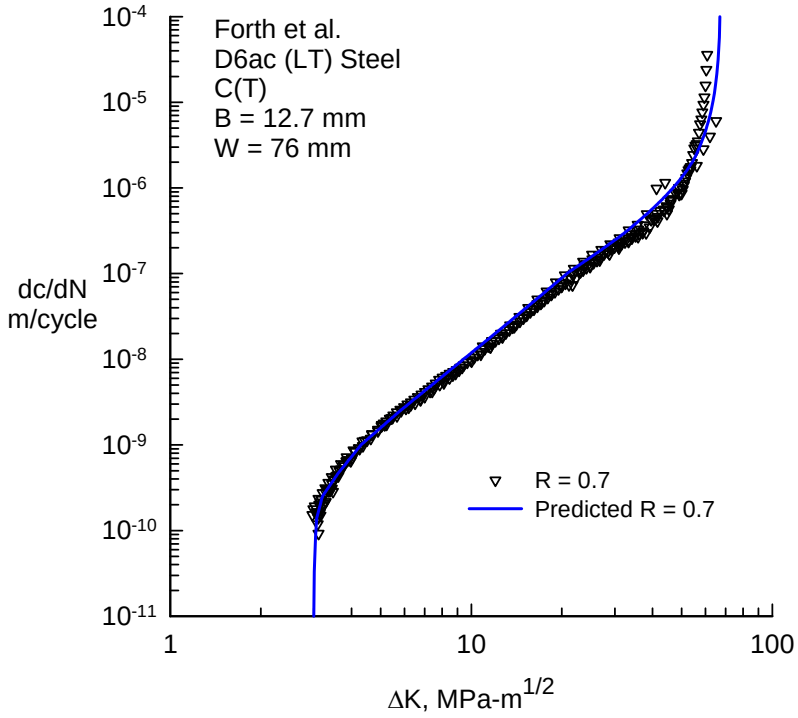

Figure 35c. Predicted Δ*K*-Rate Behavior for D6AC Steel at *R* = 0.7

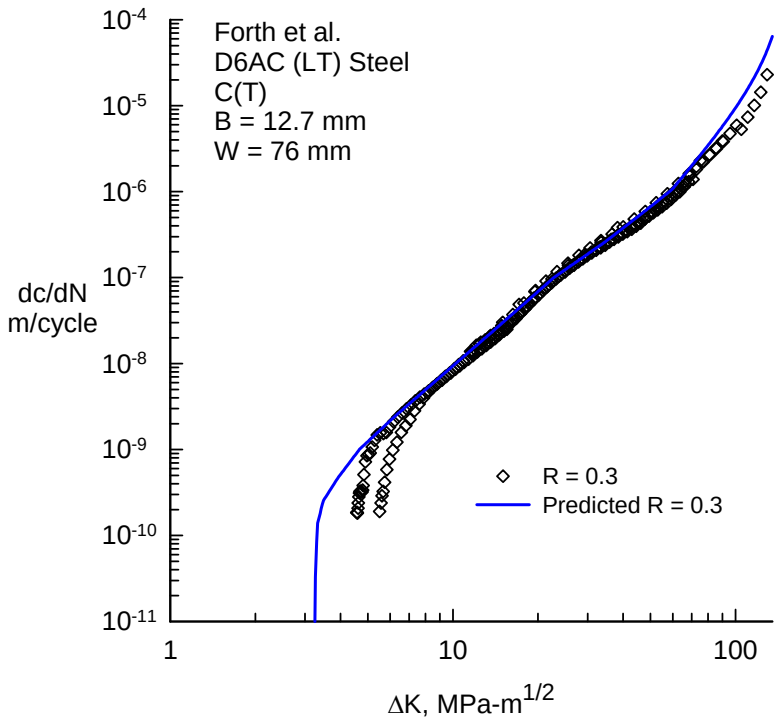

Figure 35d. Predicted Δ*K*-Rate Behavior for D6AC Steel at *R* = 0.3

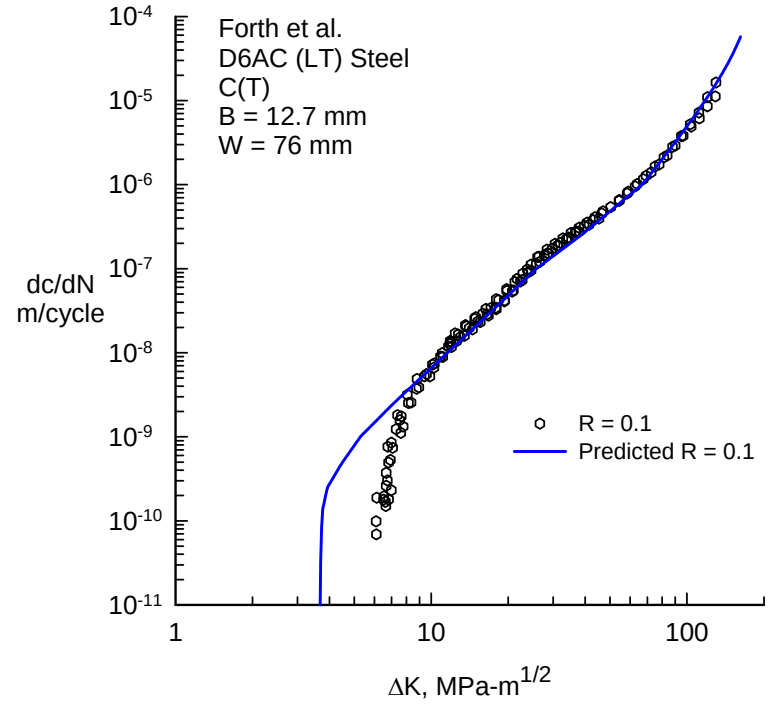

Figure 35e. Predicted Δ*K*-Rate Behavior for D6AC Steel at *R* = 0.1

Two CPCK tests were conducted on the D6AC steel to study the influence of the tensile residual stresses caused by the compressive yielding at the notch tip during compression precracking. These tests were both subjected to compressive precracking loads and then to loading, which would maintain a constant ΔK range during the duration of the test. Figures 36a and 36b show crack extension from the notch tip as a function of cycles for ΔK values of 4.4 and 7.7 MPa-m$^{1/2}$, respectively. The initial crack length is the length after the compression precracking stage. Also indicated is the compressive plastic zone size, ρ_c, using plane-stress assumptions. The results show that after crack extension of about 2 ρ_c, the crack growth rate reached a constant value over about 2 mm of crack growth (or about 6 compressive plastic zone sizes). This indicated that the influence of the tensile residual stresses is acting over about 2 ρ_c. For crack extension values greater than about 6 ρ_c, the crack began to slow down or essentially stop in the lowest ΔK test. Noting that a constant ΔK test is a load reduction test, is this a load shedding effect? The crack tip has maintained the same ΔK, but as the applied loads are reduced, the crack surface displacements are also decreasing. This may be a source for remote closure, or it could also be an interaction with the laboratory environment and buildup of oxide debris on the crack surface, which would promote higher closure loads and slower rates.

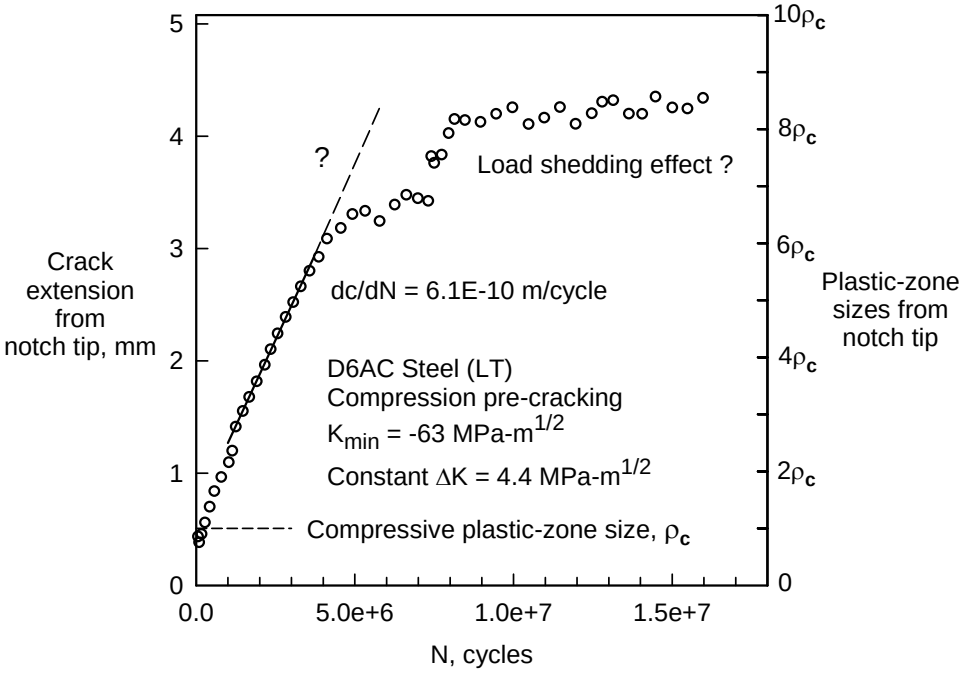

Figure 36a. Crack Growth Rates During CPCK Testing at ΔK = 4.4 MPa-m$^{1/2}$

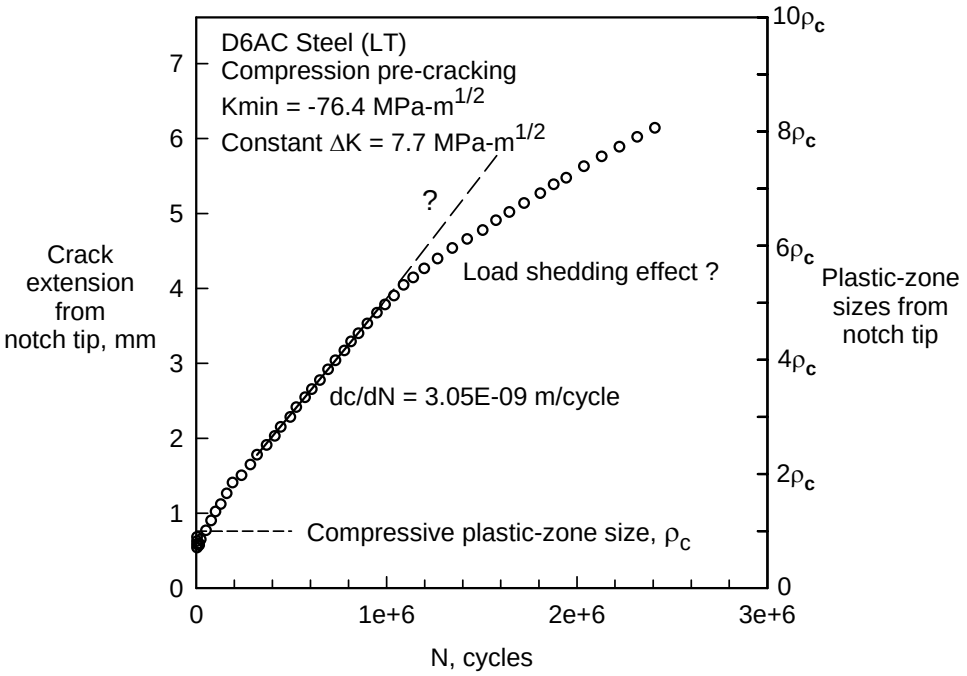

Figure 36b. Crack Growth Rates During CPCK Testing at ΔK = 7.7 MPa-m$^{1/2}$

An interesting result from the two CPCK tests is the constant rate before the crack slowed down or stopped. Figure 37 shows a comparison of these rates and the near-threshold behavior from a variety of tests on D6AC steel specimens at R = 0.1. This figure shows the ΔK-rate data from various tests (symbols), the ΔK_{eff}-rate curve (solid curve), and the predicted ΔK behavior at R = 0.1 (dashed curve). The solid symbols show the rates measured from the two CPCK tests, which agreed well with the predicted R = 0.1 behavior. The open circles show the load reduction test on a 76-mm-wide C(T) specimen; whereas, the square symbols show results on a smaller 51-mm-wide specimen. The smaller specimen produced a much lower load reduction threshold and the results were only slightly different than the predicted behavior. Would a smaller width C(T) specimen produce results that would be closer to the predicted results? One CPCA test, at an initial ΔK_i of 4 MPa-m$^{1/2}$, did not grow after 8 million cycles. Further CPCA tests are needed to help resolve the issue on the correct steady-state ΔK_{th} threshold at R = 0.1.

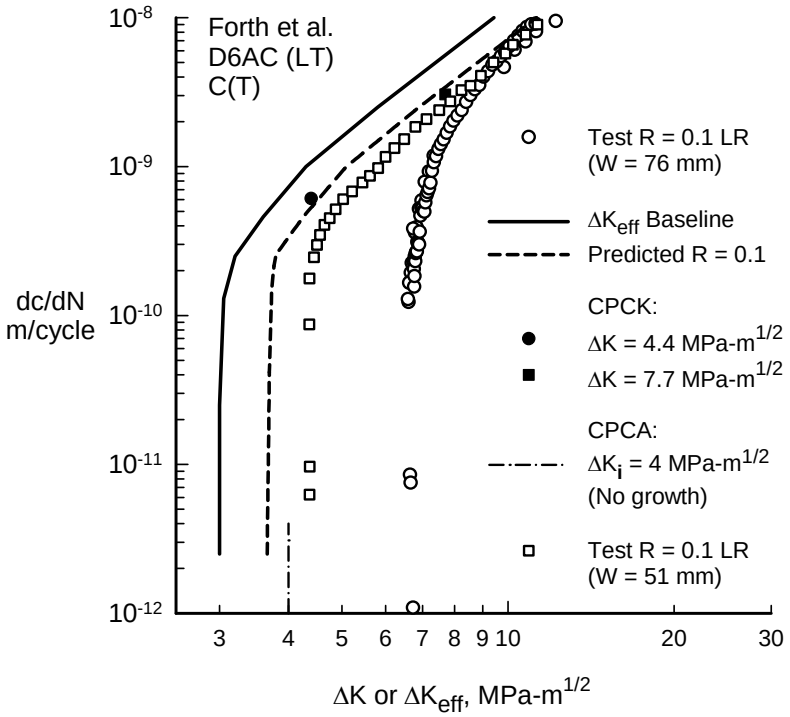

Figure 37. Comparison of Crack Growth Rates in the Near-Threshold Regime for D6AC Steel

3.6.2 4340 Steel.

The fatigue crack growth test results and material properties for the 4340 steel were obtained from references 31 and 30. C(T) specimens were used for all tests (W = 76 mm, B = 12.7 mm) [31]. Reference 30 is an AGARD study on small crack behavior in a variety of materials, high-strength 4340 steel being one of the materials. However, M(T) specimens were used in the AGARD study and they were 5.1-mm thick. The material in the AGARD study had a flow stress about twice as high as the other steel used in rotorcraft hubs. Only two test procedures were used to generate the threshold and near-threshold data: (1) load reduction and (2) constant K_{max} testing for the C(T) specimens, and only load reduction testing was used for the M(T) specimens. (Again, CPCA loading was not used in either study to determine the near-threshold behavior.)

3.6.2.1 Compact Specimens.

The fatigue crack growth rate data was generated using fixed stress ratios of 0.7, 0.3, and 0.1 and using constant K_{max} values of 12 and 33 MPa-m$^{1/2}$. Again, only the specimens tested in the LT orientation will be present here. These results are shown in figure 38a, which shows a large fanning of thresholds with stress ratio. In the mid-rate regime, the data showed a very small shift with the R ratio, which would indicate plane-strain behavior.

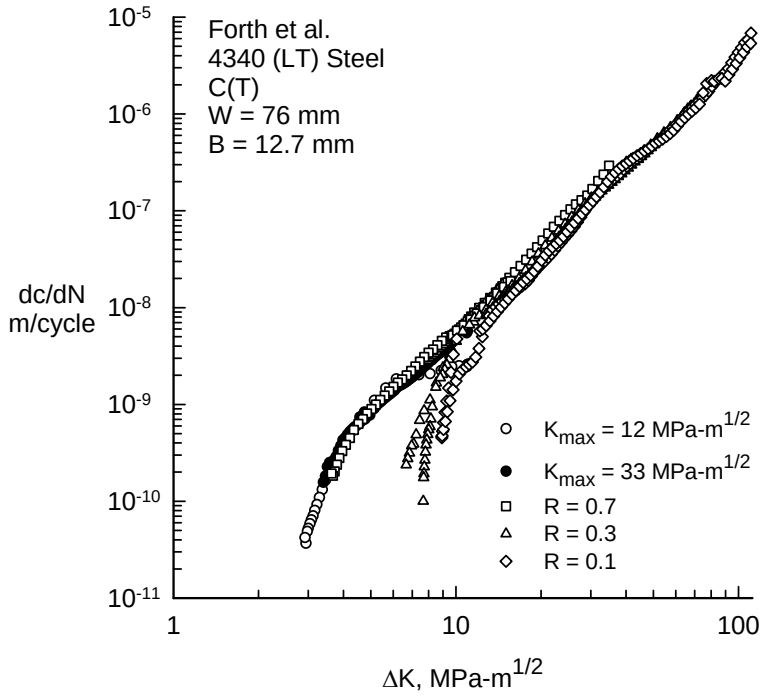

Figure 38a. Fatigue Crack Growth Rates From Various Tests on 4340 Steel

The lack of an R shift in the fatigue crack growth rate data may indicate a lack of or a very small amount of crack closure. The C(T) specimen under plane-strain conditions exhibits far less closure (almost nonexistent) than an M(T) specimen under plane-strain conditions [49]. Figure 38b shows a highly expanded mid-rate region for the steel. The data shows the traditional shift in ΔK with the R ratio, but the shift is small.

These data were analyzed with the crack closure model, and the ΔK_{eff}-rate results are shown in figure 39a. The constraint factor (α) was selected as 3, because of the observation that there was very little stress ratio shift in the ΔK-rate curves, which would indicate plane-strain behavior. However, based on the tensile properties and thickness, the $(\Delta K_{eff})_T$ was 35 MPa-m$^{1/2}$, which would indicate a flat-to-slant crack growth (or constraint loss) behavior near this value. But this could not be confirmed from the test specimens. Therefore, a single constraint factor was used for the complete data set. As can be seen from the figure, the data did not correlate onto a single curve in the low-rate regime. Again, it is suspected that the data in the near-threshold regime are being affected by the load reduction procedure, especially for the low R conditions. In this case, very little data was obtained in the high-rate regime, approaching fracture at the high R ratios. The solid curve is the ΔK_{eff} baseline curve for the 4340 steel data (see table 9). The baseline curve was chosen to fit the R = 0.7 data in the threshold regime and an average of the results in the high-rate regime.

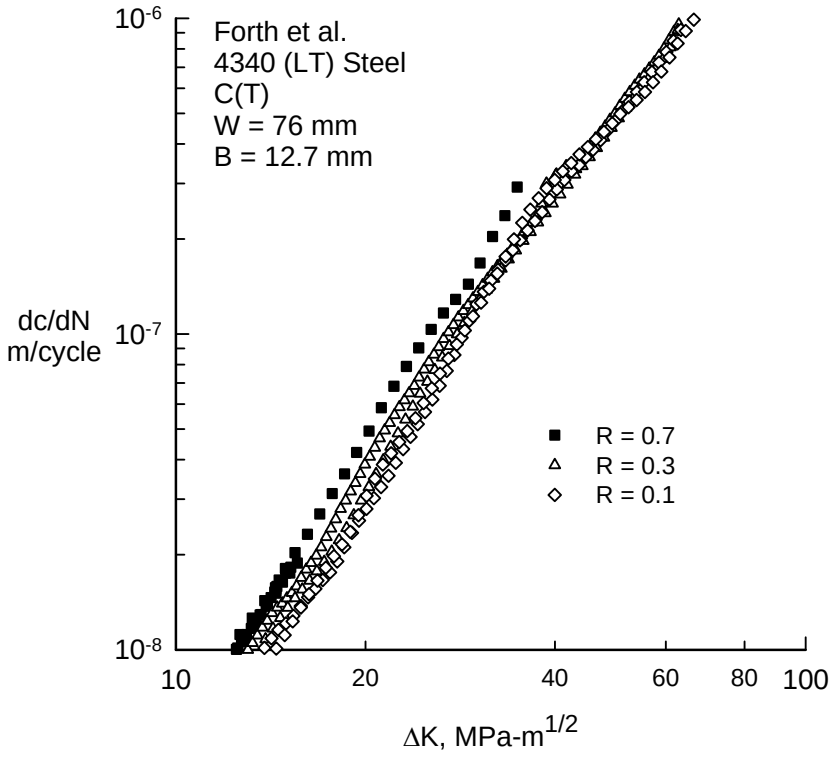

Figure 38b. Expanded View of Fatigue Crack Growth Rates Showing Effects of Stress Ratio

The dashed curve in figure 39a is the ΔK_{eff}-rate curve from M(T) specimens in the AGARD study of a thinner and higher strength 4340 steel [30]. The M(T) curve (dashed) exhibited the same threshold, but produced faster rates in the mid-rate regime than the C(T) specimens. The curves then merged at the higher rates. Whether these differences are due to specimen type, material thickness, or strength level requires further study.

The ΔK_{eff}-rate table for the C(T) specimens is shown in table 9. Because test data was not generated at high R ratios in the fracture regime, an estimate was made of C_5 and q. Further testing would be required to help establish the correct values.

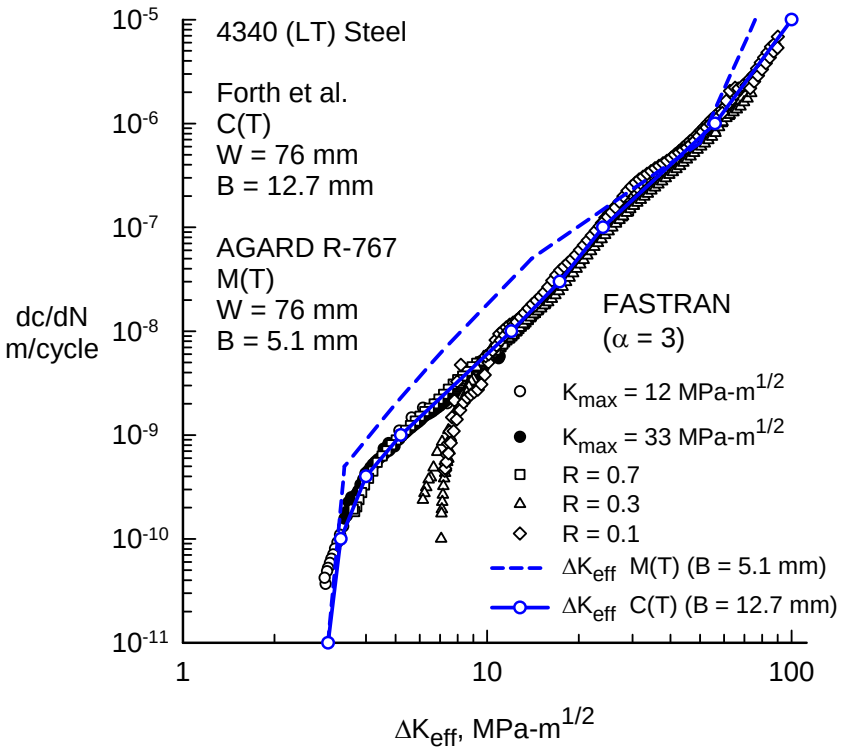

Figure 39a. Effective Stress-Intensity Factor for Various Tests on 4340 Steel

Table 9. Effective Stress-Intensity Factor Relation and Properties for Thick 4340 Steel

ΔK_{eff} MPa-m$^{1/2}$	*dc/dN* m/cycle
3.00	1.0E-11
3.30	1.0E-10
4.00	4.0E-10
5.20	1.0E-09
12.0	1.0E-08
17.3	3.0E-08
24.0	1.0E-07
56.0	1.0E-06
100.0	1.0E-05
180.0	1.0E-04
$\alpha = 3.0$	All
$C_5 = 200$	$q = 3$

Figure 38b showed an expanded view of the ΔK-rate test data in the mid-rate regime, which showed a small shift in ΔK for the same rate with stress ratio. Figure 39b shows the same data, but in terms of ΔK_{eff}. Using the crack closure model with $\alpha = 3$, the test data at $R = 0.7$ is unaffected, that is $\Delta K = \Delta K_{eff}$. But the $R = 0.1$ data over corrected and shifted too much to lower ΔK_{eff} values, which indicated that the closure model was predicting a higher opening load than

may have occurred in the tests. The crack closure model (α = 3) predicted an opening load of 27% of the maximum load for R = 0.1 loading; whereas, an analysis to make the low R data agree with the high R data gave an opening load value of 22% of the maximum load. This difference in opening loads would cause about a 20% change in crack growth rate. The upper and lower dashed curves in the figure shows the ± 20% error bands.

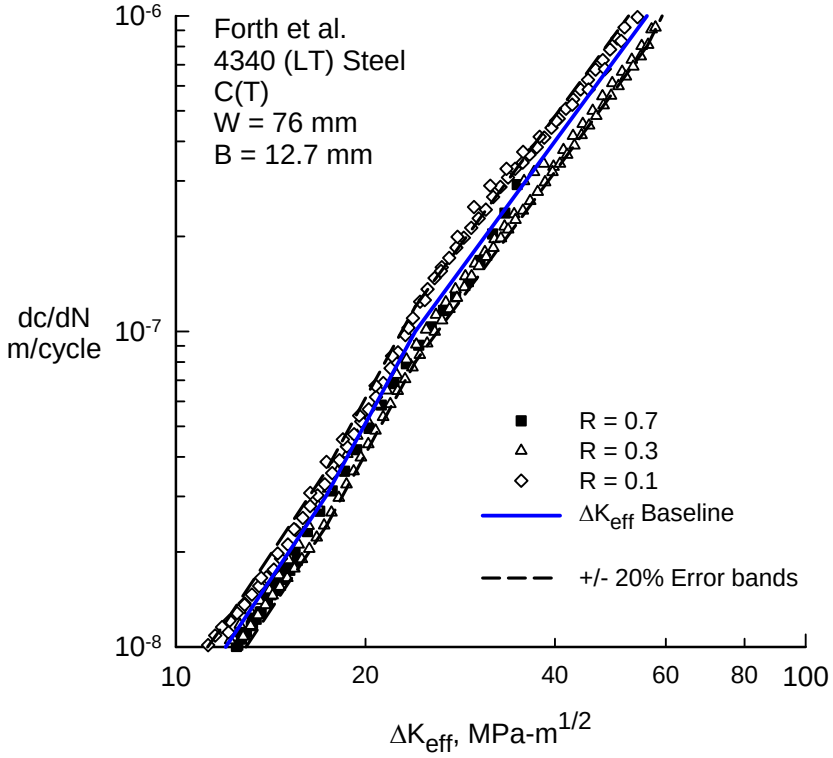

Figure 39b. Expanded View of Fatigue Crack Growth Rates Showing Effects of Stress Ratio on the ΔK_{eff}

Again, to see how well equation 11 fit these data, figure 40 shows the predicted ΔK-rate curves for the various constant R test results using the computer code described in appendix B. The equation correlated fairly well the behavior at the high R results in the near-threshold regime, as well as fitting the low R tests as the cracks grew to failure. In the threshold regime, the R = 0.7 and 0.9 curves fall together and produce the same ΔK_{th}. Further testing at high R ratios and high rates would be required to verify the use of equation 11 in the fracture regime. But the main issue is the low R ratio load reduction tests, which show much higher thresholds than those predicted from plasticity-induced crack closure theory. The predicted threshold for R = 0.1 is more than a factor of 2 lower (4 versus 9 MPa-m$^{1/2}$) than the load reduction threshold. But further study is needed on this material to resolve the apparent problem with the load reduction threshold data, such as conducting CPCA tests.

3.6.2.2 Middle Crack Tension Specimens.

From the testing at NASA LaRC and the data in NASGRO, it has become apparent that C(T) specimens are producing higher ΔK thresholds than M(T) specimens made of the same material and tested under the same stress ratio. Thus, it was of interest to revisit the AGARD Short Crack

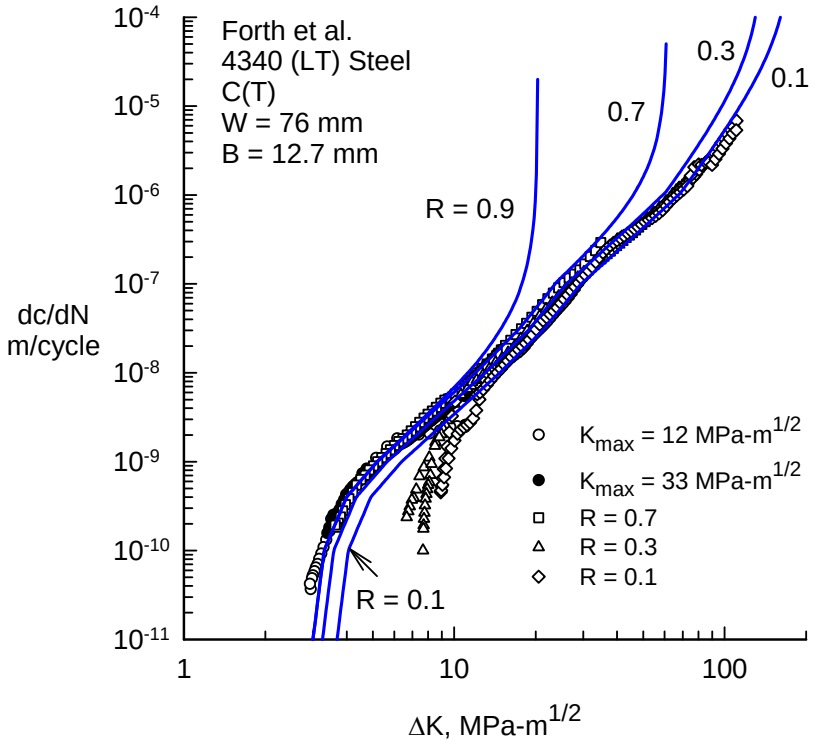

Figure 40. Predicted ΔK-Rate Behavior for 4340 Steel at Various R Ratios

Program data [30] on high-strength 4340 steel M(T) specimens tested under the load reduction procedure. These results are shown in figure 41 for stress ratios ranging from -1 to 0.5. These specimens were machined from 5.1-mm-thick steel and were tested in the LT orientation over a wide range in rates from threshold to fracture.

These data had previously been analyzed with the crack closure model [30], and the ΔK_{eff}-rate results are shown in figure 42. Based on the tensile properties and thickness, the $(\Delta K_{eff})_T$ was 52 MPa-m$^{1/2}$, which would indicate a flat-to-slant crack growth (or constraint loss) behavior near this value. On the ΔK_{eff} plot, the sharp knee in the data is the approximate location where shear lips began to form on the specimens (flat-to-slant crack growth). Slant crack growth behavior developed in the specimens at the higher rates. This corresponded very closely with the flat-to-slant crack growth equation (equation 10). Thus, a constraint loss behavior was assumed. For rates less than 5E-07 m/cycle, α was 2.5 (near plane-strain behavior), but for rates greater than 2.5E-05 m/cycle, α was 1.2 (plane-stress behavior). The data correlated fairly well, except in the near-threshold regime. At the time (1990), this was not considered to be a major problem. However, it does appear that the low R results on the M(T) specimens may have been affected by

the load reduction scheme. The fanning of thresholds with the *R* ratio was not as severe as those with the C(T) specimens under load reduction tests.

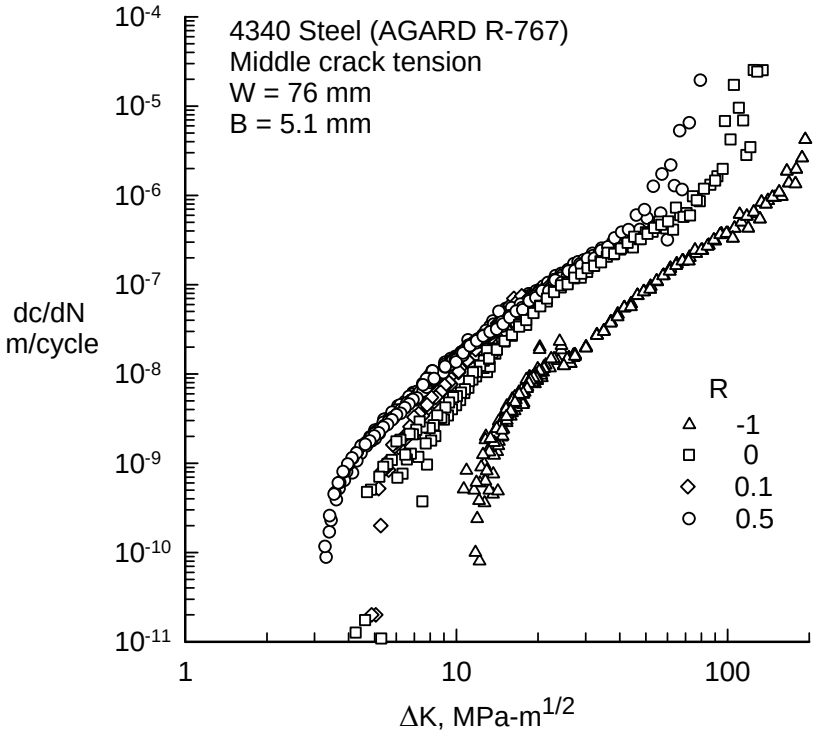

Figure 41. Fatigue Crack Growth Rates From AGARD Study on 4340 Steel

The solid curve in figure 42 shows the ΔK_{eff} baseline curve (see table 10). This curve was fit to the high *R* results in the near-threshold regime and an average of the results in the mid- and upper-rate regimes. Appendix B demonstrates how well equation 10 correlates and predicts the ΔK-rate curves for various stress ratios for the high-strength steel using the multicurve computer code.

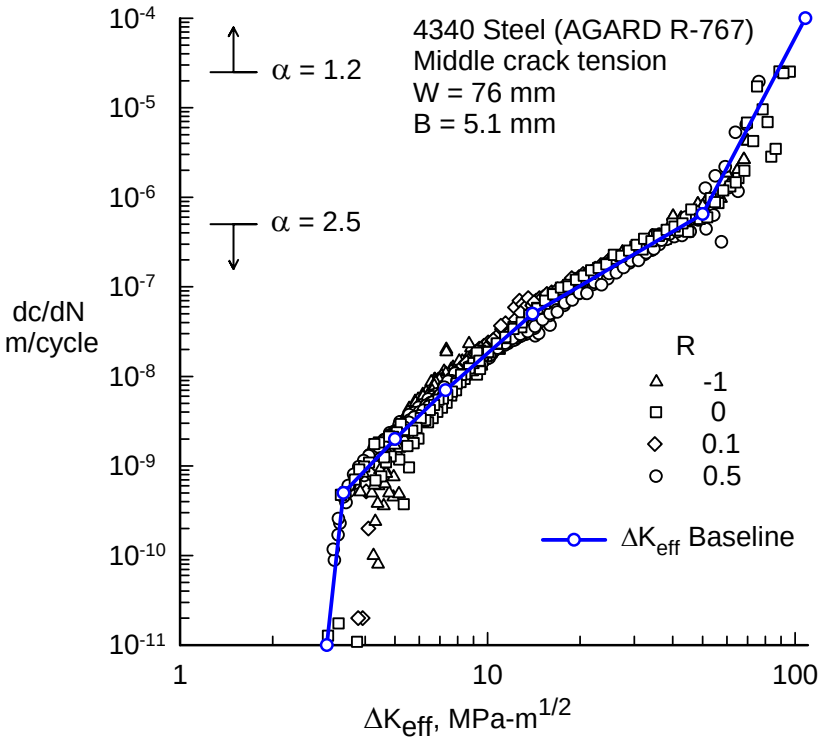

Figure 42. Effective Stress-Intensity Factors on 4340 Steel From AGARD Study

Table 10. Effective Stress-Intensity Factor Relation and Properties for Thin 4340 Steel

ΔK_{eff} MPa-m$^{1/2}$	*dc/dN* m/cycle
3.0	1.0E-11
3.4	5.0E-10
5.0	2.0E-09
7.3	7.0E-09
14.0	5.0E-08
50.0	6.5E-07
108.0	1.0E-04
$\alpha_1 = 2.5$	5.0E-07
$\alpha_2 = 1.2$	2.5E-05
$C_5 = 180$	$q = 3$

Figure 43 compares the ΔK-rate curves for C(T) and M(T) specimens made of the appropriate steel. These results show that the predicted threshold at $R = 0.1$ was more than a factor of 2 lower than the load reduction test data on the C(T) specimens, but was only about 20% lower on the M(T) specimens. Whether the differences between the C(T) and M(T) specimens are due to the specimen type, thickness, or strength level requires further study. CPCA tests also need to be conducted on the C(T) specimens to verify whether the low R thresholds are as low as predicted and whether the CPCA crack growth behavior is independent of specimen width.

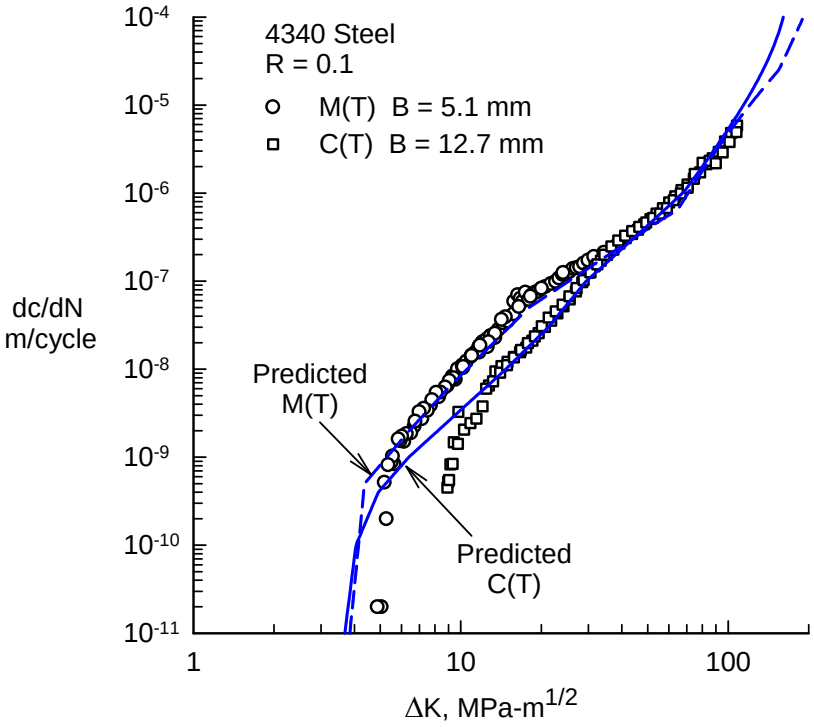

Figure 43. Comparison of M(T) and C(T) Specimen Results on 4340 Steel

3.7 DISCUSSION OF RESULTS.

A large portion of the fatigue crack growth threshold data in the report is inappropriate due to the load reduction test procedure that was used to generate these data. These data are inappropriate because the technical community uses these data as if they are steady-state constant-amplitude results. Approximately 20 years ago, tests [14] and analyses [12] indicated that a rise in the crack closure behavior accompanied the development of the linear elastic ΔK_{th}. This rise in crack closure behavior in the literature was attributed to an increase in crack surface roughness or oxide debris [38 and 39] and was thought to be a natural behavior that would also occur under constant-amplitude loading. But the analyses indicated that the rise in crack closure behavior was caused by remote closure from residual plastic deformations and that the behavior may be a load history effect.

The author, in collaboration with NASA LaRC personnel, was developing a new test method to generate threshold data under steady-state constant-amplitude loading conditions without any load history effects. This new test method was the CPCA threshold test procedure. A large test program on the development of these fatigue crack growth databases, for use in damage-tolerant analyses for aircraft propellers and rotorcraft components, was conducted at NASA LaRC under a Memorandum of Agreement with the FAA [31]. This test program was conducted to generate more accurate representations of the fatigue crack growth behavior in the near-threshold regime and approaching fracture under a wide range of constant-amplitude stress ratio conditions.

The objective of the research grant was to analyze the test data on selected propeller and rotorcraft materials to develop the ΔK_{eff} against crack growth rate relationship for use in damage-tolerant analyses. The resulting relationships could then be used in the strip-yield model in NASGRO (Stripy) [4] or used to generate the stress-intensity factor ΔK-rate curves for use in AFGROW [5] or any other life prediction code requiring LEFM procedures.

The materials tested and analyzed were 7050-T7451 and 7075-T7351 aluminum alloys and D6AC and 4340 steels. Only the steels were tested as part of the FAA test program at NASA LaRC. The 7075 (TL) alloy was tested at the NASA JSC, and the 7050 and 7075 (LT) alloys were tested at NASA LaRC.

The 7050 alloy [26 and 27] was not part of the FAA test program, and thus, a wide range in loading conditions were not used to generate the fatigue crack growth rate data. Only stress ratios ($R = P_{min}/P_{max}$) of 0.1 and 0.7 were tested. But, testing on this alloy did involve three test methods (load reduction, constant $K_{max,}$ and CPCA loading) to generate the threshold data. The results indicated that there was very little difference in the load reduction and CPCA threshold test methods. Each method produced essentially the same near-threshold and threshold results. A crack closure analysis of the data also indicated that there was very little fanning with the stress ratio at threshold, i.e., the spread in the low and high R ratio test data in the mid-rate regime was nearly the same as in the threshold regime. Further testing on this alloy would be required to generate the fatigue crack growth rate database.

The 7075 alloy [26 and 27] was also not part of the FAA test program. But fatigue crack growth rate data was obtained from both NASA LaRC and JSC. The database from NASA JSC (unpublished) on the TL orientation had data over a wide range in rates and stress ratios, but tests were only conducted with the load reduction and constant K_{max} test methods. For this alloy, the crack closure model was used to predict the threshold behavior in the low R regime. Further testing would be required to verify these predictions. (Testing at MSU under an ONR grant has confirmed the model predictions in threshold behavior for this alloy.) Data from NASA LaRC, again, used the three test methods to generate threshold data. Only stress ratios of 0.1 and 0.7 were tested. But here the results indicated a large difference in the load reduction and CPCA threshold behavior. These results show that the CPCA loading produces lower thresholds at low R and produces data with very little fanning with stress ratio at threshold. However, the CPCA results exhibited significant scatter in the data. Again, further testing on this alloy would be required to generate the fatigue crack growth rate database.

The D6AC steel [31] was part of the FAA test program. But here only two methods (load reduction and constant K_{max} testing) were used in threshold testing. Some tests were conducted under the CPCK test procedure. CPCA loading was not used to generate any fatigue crack growth rate data. But this database did include results over a wide range in rates and in stress ratios (R = 0.1, 0.3, 0.7, 0.8, and 0.9). In the mid-rate regime, these results exhibited very small shifts in the ΔK-rate curves with stress ratio, indicating a small amount of crack closure and nearly plane-strain behavior. A crack closure model analysis correlated the data fairly well in the mid-rate regime, but indicated that the model was slightly overpredicting the amount of crack closure. In the fracture region (high rates), the use of a fracture term in the multilinear equation fit the various R ratio data extremely well as the cracks grew to failure. But in the threshold

regime, an extremely large amount of fanning with the stress ratio was observed. For this material, the crack closure model was used to predict the threshold behavior in the low R regime. For R = 0.1 loading, the predicted ΔK_{th} threshold was 3.6 instead of 6.6 MPa-$m^{1/2}$. Further testing would be required to verify these predictions.

For the D6AC steel, the CPCK test results presented an interesting result on constant ΔK testing. These two tests, at different values of ΔK (4.4 and 7.7 MPa-$m^{1/2}$), indicated that the influence of the tensile residual stresses (caused by compressive yielding) were less than about 2 compressive plastic zone sizes (ρ_c). The cracks grew at a very constant rate from 2 to 6 compressive plastic zone sizes. However, the crack stopped or grew at much slower rates after crack growth beyond 6 ρ_c. But why did the crack stop or slow down? It cannot be due to the compressive yielding or the tensile residual stresses. A constant ΔK test is a load-shedding test to maintain the same stress-intensity factor as the crack grows. The crack tip has the same stress-intensity factor, but the crack surface displacements have been reduced. This may lead to premature closure due to remote closure or oxide-debris accumulation on the crack surfaces. If these tests had been conducted at a constant load, would the crack continue to grow? Noting that the crack surface displacements would be increasing as the crack grows and the likelihood of remote closure or oxide-debris accumulation is less likely. But further testing would be required to answer these questions.

The 4340 steel [31] was also part of the FAA test program. Tests were conducted for three material orientations, but only the LT orientation was analyzed herein. Again, only two methods (load reduction and constant K_{max} testing) were used in threshold testing. CPCA loading was not used to generate any fatigue crack growth rate data for this material. This database on the LT orientation had a more limited range of stress ratios (R = 0.1, 0.3, 0.7) and test results were not available in the fracture regime. In the mid-rate regime, these results also exhibited a very small shift in the ΔK-rate curves with stress ratio. A crack closure model analysis, under plane-strain conditions (constraint factor α = 3), correlated the data fairly well in the mid-rate regime, but indicated that the model was slightly overpredicting the amount of crack closure. For R = 0.1 loading, the model predicted an opening load of 27%; whereas, an estimate of what would be required to correlate the low and high R results gave 22%. Thus, improvements need to be made in the crack closure model to predict lower crack-opening behavior in bend-type configurations under high-constraint conditions. Again, in the threshold regime, an extremely large amount of fanning with the stress ratio was observed. For this material, the crack closure model was used to predict the threshold behavior in the low R regime. For R = 0.1 loading, the predicted ΔK_{th} threshold was 4 instead of about 9 MPa-$m^{1/2}$. Further testing would be required to verify these predictions.

The data on the 4340 steel from NASA LaRC was generated with compact, C(T), specimens. However, data had previously been generated in an AGARD test program [30] on a thinner, higher strength 4340 steel. These results indicated that M(T) specimens produced lower thresholds than the C(T) specimens and produced faster crack growth rates in the mid-rate regime. Whether these differences were due to specimen type, thickness, or strength level must await further testing. These observations are extremely important to the transferability of crack growth prediction methodology from laboratory specimens to propeller and rotorcraft components.

Use of the multilinear equation to fit fatigue crack growth rate data gives the advantages of a table lookup with a fracture term, which is needed to fit data that has been generated in the fracture regime at high-stress ratios. Also, many materials have sharp changes in slope, especially the aluminum alloys, that cannot fit very well with multiple parameter equations. The table lookup form allows for very accurate representation of the crack growth rate data. The computer codes (appendix A and B) were developed to help users generate the ΔK_{eff}-rate curve for a given material, thickness, and test conditions, and to predict the ΔK-rate for a given material at any specified R ratio.

4. CONCLUSIONS.

The main conclusions that were drawn from this study are:

- For use in damage-tolerant designs of propeller and rotorcraft components, fatigue crack growth rate data over a wide range in rates from threshold to fracture for a wide range in stress ratios ($R = P_{min}/P_{max}$ from -1 to 0.9) are needed, especially the high R ratio results.

- The compression-compression precracking constant-amplitude (CPCA) threshold testing procedure appears to be a method to generate steady-state constant-amplitude data, after the crack has grown about 3 compressive plastic zone sizes away from the crack starter notch. Further testing and analyses are needed to develop this method.

- Significant testing will be required to fully understand the fatigue crack growth threshold behavior under both load reduction and CPCA loading. The influence of specimen type, specimen width, and environment on load reduction and CPCA threshold testing needs to be investigated.

- Improvements are needed in the plasticity-induced crack closure model. For both load reduction and CPCA threshold testing, the current model predicts the trends in the behavior, but did not match the test data very well. For three-dimensional effects (such as plane stress and plane-strain behavior through-the-thickness), roughness and oxide-debris induced crack closure mechanisms need to be incorporated into the plasticity-induced crack closure model.

- A multilinear equation has been developed to fit the fatigue crack growth rate data over a wide range in rates and stress ratios from threshold to fracture.

- Equations have been developed to account for the influence of the crack mouth-opening displacement gage force on stress-intensity factors, when low applied loads are used on compact specimens in threshold testing, especially for thin-sheet materials.

- Computer codes have been developed to help users generate the effective stress-intensity factor range against rate relations and to predict the stress-intensity factor range against rate curves for various constant-amplitude stress ratios from threshold to fracture.

5. REFERENCES.

1. Standard Test Method for Measurement of Fatigue Crack Growth Rates, ASTM STP E-647, 2003, pp. 615-657.

2. Herman, W., Hertzberg, R., and Jaccard, R., "A Simplified Laboratory Approach for the Prediction of Short Crack Behavior in Engineering Structures," *Fatigue and Fracture of Engineering Materials and Structures*, Vol. 11, 1988, pp. 303-320.

3. Pippan, R., Plöchl, L., Klanner, F., and Stüwe, H.P., "The Use of Fatigue Specimens Precracked in Compression for Measuring Threshold Values and Crack Growth," ASTM Journal of Testing and Evaluation, Vol. 22, 1994, pp. 98.

4. NASGRO Reference Manual 4.02, Southwest Research Institute and NASA Johnson Space Center, 2002.

5. AFGROW Reference Manual 4.0, Wright-Patterson Air Force Base, AFRL/VASM, 2004.

6. Paris, P.C. and Erdogan, F., "A Critical Analysis of Crack Propagation Laws," *Transactions of the ASME, Journal of Basic Engineering*, Series D, Vol. 85, No. 3, 1963.

7. Barsom, J.M., "Fatigue-Crack Propagation in Steels of Various Yield Strengths," *Transactions of the ASME, Journal of Engineering for Industry*, Series B, Vol. 93, No. 4, November 1971.

8. Frost, N.E., "The Growth of Fatigue Cracks," *Proceedings of the First International Conference on Fracture*, Sendai, Japan, 1966, pp. 1433.

9. Hudak, S., Jr., Saxena, S., Bucci, R., and Malcolm, R., "Development of Standard Methods of Testing and Analyzing Fatigue Crack Growth Rate Data—Final Report," AFML TR 78-40, Air Force Materials Laboratory, Wright-Patterson Air Force Base, OH, 1978.

10. "Damage Tolerance and Fatigue Evaluation of Structure," Federal Aviation Regulations, Title 14 Code of Federal Regulations, Part 25, Section 571.

11. Pearson, S., "Initiation of Fatigue Cracks in Commercial Aluminum Alloys and the Subsequent Propagation of Very Short Cracks," *Engineering Fracture Mechanics*, Vol. 7, No. 2, 1975, pp. 235-247.

12. Newman, J.C., Jr., "A Nonlinear Fracture Mechanics Approach to the Growth of Small Cracks," Behavior of Short Cracks in Airframe Components, *AGARD Conference Proceedings*, No. 328, 1983.

13. Newman, J.C., Jr., "The Merging of Fatigue and Fracture Mechanics Concepts, "A Historical Perspective," *Fatigue and Fracture Mechanics*, 28th Volume, ASTM 1321, 1997, pp. 3-51.

14. Minakawa, K. and McEvily, A.J., "On Near-Threshold Fatigue Crack Growth in Steels and Aluminum Alloys," *Proceedings International Conference on Fatigue Thresholds*, Vol. 2, Stockholm, Sweden, 1981, pp. 373-390.

15. Marci, G., "A Fatigue Crack Growth Threshold," *Engineering Fracture Mechanics*, Vol. 42, 1992, pp. 367-385.

16. Tabernig, B., Powell, P., and Pippan, R., "Resistance Curves for the Threshold of Fatigue Crack Propagation in Particle Reinforced Aluminum Alloys," ASTM STP 1372, J. Newman, Jr. and R. Piascik, eds., W. Conshohocken, PA, 2000, pp. 96.

17. Marci, G., "Fatigue Crack Growth Threshold Concept and Test Results for Al- and Ti-Alloys," ASTM STP 1372, J. Newman, Jr. and R. Piascik, eds., 2000, pp. 81-95.

18. Newman, J.A., Riddell, W.T., and Piascik, R.S., "Effects of K_{max} on Fatigue Crack Growth Threshold in Aluminum Alloys," ASTM STP 1372, J.C. Newman, Jr. and R.S. Piascik, eds., W. Conshohocken, PA, 2000, pp. 63-77.

19. Vasudevan, A.K., Sadananda, K., and Louat, N., "A Review of Crack Closure, Fatigue Crack Threshold and Related Phenomena," *Materials Science and Engineering*, Vol. A188, 1994, pp. 1-22.

20. Newman, J.C., Jr., "Analysis of Fatigue Crack Growth and Closure Near-Threshold Conditions," ASTM STP-1372, J.C. Newman, Jr. and R.S. Piascik, eds., American Society for Testing and Materials, West Conshohocken, PA, 2000, pp. 227-251.

21. Newman, J.C., Jr., "FASTRAN-II - A Fatigue Crack Growth Structural Analysis Program," NASA TM 104159, February 1992.

22. Hubbard, R.P., "Crack Growth Under Cyclic Compression," *Journal of Basic Engineering, Transactions ASME*, Vol. 91, 1969, pp. 625-631.

23. Topper, T.H. and Au, P. "Fatigue Test Methodology," *AGARD Lecture Series 118*, The Technical University of Denmark, Denmark, October 19-20, 1981.

24. Au, P., Topper, T.H., and El Haddad, M.L., "The Effects of Compressive Overloads on the Threshold Stress Intensity for Short Cracks," *AGARD Conference Proceedings*, No. 328, 1983, pp. 11.1-11.7.

25. Suresh, S., "Crack Initiation in Cyclic Compression and its Application," *Engineering Fracture Mechanics*, Vol. 21, 1985, pp. 453-463.

26. Forth, S.C., Newman, J.C., Jr., and Forman, R.G., "On Generating Fatigue Crack Growth Thresholds," *International Journal of Fatigue*, Vol. 25, 2003.

27. Forth, S.C., Newman, J.C., Jr., and Forman, R.G., "Evaluation of Fatigue Crack Thresholds Using Various Experimental Methods," *Fatigue and Fracture Mechanics*, 34th Volume, ASTM 1461, S.R. Daniewicz et al., eds., ASTM International, 2004.

28. James, M.A., Forth, S.C., and Newman, J.A., "Load History Effects Resulting from Compression Precracking," *Fatigue and Fracture Mechanics*, 34th Volume, ASTM 1461, S.R. Daniewicz, J.C. Newman, Jr., and K.-H. Schwalbe, eds., ASTM International, 2004.

29. Donald, J.K. and Paris, P.C., "An Evaluation of ΔK_{eff} Estimation Procedures on 6061-T6 and 2024-T3 Aluminum Alloys," *Proceedings of Fatigue Damage of Structural Materials II*, Cape Cod, MA, September 7-11, 1998.

30. Edwards, P.R. and Newman, J.C., Jr., editors, "Short-Crack Growth Behavior in Various Aircraft Materials," AGARD report no. 767, 1990.

31. Forth, S., James, M., and Johnston, W., "Development and Validation of Advanced Test Methods to Generate Fatigue Crack Growth and Threshold Data for Use in Damage Tolerance Analyses," FAA report DOT/FAA/AR-04/22 to be published.

32. Magnusen, P.E., Bucci, R.J., Hinkle, A.J., Brockenbrough, J.R., and Konish, H.J., *International Journal of Fatigue*, Vol. 19, 1997, pp. 275.

33. Aluminum Mechanical Properties, Ryerson Tull, Chicago, IL, 2002.

34. Metals Handbook, 9th Edition, Volume 1, Properties and Selection: Irons and Steels, ASM Handbook Committee, American Society for Metals, Metals Park, OH, 1978.

35. Schmidt, R. and Paris, P.C., "Threshold for Fatigue Crack Propagation and the Effects of Load Ratio and Frequency," *Progress in Flaw Growth and Fracture Toughness Testing*, ASTM STP 536, American Society for Testing and Materials, Philadelphia, 1973, pp. 79.

36. Elber, W., "The Significance of Fatigue Crack Closure," *Damage Tolerance in Aircraft Structures*, ASTM STP 486, American Society for Testing and Materials, Philadelphia, 1971, pp. 230-242.

37. Walker, N. and Beevers, C.J., "A Fatigue Crack Closure Mechanism in Titanium," *Fatigue of Engineering Materials and Structures*, Vol. 1, No. 1, 1979, pp. 135-148.

38. Suresh, S. and Ritchie, R.O., "A Geometric Model for Fatigue Crack Closure Induced by Fracture Surface Roughness," *Metallurgical Transactions*, Vol. 13A, 1982, pp. 1627-1631.

39. Suresh, S., Parks, D., and Ritchie, R., "Crack Tip Oxide Formation and Its Influence on Fatigue Thresholds," *Proceedings Symposium on Fatigue Thresholds*, J. Backlund, A. Blom, and C. Beevers, EMAS Ltd., Warley, UK, 1982, pp. 391-408.

40. McClung, R.C., "Finite-Element Analysis of Specimen Geometry Effects on Fatigue Crack Closure," *Fatigue and Fracture of Engineering Materials and Structures*, Vol. 17, No. 8, 1994, pp. 861-872.

41. Daniewicz, S.R. and Bloom, J.M., "An Assessment of Geometry Effects on Plane Stress Fatigue Crack Closure Using a Modified Strip-Yield Model," *International Journal of Fatigue*, Vol. 18, No. 7, 1996, pp. 483-490.

42. Newman, J.C., Jr., "A Crack-Opening Stress Equation for Fatigue Crack Growth," *International Journal of Fracture*, Vol. 24, R131-R135, 1984.

43. Private Communication: Forth, S.C. and Urban, M.R., "Fatigue Crack Growth Thresholds for 7050-T7451 Aluminum," (unpublished), 2004.

44. Newman, J.C., Jr., "Effects of Constraint on Crack Growth Under Aircraft Spectrum Loading," *Fatigue of Aircraft Materials*, A. Beukers, T. deJong, J. Sinke, A. Vlot, and L. B. Vogelesang, eds., 1992, pp. 83-109.

45. Yoder G.R., Cooley L.A. and Crooker, T.W., "On Microstructural Control on Near-Threshold Fatigue Crack Growth in 7000-Series Aluminum Alloys," *Scripta Metallurgica*, Vol. 16, 1982, pp. 1021-1025.

46. Piascik, R.S. and Gangloff, R.P., "Environmental Fatigue of an Al-Li-Cu Alloy: Part II Microscopic Hydrogen Cracking Processes," *Metallurgical Transactions*, Vol. 24A, 1993, pp. 2751-2762.

47. Newman, J.C., Jr., "Fracture Analysis of Various Cracked Configurations in Sheet and Plate Materials," *Properties Related to Fracture Toughness*, ASTM STP 605, 1976, pp. 104-123.

48. Newman, J.C., Jr., Bland, J.D., and Berry, R.F., Jr., "Fracture Toughness and Critical Crack Sizes for the Space Shuttle Solid Rocket Motor D6AC Steel Case," *Fracture Mechanics*, 26th Volume, ASTM STP 1256, American Society for Testing and Materials, Philadelphia, PA, 1995, pp. 799-821.

49. Solanki, K., Daniewicz, S.R., and Newman, J.C., Jr., "Finite Element Modeling of Plasticity-Induced Crack Closure with Emphasis on Geometry and Mesh Refinement Effects," *Engineering Fracture Mechanics*, Vol. 70, 2003, pp. 1475-1489.

APPENDIX A—INFLUENCE OF THE CRACK MOUTH-OPENING DISPLACEMENT GAGE ON THE COMPACT SPECIMEN

The compact tension C(T) specimen is the most widely used test specimen to measure fatigue crack growth rates in metallic materials. Two methods have been used to monitor crack length in the C(T) specimens: (1) the crack mouth-opening displacement gage and (2) the back-face strain gage, as shown in figure A-1. Under normal loading conditions, the external forces applied to the specimen by the displacement gage (20 to 60 Newton (N) or 5 to 15 pounds) are very low compared to the applied load, *P*. But for threshold testing, the displacement gage can have a significant influence on the stress-intensity factors and, consequently, the crack growth rates, if the applied load *P* is low (less than 400 N or 100 pounds). One objective was to develop the equations to account for the influence of the displacement gage forces on the calculated stress-intensity factors. This would allow the use of displacement gage to obtain accurate results at the low applied load levels for threshold testing.

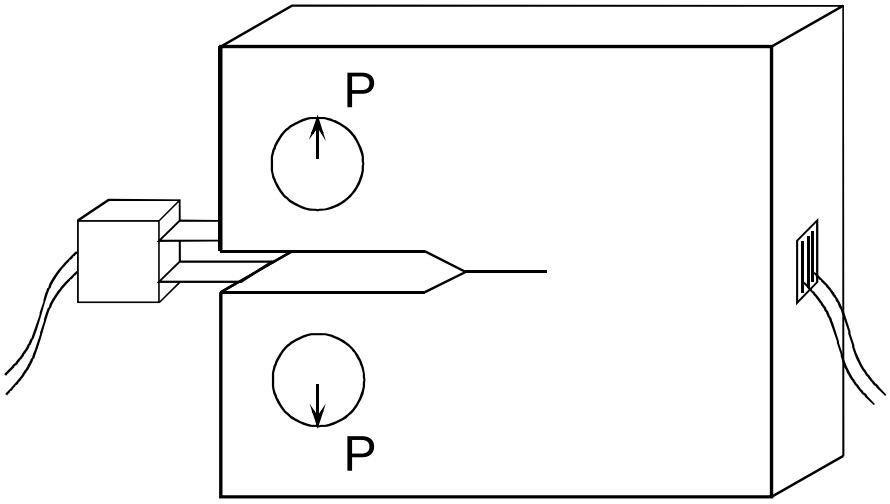

Figure A-1. Compact Tension Specimen With Crack Mouth-Opening Displacement Gage and Back-Face Strain Gage

Crack mouth-opening displacement gages, which are used to monitor crack growth in C(T) specimens, may have a significant influence on the test results when small loads are applied to the specimen. In threshold testing, small loads are generally needed to reach the very low stress-intensity factor range thresholds. The displacement gage measures the total crack mouth displacement, which is a combination of the displacement due to the applied load and that due to the force of the displacement gage. This section covers the analyses and procedures used to combine two different loading conditions on the C(T) specimen and to relate them using a displacement-compatibility equation. The relationship derived has only one unknown (crack-to-length ratio, c/W). Once the c/W ratio is found, the force that the gage exerts on the specimen can be calculated and the total stress-intensity factor due to both the applied loading and the gage force can be calculated.

The FADD2D (Version 1.0) boundary element code [A-1] was used to calculate the influence of the displacement gage force on the stress-intensity factor and the crack mouth-opening

displacements, in addition, to the applied load, *P*. The displacement gage was assumed to act like a spring applied at the crack mouth. The relationship between displacement gage force (f) and the gage displacement (V_g) is given by

$$f = k_g V_g \tag{A-1}$$

where k_g is the gage (spring) stiffness. A force *f* was applied at the crack mouth to simulate the displacement gage (see figure A-2). The force was simulated by uniform shear tractions applied over a small region along the edge of the compact specimen. Stress-intensity factors (K_f) and crack-opening displacements (V_f) at the crack mouth were calculated for various crack length-to-width ratios (c/W = 0.2 to 0.8). Convergence studies were made using the FADD2D code for some extreme cases (low c/W, large c/W, different shear tractions and areas) to study the effects of the number and distribution of boundary elements on the stress-intensity factor and displacement solutions. (Comparisons were also made between the *K* and displacement solutions for the pin-loaded C(T) specimen in American Society for Testing and Materials (ASTM) E 647 [A-2] and the results were within 0.5% of the standard equations.) Equations were developed for both stress-intensity factors and crack-opening displacements, using the same functional form, as those that are in the ASTM E 647 standard.

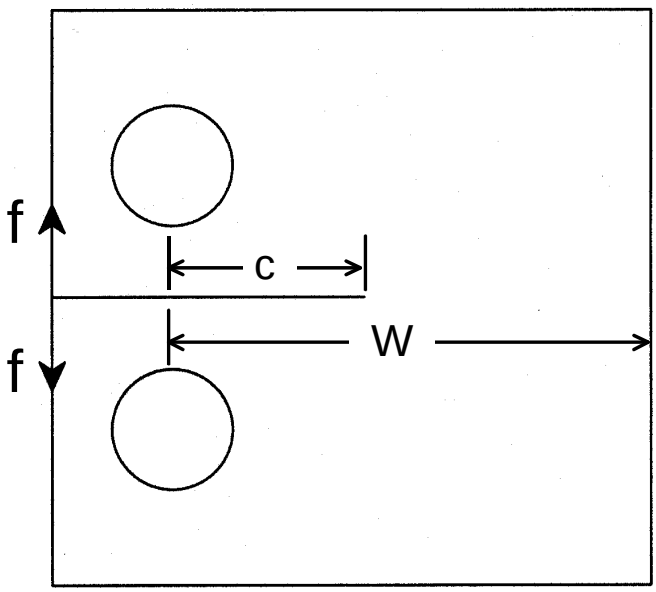

Figure A-2. Compact Tension Specimen Subjected Crack Mouth-Opening Displacement Gage Forces

The FADD2D boundary element code was used to calculate stress-intensity factors and crack mouth-opening displacements due to a force applied at the crack mouth over a wide range in crack length-to-width (c/W) ratios. The stress-intensity factor equation is

$$K_f = f /(B \sqrt{W})\, F_f \tag{A-2}$$

where f is the force applied by displacement gage and F_f is the boundary-correction factor. The function F_f is given by

$$F_f = 2.536 - 2.129\,(c/W) + 0.433\,(c/W)^2 + 1.557\,(c/W)^3 - 0.76\,(c/W)^4 \qquad \text{(A-3)}$$

A comparison of the FADD2D results and the equation is shown in figure A-3. The equation is within 1% of the numerical results over a wide range in c/W ratios (0.2 to 0.8).

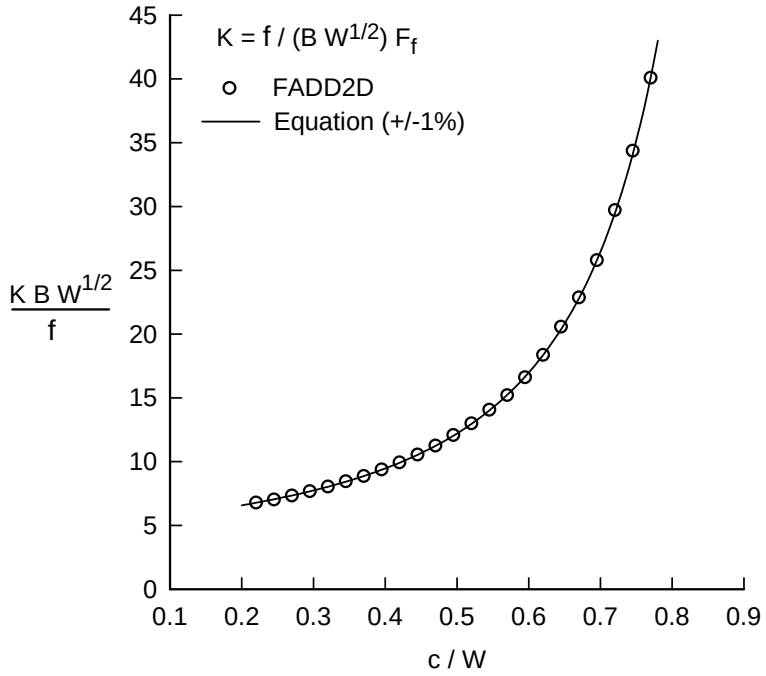

Figure A-3. Normalized Stress-Intensity Factors for a Force Applied at the Crack Mouth of a Compact Specimen

The crack mouth-opening displacement equation is given by

$$V_f = f/(E\,B)\,G_f \qquad \text{(A-4)}$$

where G_f is the boundary-correction factor on displacements, E is modulus of elasticity, and B is specimen thickness. The function G_f is given by

$$G_f = 19.75\,G_1 / (1 - c/W)^2 \qquad \text{(A-5)}$$

$$G_1 = 1.442 - 0.405\,(c/W) - 0.173\,(c/W)^2 - 1.293\,(c/W)^3 + 1.67\,(c/W)^4 \qquad \text{(A-6)}$$

A comparison of the FADD2D normalized displacements and the equation is shown in figure A-4. Again, the equation was within 1% over a wide range in c/W ratios (0.2 to 0.8).

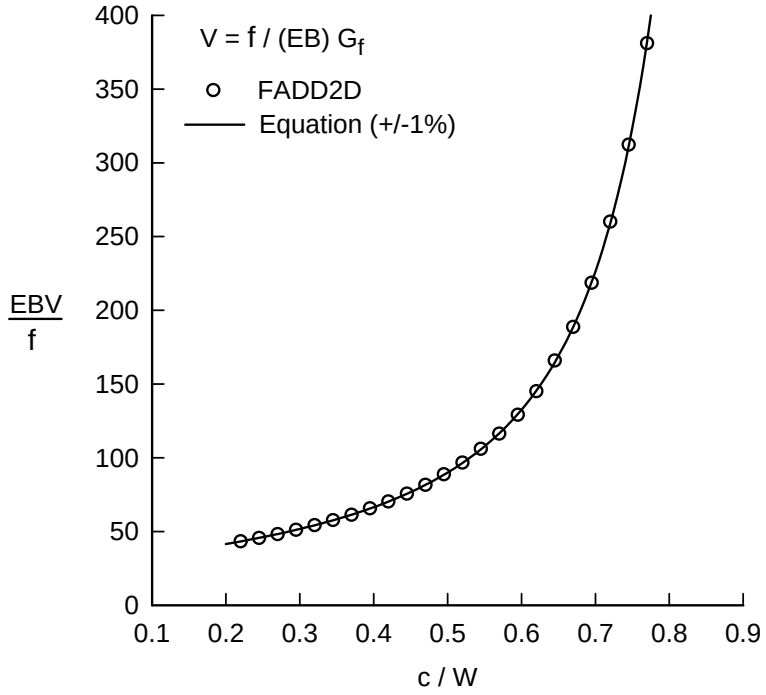

Figure A-4. Normalized Crack Mouth-Opening Displacements for a Force Applied at the Crack Mouth of a Compact Specimen

The displacement compatibility equation at the crack mouth was used to solve for the unknown displacement gage forces, *f*. Using displacement compatibility at the displacement gage location, an equation was developed to account for the influence of the displacement gage on test results that are generated at low applied loads on the compact specimen. Thus, the displacement gage force, *f*, is given by

$$f = [N_g - N_c - P\ G_P/(EB)]/[1/k_g + G_f/(EB)] \tag{A-7}$$

where N_g is the initial gage length, N_c is the notch knife-edge length, P is the applied load, E is modulus of elasticity, B is thickness, k_g is the gage spring stiffness ($f = k_g\ V_g$, where V_g is the displacement), G_P is the displacement function for the applied loading, P, and G_f is the displacement function for the gage force, f. The functions G_P and G_f are functions of c/W. Once c/W is known from the crack mouth-opening gage or back-face strain gage calibration, then the gage force, f, can be calculated. The stress-intensity factor due to the gage is then given by equation A-2.

The stress-intensity factor K_P and crack mouth-opening displacement V_P equations have already been developed for the pin-loaded compact specimen, as shown in figure A-5. These equations are given in the ASTM E 647 standard and reference A-3. The stress-intensity factor equation is

$$K_P = P\ /(B\ \sqrt{W})\ F_P \tag{A-8}$$

where P is the applied load, and F_P is the boundary-correction factor. The function F_P is given by

$$F_P = F_1 \left(0.886 - 4.64 \left(c/W\right) + 13.32 \left(c/W\right)^2 + 14.72 \left(c/W\right)^3 - 5.6 \left(c/W\right)^4\right) \quad \text{(A-9)}$$

$$F_1 = (2 + c/W)/(1 - c/W)^{3/2} \quad \text{(A-10)}$$

where the equation is valid over the range $0.2 < c/W < 1$ and is accurate to within 1% of the boundary-collocation results [A-4].

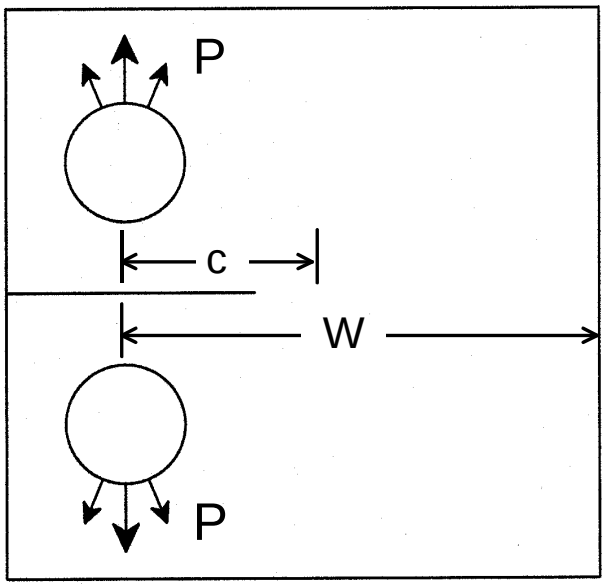

Figure A-5. Compact Tension Subjected to Pin Loading

The crack mouth-opening displacement equation is

$$V_P = P /(E\, B)\, G_P \quad \text{(A-11)}$$

where G_P is the boundary-correction factor on displacements. The function G_f is given by

$$G_P = 19.75\, G_2 / (1 - c/W)^2 \quad \text{(A-12)}$$

$$G_2 = 0.5 - 0.192 \left(c/W\right) + 1.385 \left(c/W\right)^2 - 2.919 \left(c/W\right)^3 + 1.842 \left(c/W\right)^4 \quad \text{(A-13)}$$

REFERENCES

A-1. Chang, C.C. and Mear, M.E., "A Boundary Element Method for Two-Dimensional Linear Elastic Fracture Analysis," *International Journal of Fracture*, Vol. 74, 1996, pp. 219-251.

A-2. Standard Test Method for Measurement of Fatigue Crack Growth Rates, ASTM STP E-647, 2003, pp. 615-657.

A-3. Saxena A. and Hudak, S.J., "Review and Extension of Compliance Information for Common Crack Growth Specimens," *International Journal of Fracture*, Vol. 14, No. 5, 1978.

A-4. Newman, J.C., Jr., "Stress Analysis of the Compact Specimen Including the Effects of Pin Loading," ASTM STP-560, 1974, pp. 105-121.

APPENDIX B—COMPUTER CODES TO ANALYZE FATIGUE CRACK GROWTH RATE DATA

In the following, two Fortran computer codes are given: (1) dkeffs.f and (2) multi-curve.f along with sample input and output files. In the first code (dkeffs.f), the program calculates effective stress-intensity factor range against rate (ΔK_{eff}-rate) from an input file of (ΔK-rate) from three types of tests (constant-amplitude, load reduction, or K_{max}) on compact tension (C(T)) or middle crack tension (M(T)) specimens. In the second code (multi-curve.f), the program calculates the ΔK against rate curves for a given stress ratio (R) over a wide range in rates using the ΔK_{eff} against rate input curve from the material, thickness, and environment of interest. (Each code gives a comment section that defines the input and output parameters.)

Both codes are considered "small-scale" yielding analyses of the fatigue crack growth rate data. The FASTRAN Version 3.8 life-prediction code [B-1] is considered a large-scale yielding code, which allows for plastic-zone sizes at the crack tip to be orders of magnitude larger than the crack length in M(T)-type specimens or for cracks emanating from open holes. Thus, the crack-opening stresses are a function of stress ratio (R), stress level (S_{max}), constraint factor(s), and the material tensile properties. (Stress-intensity factor or K-analogy is often used to relate the crack-opening stresses from M(T) specimens to those in other crack configurations or components, such as the C(T) specimen.) Unfortunately, fatigue crack growth rate data often presented in the literature and in handbooks do not have the associated load or stress levels and crack lengths given. Thus, the two data analysis codes have the S_{max}/σ_o ratio automatically set to 0.1 (small-scale yielding). Herein, for M(T) or C(T) specimens tested at "low" applied loads or stresses, the crack-opening stresses will only be a function of stress ratio (R) and the appropriate constraint factor(s) and will have the same value (S_o/S_{max} or P_o/P_{max}) for both specimen types. It has been found that small-scale yielding analyses are often adequate for most damage-tolerant life calculations.

B.1 EFFECTIVE STRESS-INTENSITY FACTOR RANGE.

For most damage tolerance and durability analyses, linear elastic fatigue crack growth analyses have been found to be quite adequate. The linear elastic effective stress-intensity factor range developed by Elber [B-2] is given by

$$\Delta K_{eff} = (S_{max} - S_o) \sqrt{(\pi c)}\ F \tag{B-1}$$

where S_{max} is the maximum stress, S_o is the crack-opening stress, and F is the usual boundary-correction factor. In general, for any crack configuration, the effective stress-intensity factor range is given by

$$\Delta K_{eff} = U\,\Delta K = [(1 - S_o/S_{max})/(1 - R)]\,\Delta K \tag{B-2}$$

B.2 EFFECTIVE STRESS-INTENSITY FACTOR AGAINST RATE ANALYSIS.

```
C PROGRAM DKEFFS
C-----------------------------------------------------------------------
C This program calculates DKeff against Rate from an input file of DK
C against Rate (max number of points = 999) at a given R (stress ratio).
C This is a "small-scale" yielding solution using FASTRAN Version 3.8
C crack opening stress equations (Note: Smax/Sflow = 0.1 and the crack-
C opening stress is only a function of R and constraint factor).
C
C Create an input filename (<16 characters, free Format input):
C     TITLE OF DATASET (<80 characters)
C     NALP, ALP
C     RATE1  ALP1  RATE2  ALP2  (Only if NALP = 1; otherwise skip)
C       NTYPE  NUM  R   $Constant-amplitude test
C         DK(1)  CGR(1)
C         DK(2)  CGR(2)
C          ...
C         DK(NUM)  CGR(NUM)
C       NTYPE  NUM  R   $Load-reduction test
C         DK(1)  CGR(1)
C         DK(2)  CGR(2)
C          ...
C         DK(NUM)  CGR(NUM)
C       NTYPE  NUM  KMAX  $Kmax test
C         DK(1)  CGR(1)
C          ...
C         DK(NUM)  CGR(NUM)
C       0  0  0  (END OF FILE)
C
C Multiple data sets can be analyzed in one file, if they have the
C same constraint variations.  NUM is the number of data points for
C each test type (NTYPE).
C
C   NTYPE = 1  Constant-amplitude loading, R = stress ratio
C         = 2  Load-reduction test, R = stress ratio
C         = 3  Kmax test, Kmax value is input
C
C NTYPE may be the same for all tests or different for each test
C
C Select an output filename (<16 characters), like ot4340v.txt
C
c Definitions:
C   ALP = Constraint Factor = 1    Plane Stress
C                           = 1.73 Irwin's Plane Strain
C                           = 3    Plane Strain
C
C   NALP = 0  Constraint factor (ALP) is constant as input
C        = 1  Constraint factors are variable
C             (ALP varies from ALP1 to ALP2)
C
C   RATE1 = Crack-growth rate near "start" of constraint-loss regime
C         (transition from flat-to-slant crack growth in some materials)
C         (ALP = ALP1 for rates less than RATE1)
C   RATE2 = Crack-growth rate near "end" of constraint-loss regime
C           (ALP = ALP2 for rates greater than RATE2)
```

```
C   RATE1, ALP1, RATE2 and ALP2 are used only with the NALP = 1 option
C
C   Elastic stress-intensity factor range:
C        DK = DS (PI*c)^0.5  F(c/w,...)
C        DS = Smax - Smin
C (Note: Stress-intensity factor for a negative R ratios is full range.)
C
C   Effective stress-intensity factor range:
C        DKeff = DSeff (PI*c)^0.5  F(c/w,...)
C        DSeff = Smax - So
C
C---------------------------------------------------------------------
C
      IMPLICIT REAL*8 (A-H,O-Z)
      CHARACTER*4 TITLE(20)
      CHARACTER*16 INFILE,OUTFILE
C
      PRINT *,'ENTER INPUT FILENAME'
      READ(5,11) INFILE
      PRINT *,'ENTER OUTPUT FILENAME'
      READ(5,11) OUTFILE
   11 FORMAT(A16)
      OPEN(3,FILE=INFILE,STATUS='UNKNOWN')
      OPEN(4,FILE=OUTFILE,STATUS='UNKNOWN')
C
      READ(3,12) TITLE
   12 FORMAT(20A4)
      WRITE(4,13) TITLE
   13 FORMAT(1X,19A4)
      READ(3,*) NALP, ALP
      WRITE(4,14) NALP
   14 FORMAT(5X,'NALP= ',I1)
      IF(NALP.EQ.1) THEN
      WRITE(4,15)
   15 FORMAT(/5X,'VARIABLE CONSTRAINT'/5X,'(ALP1-TO-ALP2)')
      ELSE
      WRITE(4,16) ALP
   16 FORMAT(/5X,'CONSTANT CONSTRAINT'/5X,'(ALP= 'F4.2')')
      ENDIF
C
      IERR=0
      IF(NALP.EQ.1) THEN
      READ(3,*) RATE1,ALP1,RATE2,ALP2
      WRITE(4,18) RATE1,ALP1,RATE2,ALP2
   18 FORMAT(/5X,'RATE1=',E10.3,/6X,'ALP1= ',F4.2,/
     1 /5X,'RATE2=',E10.3,/6X,'ALP2= ',F4.2)
      IF(RATE1.GT.RATE2) IERR=3
      IF(ALP1.LT.ALP2) IERR=4
      IF(IERR.EQ.3) WRITE(4,73)
      IF(IERR.EQ.4) WRITE(4,74)
      IF(IERR.GT.0) GOTO 99
      ENDIF
C
   20 READ(3,*) NTYPE,NUM,R
      IF(NTYPE.EQ.0) GOTO 99
      IF(NTYPE.EQ.1) WRITE(4,21) R
      IF(NTYPE.EQ.2) WRITE(4,22) R
```

```
      IF(NTYPE.EQ.3) THEN
      XKMAX=R
      WRITE(4,23) XKMAX
      ENDIF
   21 FORMAT(/5X,'Constant-amplitude',3x,'R= ',F6.2)
   22 FORMAT(/5X,'Load-reduction',3x,'R= ',F6.2)
   23 FORMAT(/5X,'Kmax-test',3x,'Kmax= ',F6.2)
      IF(NTYPE.LT.0.or.NTYPE.GT.3) IERR=5
      IF(IERR.EQ.5) WRITE(4,75)
      IF(IERR.GT.0) GOTO 99
C
      IF(NALP.EQ.0) WRITE(4,24)
   24 FORMAT(8X,'DKeff',9X,'Rate',8X,'U-factor')
      IF(NALP.EQ.1) WRITE(4,25)
   25 FORMAT(8X,'DKeff',9X,'Rate',8X,'U-factor',3X,'ALP')
C
      DO 30 I=1,NUM
      READ(3,*) DK,CGR
      IF(NTYPE.EQ.3) R=1-DK/XKMAX
Closure analysis to determine DKEFF against rate at R
      IF(NALP.EQ.1) THEN
      FX=(DLOG(CGR)-DLOG(RATE2))/(DLOG(RATE1)-DLOG(RATE2))
      ALP=ALP2+(ALP1-ALP2)*FX
      IF(CGR.LT.RATE1) ALP=ALP1
      IF(CGR.GT.RATE2) ALP=ALP2
      ENDIF
      PI=3.14159
      SMSO=0.1
      ANG=SMSO*PI/2
      A0=(0.825-0.34*ALP+0.05*ALP**2)*(DCOS(ANG))**(1/ALP)
      A1=(0.415-0.071*ALP)*SMSO
      A3=2*A0+A1-1
      A2=1-A0-A1-A3
      So=A0+A1*R+A2*R**2+A3*R**3
      IF(R.LT.0.0) So=A0+A1*R
      IF(So.LT.R) So=R
      U=(1-So)/(1-R)
      DKEFF=DK*U
C
      IF(NALP.EQ.0) WRITE(4,26) DKEFF,CGR,U
   26 FORMAT(5X,F8.3,6X,E11.4,5X,F5.3)
      IF(NALP.EQ.1) WRITE(4,27) DKEFF,CGR,U,ALP
   27 FORMAT(5X,F8.3,6X,E11.4,5X,F5.3,5X,F4.2)
   30 CONTINUE
      GOTO 20
C Error messages
   71 FORMAT(/5X,'DKETAB must be in ascending order!')
   72 FORMAT(/5X,'CGRTAB must be in ascending order!')
   73 FORMAT(/5X,'ALP2 must be less than ALP1!')
   74 FORMAT(/5X,'RATE2 must be greater than RATE1!')
   75 FORMAT(/5X,'NTYPE out of range!')
   99 STOP
      END
```

A sample input file, d4340v.txt, is given for the 4340 steel tested at NASA Langley. (Note that the data input has been greatly reduced and simplified for illustration purposes only.) The input file is:

```
d4340v.txt - 4340 Steel Compact Tension Specimens
 1  3.0
 1.0e-8  2.5   1.25e-7   1.2
 3    14   22.0   $Kmax test
  19.73   5.63e-8
  17.11   3.83e-8
  14.28   2.44e-8
  11.93   1.53e-8
   9.97   9.93e-9
   8.33   6.35e-9
   6.95   4.08e-9
   5.28   2.08e-9
   4.50   1.33e-9
   4.05   9.09e-10
   3.87   8.53e-10
   3.45   4.62e-10
   3.25   3.45e-10
   3.02   1.90e-10
 1    13   0.7    $Constant-amplitude test
   8.91   7.46e-9
   9.90   1.03e-8
  11.02   1.39e-8
  12.26   1.93e-8
  13.64   2.66e-8
  15.18   3.63e-8
  16.89   5.18e-8
  18.80   7.21e-8
  21.24   1.25e-7
  22.55   1.27e-7
  23.37   1.45e-7
  24.23   1.59e-7
  25.88   2.01e-7
 2    15   0.1    $Load-reduction test
   9.033   5.562e-9
   8.550   4.216e-9
   8.066   3.175e-9
   7.824   2.743e-9
   7.605   2.280e-9
   7.176   1.442e-9
   6.967   1.125e-9
   6.758   7.620e-10
   6.451   3.225e-10
   6.341   2.590e-10
   6.121   1.889e-10
   6.110   1.854e-10
   6.099   6.908e-11
   6.088   1.104e-10
   6.078   9.880e-11
  0   0   0
```

The corresponding output file, ot4340v.txt, generates the ΔK_{eff}-rate analysis of the ΔK-rate input data using either constant constraint (NALP = 0) or variable-constraint conditions (NALP = 1). This particular example is a variable-constraint analysis where fatigue crack growth rates below RATE1 have a constant-constraint factor of ALP1 and for rates above RATE2 have a constant-constraint factor of ALP2. A linear interpolation on log(rate) is used for rates between these two input rate values. The output is DKeff, Rate, U-factor, and ALP in the same units (MPa-$m^{1/2}$ and m/cycle; or ksi-$in^{1/2}$ and in/cycle) as the input data. The U-factor (Elber's ratio, see equation B-2) is the ratio of $\Delta K_{eff}/\Delta K$, and the ALP value is the constraint factor at this particular crack growth rate.

The output file is given as:

```
d4340v.txt - 4340 Steel Compact Tension Specimens

    NALP= 1

    VARIABLE CONSTRAINT
    (ALP1-TO-ALP2)

    RATE1= 0.100E-07
     ALP1= 2.50

    RATE2= 0.125E-06
     ALP2= 1.20

    Kmax-test   Kmax=  22.00
       DKeff         Rate        U-factor   ALP
      12.877       0.5630E-07     0.653     1.61
      12.851       0.3830E-07     0.751     1.81
      12.124       0.2440E-07     0.849     2.04
      11.001       0.1530E-07     0.922     2.28
       9.676       0.9930E-08     0.970     2.50
       8.220       0.6350E-08     0.987     2.50
       6.929       0.4080E-08     0.997     2.50
       5.280       0.2080E-08     1.000     2.50
       4.500       0.1330E-08     1.000     2.50
       4.050       0.9090E-09     1.000     2.50
       3.870       0.8530E-09     1.000     2.50
       3.450       0.4620E-09     1.000     2.50
       3.250       0.3450E-09     1.000     2.50
       3.020       0.1900E-09     1.000     2.50

    Constant-amplitude   R=   0.70
       DKeff         Rate        U-factor   ALP
       8.901       0.7460E-08     0.999     2.50
       9.880       0.1030E-07     0.998     2.48
      10.876       0.1390E-07     0.987     2.33
      11.926       0.1930E-07     0.973     2.16
      13.054       0.2660E-07     0.957     2.00
      14.269       0.3630E-07     0.940     1.84
      15.509       0.5180E-07     0.918     1.65
      16.844       0.7210E-07     0.896     1.48
      18.152       0.1250E-06     0.855     1.20
      19.271       0.1270E-06     0.855     1.20
```

```
  19.972       0.1450E-06     0.855     1.20
  20.707       0.1590E-06     0.855     1.20
  22.117       0.2010E-06     0.855     1.20

Load-reduction   R=   0.10
   DKeff          Rate        U-factor   ALP
   7.036       0.5562E-08     0.779     2.50
   6.660       0.4216E-08     0.779     2.50
   6.283       0.3175E-08     0.779     2.50
   6.094       0.2743E-08     0.779     2.50
   5.924       0.2280E-08     0.779     2.50
   5.589       0.1442E-08     0.779     2.50
   5.427       0.1125E-08     0.779     2.50
   5.264       0.7620E-09     0.779     2.50
   5.025       0.3225E-09     0.779     2.50
   4.939       0.2590E-09     0.779     2.50
   4.768       0.1889E-09     0.779     2.50
   4.759       0.1854E-09     0.779     2.50
   4.750       0.6908E-10     0.779     2.50
   4.742       0.1104E-09     0.779     2.50
   4.734       0.9880E-10     0.779     2.50
```

B.3 ELASTIC STRESS-INTENSITY FACTOR AGAINST RATE ANALYSIS.

The crack growth relation used in FASTRAN is

$$dc/dN = C_i\,(\Delta K_{eff})^{n_i}/[1-(K_{max}/C_5)^q] \qquad \text{(B-3)}$$

where C_i and n_i are the coefficient and power for each linear segment, K_{max} is the maximum stress-intensity factor, C_5 is the cyclic fracture toughness, and q is the power on the fracture term. The table lookup form is used because many materials, especially aluminum alloys, show sharp changes in the crack growth rate curves at unique values of rate. These sharp changes have been associated with monotonic and cyclic plastic zone sizes, grain sizes, and environments [B-3 and B-4]. The fracture term is very similar to the term used by Forman in the crack growth rate equation in the NASGRO code [B-5]. In general, C_5, which is equal to K_{Ie}, the elastic stress-intensity factor at failure (under cyclic loading), is a function of crack length, specimen width, and specimen type. A method to correlate fracture and to predict K_{Ie} or C_5 for a given material and crack configuration has been developed by Newman [B-6]. Herein, C_5 and q are held constant; and they are treated as fitting parameters.

```
C PROGRAM MULTI-CURVE
C-----------------------------------------------------------------------
C This program creates an output file of DK-Rate points (NMAX) at a
C given input stress ratio (R) from input DKeff-Rate table-lookup,
C C5 = cyclic fracture toughness and q = power on fracture term in
C fatigue-crack growth equation:
C
C              dc/dN = C1(DKeff)^C2/[1 - (Kmax/C5)^q]
C
C    MTAB = number of DKETAB(i) and CGRTAB(i) input points (MTAB < 35)
C    DKETAB(i) = "elastic" DKeff (MPa-m^1/2 or ksi-in^1/2) at point i
C    CGRTAB(i) = crack-growth rate (m/cycle or in/cycle) at point i
```

```
C    where i = 1 to MTAB
C    C1 and C2 are coefficient and power of each multi-linear segment
C    defined by the table of DKETAB and CGRTAB values
C
C This is a "small-scale" yielding solution using FASTRAN Version 3.8
C crack opening stress equations (Note: Smax/Sflow set to 0.1, and the
C crack opening stress is only a function of R and constraint factor).
c Note that C5 is generally larger than the monotonic fracture toughness
C and is used as a fitting parameter. (C5 is the elastic stress-
C stress-intensity factor at failure and is sometimes denoted as KIe.
C In general, KIe varies with thickness, crack length, width and loading
C conditions for ductile materials. Only for brittle materials would
C KIe be considered a constant.)
C
C Note: C3 and C4 are "threshold" constants which are "not" used.
C Near threshold behavior is modeled with the DKeff-Rate table and
C the closure model with the appropriate constraint factor will
C predict the value of the DKth threshold at a given R ratio.
C
C Note: NMAX should be large, like 400, to define a smooth curve and
C negative R ratios are full-range DK.
C
C Create an input filename (<16 characters, free Format input):
C     TITLE OF DATASET (<80 characters)
C     MTAB, NALP, ALP
C     DKETAB(1)  CGRTAB(1)
C     DKETAB(2)  CGRTAB(2)
C      ...
C     DKETAB(MTAB)  CGRTAB(MTAB)
C     RATE1  ALP1  RATE2  ALP2  (Only if NALP = 1)
C     NMAX, R, C5, q
C
C Select an output filename (<16 characters), like otd4340.txt
C
C Definitions:
C   ALP = Constraint Factor = 1    Plane Stress
C                           = 1.73 Irwin's Plane Strain
C                           = 3    Plane Strain
C
C   NALP = 0  Constraint factor (ALP) is constant as input
C        = 1  Constraint factors are variable
C             (ALP varies from ALP1 to ALP2)
C
C   RATE1 = Crack-growth rate near "start" of constraint-loss regime
C         (transition from flat-to-slant crack growth in some materials)
C         (ALP = ALP1 for rates less than RATE1)
C   RATE2 = Crack-growth rate near "end" of constraint-loss regime
C           (ALP = ALP2 for rates greater than RATE2)
C   RATE1, ALP1, RATE2 and ALP2 are used only with the NALP = 1 option
C
C   Elastic stress-intensity factor range:
C        DK = DS (PI*c)^0.5  F(c/w,...)
C        DS = Smax - Smin
C (Note: Stress-intensity factor for a negative R ratios is full range.)
C
C   Effective stress-intensity factor range:
C        DKeff = DSeff (PI*c)^0.5  F(c/w,...)
```

```
C        DSeff = Smax - So
C
C-----------------------------------------------------------------------
C
      IMPLICIT REAL*8 (A-H,O-Z)
      DIMENSION DKETAB(35),CGRTAB(35),C1(35),C2(35)
      CHARACTER*4 TITLE(20)
      CHARACTER*16 INFILE,OUTFILE
C
      PRINT *,'ENTER INPUT FILENAME'
      READ(5,11) INFILE
      PRINT *,'ENTER OUTPUT FILENAME'
      READ(5,11) OUTFILE
   11 FORMAT(A16)
      OPEN(3,FILE=INFILE,STATUS='UNKNOWN')
      OPEN(4,FILE=OUTFILE,STATUS='UNKNOWN')
C
      READ(3,12) TITLE
   12 FORMAT(20A4)
      WRITE(4,13) TITLE
   13 FORMAT(1X,19A4)
      READ(3,*) MTAB, NALP, ALP
      WRITE(4,14) MTAB, NALP
   14 FORMAT(5X,'MTAB= ',I2,/5X,'NALP= 'I1)
      IF(NALP.EQ.1) THEN
      WRITE(4,15)
   15 FORMAT(/5X,'VARIABLE CONSTRAINT'/5X,'(ALP1-TO-ALP2)'/)
      ELSE
      WRITE(4,16) ALP
   16 FORMAT(/5X,'CONSTANT CONSTRAINT'/5X,'(ALP= 'F4.2')'/)
      ENDIF
      IERR=0
      WRITE(4,18)
   18 FORMAT(7X,'DKeff',10X,'Rate')
C
      DO 20 I=1,MTAB
      READ(3,*) DKETAB(I),CGRTAB(I)
      WRITE(4,19) DKETAB(I),CGRTAB(I)
   19 FORMAT(5X,F7.2,7X,E10.3)
      IF(I.GT.1) THEN
      II=I-1
      IF(DKETAB(I).LE.DKETAB(II)) IERR = 1
      IF(CGRTAB(I).LE.CGRTAB(II)) IERR = 2
      IF(IERR.EQ.1) WRITE(4,71)
      IF(IERR.EQ.2) WRITE(4,72)
      IF(IERR.GT.0) GOTO 99
      ENDIF
      IF(I.GT.1) THEN
      I2=I
      I1=I-1
      C2(I1)=(DLOG(CGRTAB(I2))-DLOG(CGRTAB(I1)))/
     1 (DLOG(DKETAB(I2))-DLOG(DKETAB(I1)))
      C1(I1)=CGRTAB(I1)/(DKETAB(I1)**C2(I1))
      ENDIF
   20 CONTINUE
C
      IF(NALP.EQ.1) THEN
```

```
      READ(3,*) RATE1,ALP1,RATE2,ALP2
      WRITE(4,21) RATE1,ALP1,RATE2,ALP2
   21 FORMAT(/5X,'RATE1=',E10.3,/6X,'ALP1= ',F4.2,/
     1 /5X,'RATE2=',E10.3,/6X,'ALP2= ',F4.2)
      IF(RATE1.GT.RATE2) IERR=3
      IF(ALP1.LT.ALP2) IERR=4
      IF(IERR.EQ.3) WRITE(4,73)
      IF(IERR.EQ.4) WRITE(4,74)
      IF(IERR.GT.0) GOTO 99
      ENDIF
      READ(3,*) NMAX, R, C5, q
      WRITE(4,23) NMAX, R, C5, q
   23 FORMAT(/5X,'NMAX= ',I3,/5X,'R=',F6.2,//,5X,
     1 'C5= ',F6.2,/6X,'q= ',F4.2,/)
C
      WRITE(4,24)
   24 FORMAT(9X,'DK',11X,'Rate')
      DKF=DLOG(DKETAB(1))
      RDKEFF=(DLOG(DKETAB(MTAB))-DLOG(DKETAB(1)))/NMAX
      DKF=DLOG(DKETAB(1))-RDKEFF
   40 DKF=DKF+RDKEFF
      DKFF=DEXP(DKF)
      IF(DKFF.GT.DKETAB(MTAB)) GOTO 99
      DO 50 I=2,MTAB
      IF(DKFF.LE.DKETAB(I)) GOTO 60
   50 CONTINUE
      I=MTAB
   60 I1=I-1
      CGR=C1(I1)*DKFF**C2(I1)
c     WRITE(4,62) DKFF,CGR
c  62 FORMAT(5X,F8.4,4X,E12.5)
C
Closure analysis to determine DK against rate at R
      IF(NALP.EQ.1) THEN
      FX=(DLOG(CGR)-DLOG(RATE2))/(DLOG(RATE1)-DLOG(RATE2))
      ALP=ALP2+(ALP1-ALP2)*FX
      IF(CGR.LT.RATE1) ALP=ALP1
      IF(CGR.GT.RATE2) ALP=ALP2
      ENDIF
      PI=3.14159
      SMSO=0.1
      ANG=SMSO*PI/2
      A0=(0.825-0.34*ALP+0.05*ALP**2)*(DCOS(ANG))**(1/ALP)
      A1=(0.415-0.071*ALP)*SMSO
      A3=2*A0+A1-1
      A2=1-A0-A1-A3
      So=A0+A1*R+A2*R**2+A3*R**3
      IF(R.LT.0.0) So=A0+A1*R
      IF(So.LT.R) So=R
      U=(1-So)/(1-R)
      DK=DKFF/U
      XKMAX=DK/(1-R)
      CGR1=CGR/(1-(XKMAX/C5)**q)
C
      IF(CGR1.GT.0.0) WRITE(4,64) DK,CGR1
   64 FORMAT(5X,F8.3,6X,E11.4)
      GOTO 40
```

```
C Error messages
   71 FORMAT(/5X,'DKETAB must be in ascending order!')
   72 FORMAT(/5X,'CGRTAB must be in ascending order!')
   73 FORMAT(/5X,'ALP2 must be less than ALP1!')
   74 FORMAT(/5X,'RATE2 must be greater than RATE1!')
   99 STOP
      END
```

A sample input file, 4340rate.txt, is given for the 4340 steel tested during the AGARD Short Crack Program [B-7]. This file was created to generate a ΔK-rate curve at $R = -1$ using the ΔK_{eff}-rate curve for the 4340 steel. This example illustrates a variable-constraint option with 400 points to define a very smooth curve. C_5 was set to 180 MPa-m$^{1/2}$ and $q = 3$. The input file is:

```
4340rate.txt  R=-1
    7  1  2.5
   3.00   1.00e-11
   3.40   5.00e-10
   5.00   2.00e-9
   7.30   7.00e-9
  14.00   5.00e-8
  50.00   6.50e-7
 108.00   1.00e-4
5.0e-7  2.5  2.5e-5  1.2
 400  -1  180.0  3.0
```

To generate curves at other stress ratios, only the stress ratio, R, has to be changed in the input data file. The corresponding output file, out4340.txt, generates the ΔK-rate curve at the specified R value. The output file is given as:

```
 4340rate.txt  R=-1

     MTAB=  7
     NALP= 1

     VARIABLE CONSTRAINT
     (ALP1-TO-ALP2)

       DKeff          Rate
        3.00        0.100E-10
        3.40        0.500E-09
        5.00        0.200E-08
        7.30        0.700E-08
       14.00        0.500E-07
       50.00        0.650E-06
      108.00        0.100E-03

     RATE1= 0.500E-06
      ALP1= 2.50

     RATE2= 0.250E-04
      ALP2= 1.20

     NMAX= 400
     R= -1.00
```

```
C5= 180.00
 q= 3.00

    DK           Rate
  8.134       0.1000E-10
  8.207       0.1323E-10
  8.281       0.1751E-10
  8.355       0.2316E-10
  8.430       0.3065E-10
  8.506       0.4055E-10
  8.583       0.5366E-10
  8.660       0.7100E-10
  8.738       0.9394E-10
  8.817       0.1243E-09
  8.896       0.1645E-09
   ...         ...        $Data intentionally removed

 51.497       0.9273E-07
 51.961       0.9442E-07
 52.428       0.9615E-07
 52.900       0.9791E-07
 53.376       0.9970E-07
 53.856       0.1015E-06
 54.341       0.1034E-06
 54.830       0.1053E-06
 55.324       0.1072E-06
 55.821       0.1092E-06
   ...         ...        $Data intentionally removed

331.860       0.1516E-03
334.847       0.1784E-03
337.860       0.2130E-03
340.900       0.2596E-03
343.968       0.3251E-03
347.064       0.4235E-03
350.187       0.5868E-03
353.338       0.9085E-03
356.518       0.1827E-02
359.726       0.2442E-01
```

B.4 EXAMPLE OF FATIGUE CRACK GROWTH RATE DATA ANALYSES.

In the AGARD Short-Crack Program [B-7], fatigue crack growth rate tests were conducted on M(T) specimens under constant-amplitude and load reduction procedures at several stress ratios. These data were analyzed to determine the ΔK_{eff}-rate curve and the constraint factors needed to correlate the data onto a single curve. The high constraint factor ($\alpha = 2.5$) correlated the data in the mid-rate regime quite well, but showed variations in the near-threshold region. It is suspected that the load reduction procedure is generating inappropriately high threshold behavior at the low R ratios even on the M(T) specimens, but the influence appears to be far less than that observed on the steel C(T) specimens. At the high rates, the sharp change in slope was caused by the flat-to-slant crack growth behavior and indicated a constraint loss regime; and a low

constraint factor ($\alpha = 1.2$) was required to correlate the data. The baseline ΔK_{eff} curve was fitted to the high R results in the near-threshold regime.

Figure B-1 shows the ΔK-rate data on the 4340 steel at three R ratios. The curves are the predicted results using the "multi-curve" program at various stress ratios from –1 to 0.9. The cyclic fracture toughness, C_5, and q were selected to help fit the data in the fracture regime. The predicted curves fit the test data quite well over the complete range in rates from threshold to fracture. Tests at R values from 0.7 to 0.9 would be required to verify the choice of the cyclic fracture toughness.

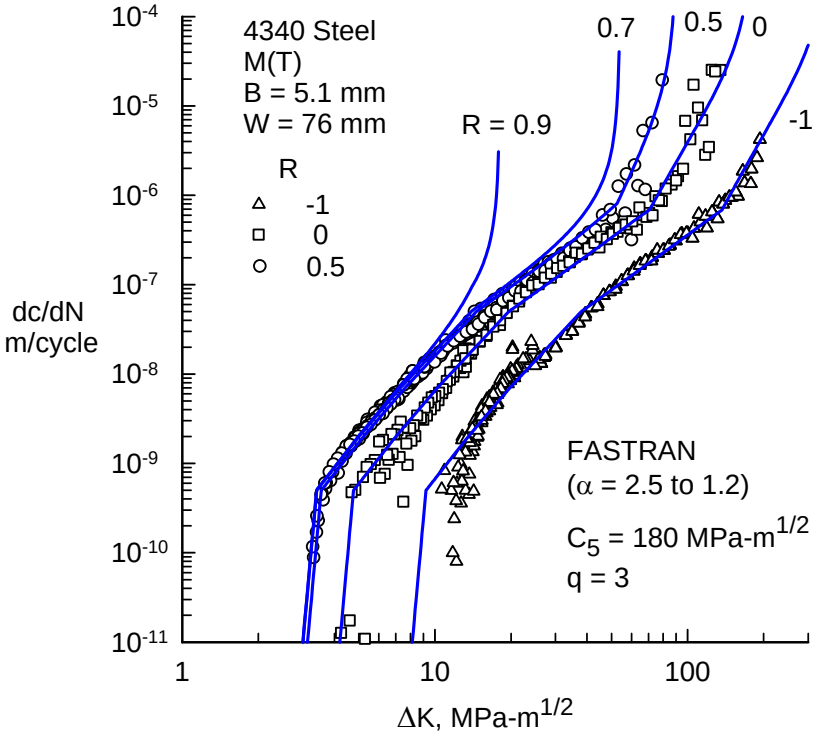

Figure B-1. Stress-Intensity Factor Range Against Rate for 4340 Steel M(T) Specimens

B.5 REFERENCES.

B-1. Newman, J.C., Jr., "FASTRAN-II - A Fatigue Crack Growth Structural Analysis Program," NASA TM 104159, February 1992.

B-2. Elber, W., "The Significance of Fatigue Crack Closure," *Damage Tolerance in Aircraft Structures*, ASTM STP 486, American Society for Testing and Materials, Philadelphia, 1971, pp. 230-242.

B-3. Yoder G.R., Cooley L.A., and Crooker, T.W., "On Microstructural Control on Near-Threshold Fatigue Crack Growth in 7000-Series Aluminum Alloys," *Scripta Metallurgica*, Vol. 16, 1982, pp. 1021-1025.

B-4. Piascik, R.S. and Gangloff, R.P., "Environmental Fatigue of an Al-Li-Cu Alloy: Part II Microscopic Hydrogen Cracking Processes," *Metallurgical Transactions*, Vol. 24A, 1993, pp. 2751-2762.

B-5. NASGRO Reference Manual 4.02, Southwest Research Institute and NASA Johnson Space Center, 2002.

B-6. Newman, J.C., Jr., "Fracture Analysis of Various Cracked Configurations in Sheet and Plate Materials," *Properties Related to Fracture Toughness*, ASTM STP 605, 1976, pp. 104-123.

B-7. Edwards, P.R. and Newman, J.C., Jr., editors, "Short-Crack Growth Behavior in Various Aircraft Materials," AGARD report no. 767, 1990.